Louisiana Tech University
Louisiana Tech Digital Commons

Doctoral Dissertations | Graduate School

Summer 2007

Fabrication and application of conducting polymer micro- and nano-patterns

Anirban Chakraborty
Louisiana Tech University

Follow this and additional works at: https://digitalcommons.latech.edu/dissertations

Part of the Electrical and Computer Engineering Commons

Recommended Citation
Chakraborty, Anirban, "" (2007). *Dissertation*. 495.
https://digitalcommons.latech.edu/dissertations/495

This Dissertation is brought to you for free and open access by the Graduate School at Louisiana Tech Digital Commons. It has been accepted for inclusion in Doctoral Dissertations by an authorized administrator of Louisiana Tech Digital Commons. For more information, please contact digitalcommons@latech.edu.

FABRICATION AND APPLICATION OF CONDUCTING POLYMER MICRO- AND NANO-PATTERNS

by

Anirban Chakraborty, BE

A Dissertation Presented in Partial Fulfillment
of the requirements for the Degree
Doctor of Philosophy

COLLEGE OF ENGINEERING AND SCIENCE
LOUISIANA TECH UNIVERSITY

August, 2007

Reproduced with permission of the copyright owner. Further reproduction prohibited without permission.

UMI Number: 3270946

INFORMATION TO USERS

The quality of this reproduction is dependent upon the quality of the copy submitted. Broken or indistinct print, colored or poor quality illustrations and photographs, print bleed-through, substandard margins, and improper alignment can adversely affect reproduction.

In the unlikely event that the author did not send a complete manuscript and there are missing pages, these will be noted. Also, if unauthorized copyright material had to be removed, a note will indicate the deletion.

UMI®

UMI Microform 3270946

Copyright 2007 by ProQuest Information and Learning Company.

All rights reserved. This microform edition is protected against unauthorized copying under Title 17, United States Code.

ProQuest Information and Learning Company
300 North Zeeb Road
P.O. Box 1346
Ann Arbor, MI 48106-1346

Reproduced with permission of the copyright owner. Further reproduction prohibited without permission.

LOUISIANA TECH UNIVERSITY

THE GRADUATE SCHOOL

07-01-07
Date

We hereby recommend that the dissertation prepared under our supervision by Anirban Chakraborty

entitled Fabrication and Application of Conducting Polymer Micro- and Nano-patterns.

be accepted in partial fulfillment of the requirements for the Degree of Ph.D. in Engineering

Supervisor of Dissertation Research

Head of Department

College of Engineering and Science
Department

Recommendation concurred in:

Advisory Committee

Approved:
Director of Graduate Studies

Approved:
Dean of the Graduate School

Dean of the College

GS Form 13
(5/03)

Reproduced with permission of the copyright owner. Further reproduction prohibited without permission.

ABSTRACT

Conducting polymers, since their discovery, have attracted significant attention due to their promise of replacing silicon and metals in building devices. They have been shown to have wide applications for biological and chemical sensing as well as for electronic devices. Previous and current efforts have concentrated on building devices of a specific function. When multiple micropatterns of different conducting polymers are fabricated on a common substrate, a versatile microsystem can be envisioned. The existing conducting polymer patterning techniques present some technical challenges of degradation, low throughput, low resolution, depth of field, and residual layer in producing conducting polymer microstructures. To circumvent these challenges in the existing technology, the Intermediate-Layer Lithography (ILL) method is proposed in this study. This approach overcomes the "depth of field" and "residual layer" issues of the traditional hot embossing process.

Conducting polymer micropatterns of various dimensions have been fabricated. The conducting polymers used for patterning include polypyrrole (PPy), poly(3,4-ethylenedioxythiophen)-poly(4-styrenesulphonate) (PEDOT-PSS), and sulphonated polyaniline (SPANI). Straight and serpentine microwires of various dimensions were fabricated and the embossing recipe was finalized for a stable reproduction of the

Reproduced with permission of the copyright owner. Further reproduction prohibited without permission.

imprinting results. The fabricated microwires were used for sensing applications using the "chemiresistor" principle. Sensitivities of conducting polymer films and microwires were compared after they were exposed to different levels of humidity. The microwires were found to be more sensitive than films at lower humidity levels. Two sets of microwires of PPy, PEDOT-PSS, and SPANI were imprinted on a common substrate. The imprinted microwires were used for sensing methanol, toluene, and acetone, individually and in mixtures of two gases. Each of the three different conducting polymer microwires was found to be more sensitive to methanol and acetone compared to toluene. An additional layer of glucose oxidase was coated over the PPy microwires to sense for glucose. The response current of the PPy microwires increased with increasing concentration of glucose (0.2 mg/ml - 0.8 mg/ml). The relationship between the surface-to-volume ratio of the microwires and their sensitivities was also investigated. PPy and PEDOT-PSS microwires of various dimensions were fabricated and exposed to acetone vapor at low concentrations. The microwires with higher surface-to-volume ratio were found to be most sensitive at lower concentrations of acetone.

PPy nanowires were fabricated effectively using the ILL method. The widths of the wires were 100 nm and 500 nm with lengths of 20 μm. In the near future, we would like to fabricate several different conducting polymer nanowires on a common substrate for sensing operations. Multiple sensors on a common substrate would result in a more functional sensor capable of sensing multiple analytes at very low concentrations.

Reproduced with permission of the copyright owner. Further reproduction prohibited without permission.

APPROVAL FOR SCHOLARLY DISSEMINATION

The author grants to the Prescott Memorial Library of Louisiana Tech University the right to reproduce, by appropriate methods, upon request, any or all portions of this Dissertation. It is understood that "proper request? consists of the agreement, on the part of the requesting party, that said reproduction is for his personal use and that subsequent reproduction will not occur without written approval of the author of this Dissertation. Further, any portions of the Dissertation used in books, papers, and other works must be appropriately referenced to this Dissertation.

Finally, the author of this Dissertation reserves the right to publish freely, in the literature, at any time, any or all portions of this Dissertation.

Author Anirban Chakraborty

Date 07-25-07

GS Form 14
(5/03)

Reproduced with permission of the copyright owner. Further reproduction prohibited without permission.

TABLE OF CONTENTS

ABSTRACT iii

LIST OF TABLES ix

LIST OF FIGURES x

ACKNOWLEDGEMENTS xv

CHAPTER 1 INTRODUCTION AND DISSERTATION OVERVIEW 1

1.1 Introduction 1

1.2 Dissertation Overview 4

CHAPTER 2 THEORY OF CONDUCTING POLYMERS 6

2.1 History of Conducting Polymers 6

2.2 Conduction Mechanisms 8

2.2.1 Role of Solitons, Polarons and Bipolarons in Conduction 11

2.2.2 Charge Hopping Mechanism 14

2.3 Three Commonly Used Conducting Polymers 17

2.3.1 PPy 17

2.3.2 PEDOT-PSS 18

2.3.3 Polyaniline (PANI) 18

2.4 Applications of Conducting Polymers 20

CHAPTER 3 CONDUCTING POLYMER PATTERNING TECHNIQUES 25

3.1 Soft Lithography Technique 25

Reproduced with permission of the copyright owner. Further reproduction prohibited without permission.

3.2 Inkjet Printing Technique 27

3.3 Hot Embossing Technique 29

CHAPTER 4 INTERMEDIATE-LAYER LITHOGRAPHY METHOD 33

4.1 Process Steps in the ILL Method 33

4.2 Key Points of the ILL Method 34

4.3 Experimental Procedure 36

4.3.1 Fabrication of the Silicon Mold for ILL 36

4.3.2 Experimental Procedure for ILL 39

4.4 Numerical Modeling of the Embossing Process 42

4.5 Experimental Results of Fabrication 47

CHAPTER 5 APPLICATIONS OF THE CONDUCTING POLYMER MICROWIRES 56

5.1 Humidity Exposure to PPy Microwire Sensor 57

5.2 Binary Sensor Configuration and Detection 59

5.2.1 Exposure of PPy and SPANI Microwires to Methanol and Toluene. 61

5.2.2 Exposure of PEDOT and SPANI Microwires to Acetone and Toluene 66

5.3 Glucose Sensing with PPy Microwires 72

5.4 Surface-to-Volume Ratio and Sensitivity Comparison 74

5.4.1. Partial Exposure of PPy Film Sensor 77

5.4.2 Experimental Comparison of Sensitivities of PPy and PEDOT Microwires and Film Sensor. 80

CHAPTER 6 FABRICATION OF PPy NANOWIRES USING THE ILL TECHNIQUE 85

6.1 Silicon Nanomolds 86

6.2 Mold and Substrate Preparation for Nanoembossing 89

Reproduced with permission of the copyright owner. Further reproduction prohibited without permission.

6.2.1 Mold Preparation for Nanoembossing 89

6.2.2 Substrate Preparation 89

6.3 Nanoembossing Experimental Results 91

6.3.1 Nanoembossing of the 500 nm Wide Silicon Channels 91

6.3.2 Nanoembossing of the 100 nm Wide Silicon Channels 92

6.3.3 Nanoembossing of the 100 nm Wide Silicon Nanochannels with a Pitch of 500 nm 95

CHAPTER 7 CONCLUSIONS AND FUTURE DIRECTION 97

7.1 Conclusions 97

7.2 Future Direction 99

REFERENCES 100

Reproduced with permission of the copyright owner. Further reproduction prohibited without permission.

LIST OF TABLES

Table 4. 1 Material properties of silicon and PMMA which were used for simulations. 45

Table 4. 2 Hot embossing machine recipe for imprinting the 300 μm wide microwires of PPy, PEDOT and SPANI. 48

Table 4. 3 Experimental results of the imprinting process using silicon molds of various dimensions. 50

Table 5. 1 Dimensions of the of the PPy and PEDOT microwires fabricated with different surface-to-volume ratios 81

Table 6. 1 Embossing recipe for imprinting the 500 nm wide PPy nanowires. 91

Table 6. 2 Hot embossing recipe for embossing the 100 nm wide silicon channels on PPy. 93

Reproduced with permission of the copyright owner. Further reproduction prohibited without permission.

LIST OF FIGURES

Figure 1.1 Conductivity of conducting polymers compared in a scale from quartz (insulator) to copper (conductor). 2

Figure 1.2 Double logarithmic plot of conducting polymer applications with respect to ionic and electronic resistances. 3

Figure 2.1 Chemical structure of polyacetylene. 7

Figure 22 Chemical structure of a heterocyclic polymer. The "X" are the hetero-atoms which are included in the chain in five-membered rings. 7

Figure 2.3 Chemical structures of the three commonly used conducting polymers: (a) polypyrrole, (b) polythiophene, and (c) polyaniline. 8

Figure 2.4 Formation of Polarons and Bipolarons during oxidative doping in PPy 12

Figure 2.5 Formation of solitons during doping of the conducting polymers. 14

Figure 2.6 Structure of conducting polymers showing the random distribution of the crystalline and amorphous regions. 15

Figure 2.7 Mechanism of "intersoliton hopping". 15

Figure 2.8 Mechanism of charge hopping which contributes to conductivity in conducting polymers. 16

Figure 2.9 Chemical structure of PPy: (a) neutral, (b) partially oxidized on low doping, (c) highly oxidized on heavy doping. 17

Figure 2.10 Chemical structure of PEDOT-PSS. 18

Figure 2.11 Chemical structure of the various redox states of PANI. 19

Figure 2.12 Working principle of an electronic nose. 22

Reproduced with permission of the copyright owner. Further reproduction prohibited without permission.

Figure 3.1 Schematic of the soft lithography pattern transfer process: (a) the rigid mold, (b) the liquid PDMS poured into the rigid mold, (c) the cured PDMS layer peeled-off from the rigid mold, (d) "ink" applied to the PDMS stamp, (e) the inked 25

Figure 3.2 Deformations of the PDMS in the soft lithography approach: (a) pairing deformation, (b) sagging deformation, and (c) shrinkage. 26

Figure 3.3 Continuous inkjet printing technique. 28

Figure 3.4 Drop-on-demand inkjet printing technique. 28

Figure 3.5 Autodrop printing system from Microdrop. 29

Figure 3.6 General scheme of a hot embossing machine. 31

Figure 3.7 Standard force and temperature profile during the hot embossing process. 32

Figure 4.1 Process steps in the ILL method. 34

Figure 4.2 (a) "Residual layer" and "height variation" obstacles which both hot embossing and nanoimprint lithography approaches faces in patterning 35

Figure 4.3 Schematic of the silicon mold fabrication steps: (a) the UV photolithography step, (b) the patterned photoresist layer, (c) the BOE etching of the SiO_2 layer, (d) the patterned SiO_2 layer, (e) the DRIE etching of silicon with SiO_2 as mask, and 37

Figure 4.4 (a) SEM of the microwire mold, (b) SEM of the serpentine microheater mold, and (c) optical picture of the silicon mold attached to the hot embossing tool. 38

Figure 4.5 HEX 01/LT Hot embossing machine from JENOPTIK Mikrotechnik GmbH. 40

Figure 4.6 Simulation results in ANSYS for fabrication of a 5μm serpentine microheater pattern: (a) before mold insertion, and (b) after mold insertion. 44

Figure 4.7 Simulation results in ANSYS for fabrication of a 50μm serpentine microheater pattern: (a) before mold insertion, and (b) after mold insertion. 45

Figure 4.8 Optical picture of straight microwires of PPy, PEDOT, and SPANI fabricated simultaneously using the ILL method. 47

Reproduced with permission of the copyright owner. Further reproduction prohibited without permission.

Figure 4.9 Optical pictures of serpentine microwire (microheater) patterns of PPy, PEDOT, and SPANI fabricated simultaneously using the ILL method. 48

Figure 4.10 Side-view SEM pictures of the (a) PPy, (b) PEDOT, and (c) SPANI microwires. 51

Figure 4.11 Serpentine microwires of width 5μm of PPy imprinted on PMMA: (a) SEM top view, and (b) SEM side view. The contact pads are 200μm X 200μm. 52

Figure 4.12 Serpentine microwires of width 50μm of PPy imprinted on PMMA: (a) SEM top view, and (b) SEM side view. The contact pads are 500 μm X 500 μm. 52

Figure 4.13 SEM pictures of serpentine PPy microwire patterns of width: (a) 50 μm, and (b) 10 μm. The silicon mold used for imprinting has a depth of 17 μm.....53

Figure 4.14 Variation in current of a 50 μm wide serpentine PPy microheater pattern when heated and cooled successively with increasing temperatures.....54

Figure 5.1 Schematic of three conducting polymer microwire sensor on a common platform.....56

Figure 5.2 SEM picture of additional silver epoxy contact with a PPy microwire. 57

Figure 5.3 Humidity exposure experimental setup.....58

Figure 5.4 Humidity response of a single microwire and a film of PPy. 59

Figure 5.5 Experimental setup for the binary sensor configuration and detection scheme. 60

Figure 5.6 Current variation of PPy microwires to methanol exposure. 61

Figure 5.7 Current variation of PPy microwires when exposed to toluene. 62

Figure 5.8 Current variation of PPy microwires when exposed to the mixture of vapors of methanol and toluene. 63

Figure 5.9 Current variation of SPANI microwires when exposed to methanol vapors.....64

Figure 5.10 Current variation of SPANI microwires to toluene exposure. 64

Reproduced with permission of the copyright owner. Further reproduction prohibited without permission.

Figure 5.11 Current variation of SPANI microwires when exposed to a mixture of methanol and tolene vapors. 65

Figure 5.12 Current variation of SPANI microwires to acetone exposure. 66

Figure 5.13 Current variation of SPANI microwires to toluene exposure. 67

Figure 5.14 Current variation of SPANI microwires to exposure to mixture of acetone and toluene. 68

Figure 5.15 Current variation of PEDOT microwires to acetone exposure. 69

Figure 5.16 Current variation of PEDOT microwires to toluene exposure. 70

Figure 5.17 Current variation of PEDOT microwires to exposure to mixture of acetone and toluene. 71

Figure 5.18 PPy microwire response to glucose solution of concentration 0.3 mg/ml. 73

Figure 5.19 Current variation of PPy microwires to glusoce solution of various concentrations. 74

Figure 5.20 Relationship between a film sensor and an individual "chemiresistor" block. 75

Figure 5.21 Comparison between a rectangular film and a microwire of same thickness where a1<<a2 and b1<<b2. 77

Figure 5.22 Experimental setup and schematic of the partial exposure experiment. 78

Figure 5.23 Relationship between the sensitivity of a PPy film to the exposed surface area. 79

Figure 5.24 Optical picture of the overall view of the imprinted PPy microwires. 80

Figure 5.25 Optical picture of the close-up view of a set of PPy microwires. Each microwire is 50 μm wide and 2000 μm long. 81

Figure 5.26 Sensitivity comparison between a PPy film and microwires of different surface-to-volume ratios. 83

Figure 5.27 Sensitivity comparison between a PEDOT film and microwires of different surface-to-volume ratios. 83

Reproduced with permission of the copyright owner. Further reproduction prohibited without permission.

Figure 6.1 AFM scan of a silicon nanomold containing 500 nm wide channels which are 20 μm long. 88

Figure 6.2 SEM picture of a silicon nanomold with channels of width 100 nm and length 5 μm. 88

Figure 6.3 AFM scan of the embossed PPy nanowires, 500 nm wide and 20 μm long. 92

Figure 6.4 SEM pictures of the partially filled PPy nanowires, 100 nm wide and 20 μm long. The pitch of the lines was 1 μm. 94

Figure 6.5 PPy nanowires 100 nm wide and 20 μm long. The pitch of the lines was 1 μm. 95

Figure 6.6 SEM pictures of the embossed PPy nanowire, 100 nm wide and 20 μm long. The pitch of the nanowires was 500 nm. 96

Reproduced with permission of the copyright owner. Further reproduction prohibited without permission.

ACKNOWLEDGEMENTS

I would like to express my sincere gratitude to my research advisor, Dr. Cheng Luo. He was my mentor, constantly guiding and supporting me in my pursuit of higher learning. I would also like to express my sincere thanks and regards to Mr. Ji Fang. I have worked closely with him, and he would always gladly offer his help when I needed and share his vast knowledge of the microfabrication field. I would like to thank Dr. Yuri Lvov, Dr. Jun-Ing Ker, and Dr. Chester Wilson for their consent to be in my dissertation committee.

I thank my current group members, Xinchuan Liu, Hao Li, Hui Wang, Ganga Parthasarathi, and Si Chen and former members, Fang Meng, Rakesh Poddar, Anand Francis, and Amitha Govindraju for their help and support. They always shared their precious research experiences whenever I needed their suggestions. It was always a pleasure working with them. Additionally, my friends, Anshul Agarwal, Anagha Patil, Pradeep Chowriappa, and Shantanu Balkundi deserve special mention for their continuous encouragement, assistance, suggestions and support.

I would like to thank my parents and my brother for their constant support and encouragement. That I was able to accomplish my academic pursuits in the United States of America was solely because of my parents' support. Finally, I dedicate this dissertation to my parents.

Reproduced with permission of the copyright owner. Further reproduction prohibited without permission.

CHAPTER 1

INTRODUCTION AND DISSERTATION OVERVIEW

1.1 Introduction

Polymers have been traditionally regarded as insulating substances. Conductivity, however little, was considered undesirable. Conducting polymers were discovered accidently in 1977. It was discovered after a post doctorate worker for Shirakawa accidentally added 1000 times more catalyst to a reaction [1]. It resulted in the formation of a silvery film. The conductivity of the film was found to be higher than the normal levels. The film was later doped to generate much higher conductivity. There are two principal reasons for the enormous interest in the area of conducting polymers. First, the scientific community is curious to understand the intrinsic behavior of this new class of polymers. Charge transfers to and from the polymer, and charge transports within the polymer matrix are being constantly investigated. Second, conducting polymers are promising for a wide range of applications, including sensors, electronic devices, energy storage, electronic displays, microsystem technologies, corrosion protection, etc. The conductivity range of the conducting polymers is represented in Figure 1.1. The conductivity of the conducting polymers may be increased by oxidative and reductive doping [1]. The main charge transport mechanisms are electron hopping between the redox sites in the polymer chains and movement of the delocalized electrons through the

Reproduced with permission of the copyright owner. Further reproduction prohibited without permission.

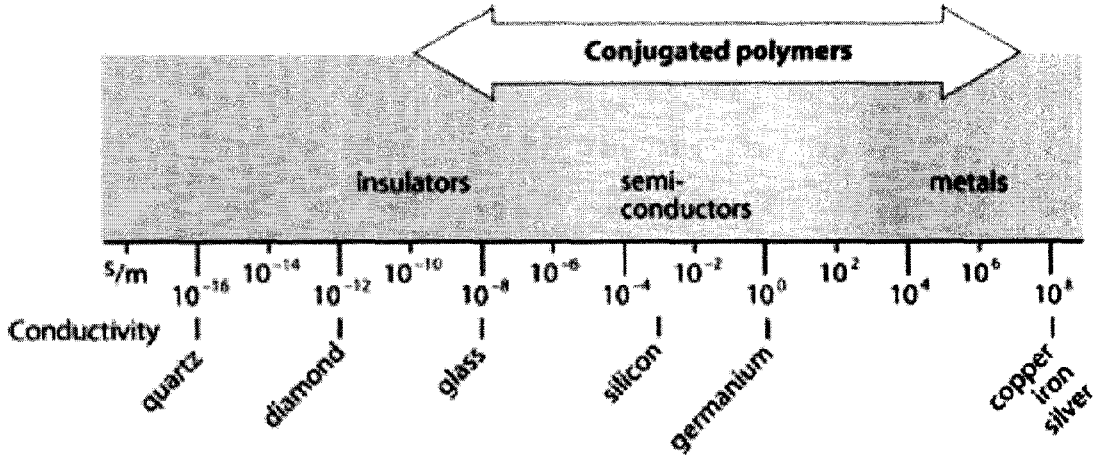

Figure 1.1 Conductivity of conducting polymers compared in a scale from quartz (insulator) to copper (conductor) [1].

conjugate system in the polymer backbone. The traditional sensor (or solid-state sensor) materials include semiconductors (Si, GaAs) [2], semiconducting metal oxides (SnO_2, ZnO_2, TiO_2, WO_3) [3,4,5], solid electrolytes (Y_2O_3 stabilized ZrO_2)[6,7,8], and membranes[9,10,11]. Silicon-based sensors are not produced any more, due to fundamental problems with reproducibility, stability, sensitivity, and selectivity. The semiconducting oxide based sensors rely on catalytic reactions. The oxides may be catalysts themselves, or additional catalysts may be added to achieve selectivity, sensitivity, and fast response. Solid electrolyte-based sensors have been used as gas and ion sensors [6,7]. Ionic mobility, rather than electron mobility, plays an important role in conduction in solid electrolytes.

The realm of applications of conducting polymers is represented by Inzelt et al. [12] in a double logarithmic plot (Figure 1.2). For reference, the position of metals, semiconductors, and insulators is given at the top of the figure.

Reproduced with permission of the copyright owner. Further reproduction prohibited without permission.

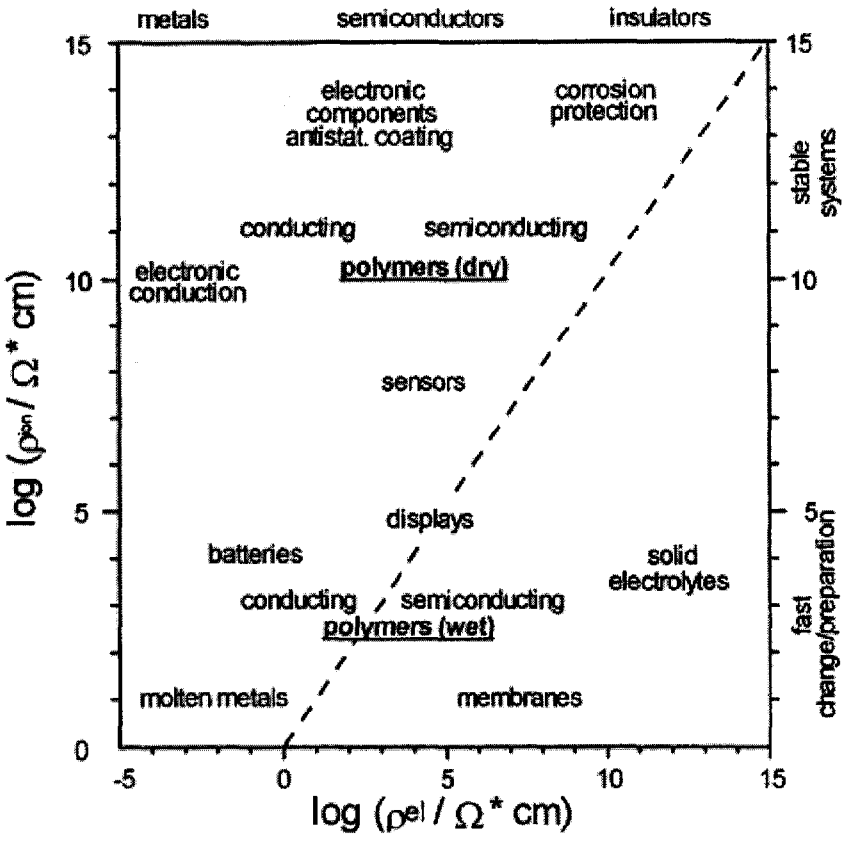

Figure 1.2 Double logarithmic plot of conducting polymer applications with respect to ionic and electronic resistances [12].

The top of the figure represents a region of high ionic resistances. In this region, dry state inert atmosphere applications of conducting polymers exist, such as membranes for corrosion protection using polymers such as PPy and polynailine [13,14,15] and various sensors such as gas [16], urea [17], hemoglobin [17], and humidity [18]. The bottom of the figure represents applications where the conducting polymer is in contact with electrolytes. Such applications include energy technologies like batteries. A Li-PPy combination battery was demonstrated [19]. The high ionic conductivity and discharge rates allow some conducting polymers to be used as electrode materials for supercapacitors [20,21]. Organic electroluminescent devices (LED) offer an alternative to

Reproduced with permission of the copyright owner. Further reproduction prohibited without permission.

liquid crystal displays and cathode tubes. The organic LEDs incorporate a sandwich structure consisting of Indium Tin Oxide (ITO) / light-emitting polymer / ITO; for example, ITO / PEDOT-PSS / ITO [22]. On application of an electric field, electrons and holes are injected into the polymer material where they recombine to emit photons. Polyaniline was introduced as one of the intermediate layers after ITO to enhance the efficiency of the LED [23]. Conducting polymer films can be considered as membranes due to their porous nature. They have been used for separation of gases and liquids. Studies have been done to control the pore sizes and selectivity based on their chemical structures and redox states [24,25].

The research into the various aspects of conducting polymer continues with new materials being synthesized, as well as novel applications being suggested. The polymer scientists and technologists need to collaborate closely to bring durable, stable, and multifunctional conducting polymer devices to human society.

1.2 Dissertation Overview

Chapter Two highlights the theory of conducting polymers. The polymer conduction mechanisms are explained. The specific chemical structures of the three commonly used conducting polymers including polypyrrole (PPy), poly(3,4-ethylenedioxythiophen)-poly(4-styrenesulphonate) (PEDOT-PSS), and sulphonated polyaniline (SPANI) are explained as well. The various applications of the conducting polymers are discussed.

Chapter Three explains the current conducting polymer patterning techniques, including soft lithography, inkjet printing, and hot embossing methods. Also, UV photolithography and the deep reactive ion etching techniques are also explained briefly.

Reproduced with permission of the copyright owner. Further reproduction prohibited without permission.

Chapter Four introduces the Intermediate-Layer Lithography (ILL) method. The key points of this method are discussed. The experimental procedures and imprinting results are explained.

Chapter Five explains the applications of the conducting polymer microwires fabricated using the ILL method. The microwires of PPy, PEDOT-PSS, and SPANI have been used for sensing humidity, glucose, and volatile organic gases including acetone, toluene, and methanol. PPy and PEDOT-PSS microwires with different surface-to-volume ratios have been fabricated and tested for sensitivity to acetone vapor at low concentrations.

Chapter Six presents details of ILL using a silicon mold with nano-channels. The widths of the channels etched in the silicon mold are 100 nm and 500 nm. The procedural details with experimental results are provided. Chapter Seven concludes this work with a summary of achievements and future direction.

Reproduced with permission of the copyright owner. Further reproduction prohibited without permission.

CHAPTER 2

THEORY OF CONDUCTING POLYMERS

2.1 History of Conducting Polymers

Since their discovery in 1977, conducting polymers have been at the center of intense scientific research. This research led to awarding the Nobel Prize in Chemistry to Heeger, MacDiarmid, and Shirakawa in the year 2000. Polyacetylene was first synthesized in 1958 by Natta, et al. The conductivity was found to be similar to semiconductors, in the range of $7X10^{-11}$ to $7X10^{-3}$ Scm^{-1}. In 1977, one of the post doctoral students of Hideki Shirakawa was trying to synthesize polyacetylene. After accidently adding the Ziegler-Natta catalyst 1000 times more than the required amount, a thin silvery film was obtained. The conductivity of the resulting film was found to be in the higher levels of the previously synthesized semiconducting film [26]. This was the first reported intrinsically conducting polyacetylene (Figure 2.1). It was later found that the conductivity of Polyacetylene could be increased 11 times by exposing it to iodine vapor. Exposing polyacetylene to iodine vapor caused charge transfer to occur from polyacetylene (donor) to iodine (acceptor), resulting in the formation of charge carriers. This process is called "doping." Beyond 2% doping, the generated charge carriers are able to move freely along the polymer chain, resulting in much increased conductivity.

Reproduced with permission of the copyright owner. Further reproduction prohibited without permission.

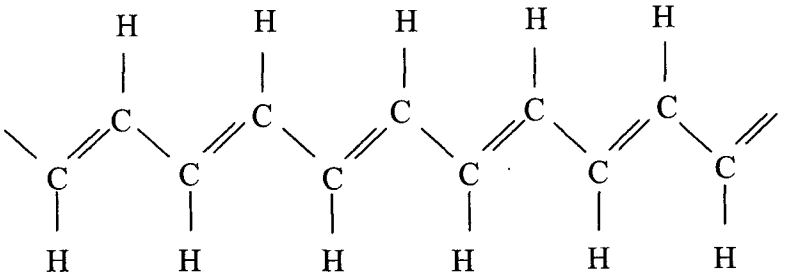

Figure 2.1 Chemical structure of polyacetylene.

Polyacetylene is a homocyclic conducting polymer with carbon and hydrogen in the polymer backbone. Later, heterocyclic polymers were synthesized. These have hetero atoms bonded to the chain in five-membered rings (Figure 2.2).

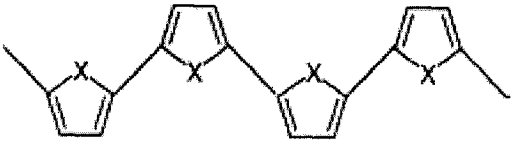

Figure 2.2 Chemical structure of a heterocyclic polymer. The "X" are the hetero-atoms which are included in the chain in five-membered rings [2].

Such heterocyclic conducting polymers include polyfuran, polythiophene, and polypyrrole. Polyfurans have oxygen, polythiophenes have sulfur, and polypyrroles have N-H in the five membered rings in the polymer chain. The most commonly used conducting polymers are polypyrrole, polythiophene, and polyaniline. Their chemical structures are as illustrated in Figure 2.3 [27]. They are shown without any charge.

Reproduced with permission of the copyright owner. Further reproduction prohibited without permission.

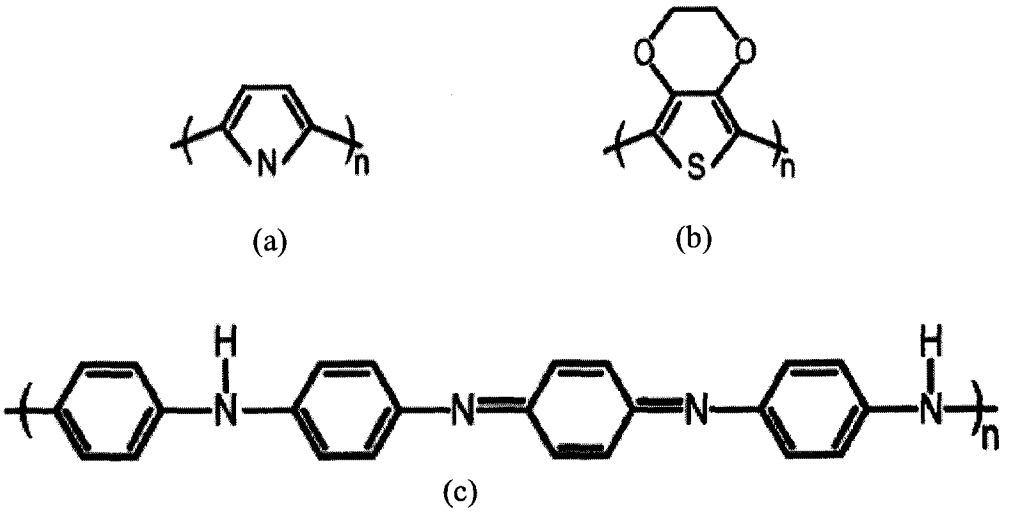

Figure 2.3 Chemical structures of the three commonly used conducting polymers: (a) polypyrrole, (b) polythiophene, and (c) polyaniline [27].

2.2 Conduction Mechanisms

The signature of an undoped conducting polymer is the alternating single and double bond architecture which constitutes the polymer backbone (Figure 2.1). The carbon atoms in the polymer backbone are SP^2 hybridised. The valency of carbon is four, and SP^2 hybridization occurs from three electrons in the outer shell of the carbon atoms (one s- and two p-orbitals). These form three "σ" bonds with neighboring carbon and hydrogen atoms. This configuration leaves one electron in the p-orbital. This π-electron cloud overlaps with the neighboring carbon atoms forming a π-band. In the case of the conducting polymers, there is alternating carbon single and double bond structure. This structure helps in reducing the energy of the system by increasing the π-electron density. The π-band exists throughout the backbone of the conducting polymers, forming a continuous delocalized π-system. A band gap results in the magnitude of 1.5 eV between

Reproduced with permission of the copyright owner. Further reproduction prohibited without permission.

the filled bonding and unfilled antibonding states. This result makes it a high energy gap semiconductor with very little conductivity.

The conductivity of conducting polymers can be increased by "doping." Doping is the addition or removal of electrons. Oxidative doping occurs when electrons are transferred from the conducting polymer backbone to the dopant. It is also called p-doping. In reductive doping, also called as n-doping, electrons are transferred to the conducting polymer backbone from the dopant. The conducting polymer stores charge by oxidative and reductive doping. In both cases, two scenarios may be possible. The polymer may either lose an electron from its bands or localize charge over a section of the polymer chain [26]. This localization of charge decreases the ionization energy and increases the electron affinity, so the polymer is better able to accommodate the newly formed charge. This accommodation is preferred over delocalization of the charge. Some oxidizing dopants include iodine, arsenic pentachloride, iron (III) chloride, and $NOPF_6$. Sodium Naphthalide is a reductive dopant.

Two different kinds of doping are redox and non-redox doping. The different kinds of redox dopings are as follows: chemical and electrochemical n- and p-type doping, photo-doping, and charge injection doping [28]. In redox doping, the number of electrons associated with the polymer backbone changes.

P-type doping was first done to *trans*-polyacetylene using iodine exposure. This doping caused partial oxidation of the polymer backbone. This oxidation increased the conductivity of polyacetylene from 10^{-5} to 10^{3} Scm^{-1}. P-doping may also be achieved by electrochemical anodic oxidation of *trans*-polyacetylene immersed in a solution of

Reproduced with permission of the copyright owner. Further reproduction prohibited without permission.

$LiClO_4$. The positive DC voltage is applied to the Polyacetylene film, and the negative terminal is immersed in the solution.

N-type doping was achieved by treating *trans*-polyacetylene with sodium amalgam or sodium naphthaline. This doping caused partial reduction of the π-backbone system. The conductivity was increased to 10^3 after the process. Reductive doping is also achieved electrochemically by immersing a *trans*-polyacetylene film in a solution of LiClO dissolved in tetrahydrofuran and attaching it to the negative terminal of the DC power supply.

Photo-doping occurs by exposing *trans*-polyacetylene to radiation of energy higher than the band gap energy. This exposure causes the formation of charges in the polymer backbone. The charges vanish, however, as soon as the exposure is stopped. In case a potential is applied during irradiation, there is some photoconductivity.

Charge injection doping is another mechanism of inducing doping in conducting polymers without using any dopant ions. This mechanism is achieved by forming a metal-insulator-semiconductor architecture. When the structure is biased, a surface charge layer forms. Polyacetylene and poly(3-hexathiophene) have been doped in this way.

In non-redox doping, the number of electrons associated with the polymer backbone does not change. The polymer energy levels are rearranged during the doping process. Polyanilne emraldine base was the first conducting polymer doped in this manner by treating it with aqueous protonic acid. The conductivity was increased by nine to ten orders of magnitude.

Reproduced with permission of the copyright owner. Further reproduction prohibited without permission.

2.2.1 Role of Solitons, Polarons and Bipolarons in Conduction

Solitons are elementary excitations in the polyacetylene chain. These discontinuities occur when a carbon atom shares a single bond with the neighboring carbon atoms [29,30]. The formation of discontinuities causes the formation of additional electronic states in the band gap. The formation of solitons does not lead to conduction in the polymer. The solitons hop from one site to the other along the length of a single polymer chain. When a vast number of solitons occur, there is soliton hopping across the polymer chains. This hopping method varies at a higher power of temperature [31]. For lightly and moderately doped samples, variable-range hopping mechanism contributes to conduction [32]. Polarons are formed by lattice deformations which cause electrons to be localized in a region of electrical potential minimum [33]. Polarons also cause the appearance of additional electronic states in the band gap. Polarons have both charge and spin, and their motion contributes to charge transport across the polymer chains. When polarons of opposite spins combine, they form bipolarons with no spins. Bipolarons may also contribute to charge transport and conduction. In case of PPy, the conductivity is increased by oxidative doping [26]. The process is illustrated in Figure 2.4.

Reproduced with permission of the copyright owner. Further reproduction prohibited without permission.

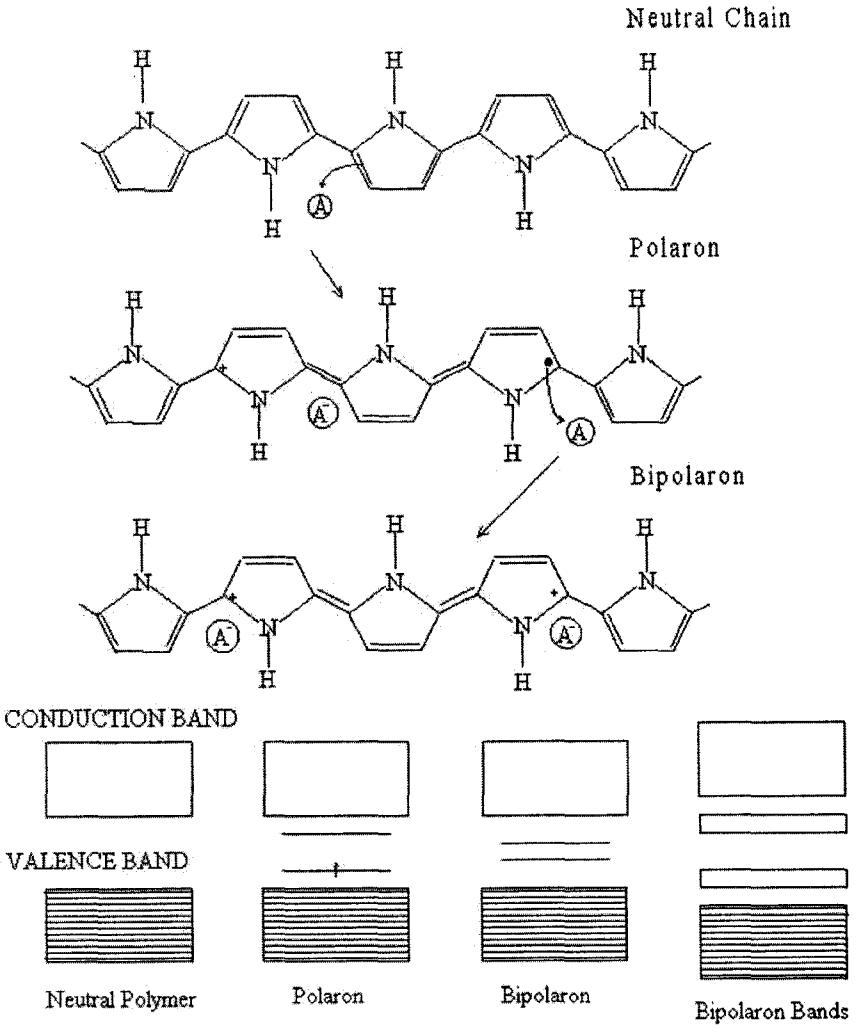

Figure 2. 4 Formation of Polarons and Bipolarons during oxidative doping in PPy [26].

In the doping process, an electron is removed, creating a positive charge and free radical. The positive charge and the free radical are coupled to each other with local resonance using the quinoid rings in the case of PPy. This process costs the polymer a considerable amount of energy, and the region of disturbance has higher energy than the rest of the polymer chain. The number of quinoid rings used to hold the charge and radical is limited. In the case of PPy, only four quinoid rings are used. The combination of the charged site and the radical is called a Polaron. Polarons create a new localized

Reproduced with permission of the copyright owner. Further reproduction prohibited without permission.

electronic state within the energy gap, with the lower energy states being occupied by a single unpaired electron. In the case of PPy, the polaron state is located about 0.5 eV from the band edges. Upon further oxidation, the free radical of the polaron is removed. This removal creates a spinless defect known as Bipolaron. At higher doping levels, polarons are converted to bipolarons. This conversion happens because formation of separate polarons uses more energy; hence, polarons combine to form bipolarons. As the level of doping is increased, there is formation of continuous bipolaron bands. At very high levels of doping the upper and lower bipolaron bands may overlap with the valence and conduction bands. This overlapping would result in metal like conductivity.

For conducting polymers which have a degenerate ground state, the conduction mechanism involves formation of solitons (Figure 2.5). In this case, the charge and the free radical are not bound with each other but are freely separated along the chain. This seperation results in the formation of independent domain. These domains may enclose two phases with opposite orientation and similar energy. Hence, the solitons can be neutral sometimes. Soliton formation creates new energy levels in the middle of the energy gap. At higher doping levels, solitons interact with each other to form bands which may overlap with the valence and conduction bands to increase conductivity [26].

Reproduced with permission of the copyright owner. Further reproduction prohibited without permission.

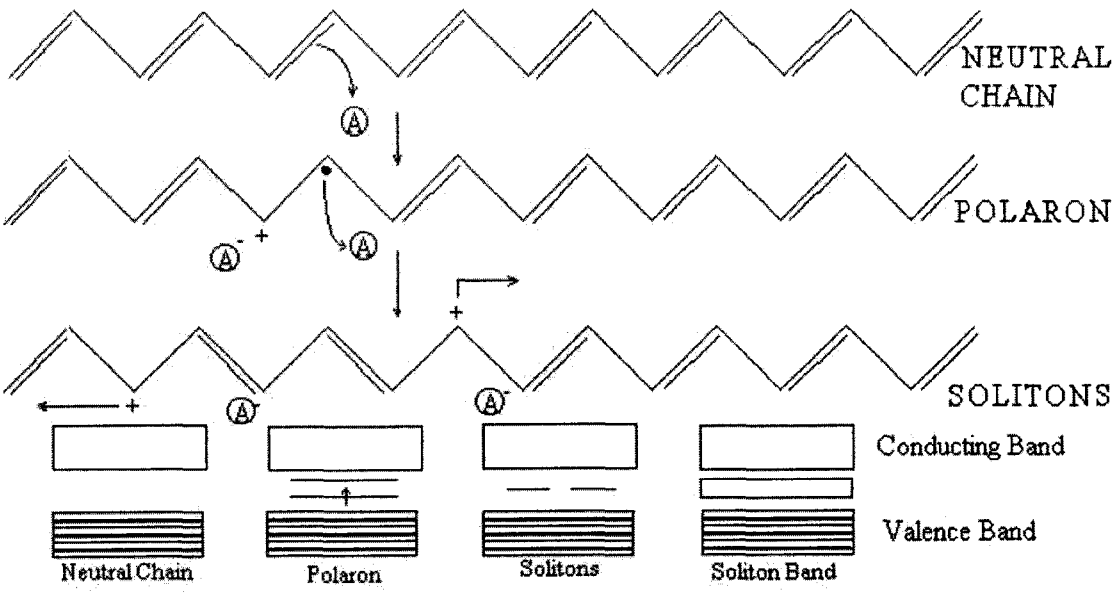

Figure 2. 5 Formation of solitons during doping of the conducting polymers [26].

2.2.2 Charge Hopping Mechanism

The precise mechanism of charge transfer in conducting polymers is still unknown. Solitions and bipolarons constitute the majority of charge carriers. This is because the conducting polymer structure is highly disordered [34]. It consists of crystalline and amorphous regions distributed randomly (Figure 2.6). Random distribution makes the task of tracing the path of the charge movement between the various domains very difficult.

Reproduced with permission of the copyright owner. Further reproduction prohibited without permission.

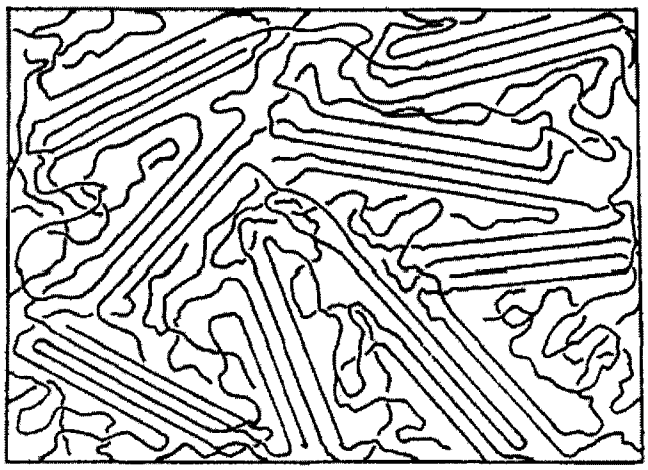

Figure 2. 6 Structure of conducting polymers showing the random distribution of the crystalline and amorphous regions [34].

The movement of charge along a specific chain has to be considered, as well as movement between the polymer chains and between the various different crystalline and amorphous domains. "Inter-soliton hopping" mechanism is one proposed technique (Figure 2.7) [1].

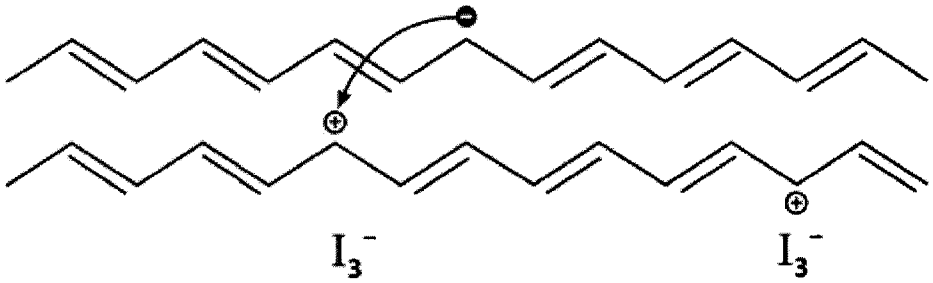

Figure 2. 7 Mechanism of "intersoliton hopping" [1].

In this mechanism, an electron jumps to other localized states in the adjacent polymer chains. The solitons move around by exchanging electrons with a nearby charged soliton.

Reproduced with permission of the copyright owner. Further reproduction prohibited without permission.

In hopping mechanism, the charge carriers tunnel from one localized state to another within the energy band gap [35,36,37,38]. The energy for hopping to take place is provided by the phonons at non-zero temperatures. Electrons hop from one energy state to the next by absorbing phonons. At zero temperature, the conductivity is zero in those conducting polymers where the hopping mechanism is dominant. As the temperature increases, more and more electrons absorb phonons and start hopping [39]. Hence, there is a relationship between temperature and conductivity. Figure 2.8 illustrates the idea of the charge hopping mechanism.

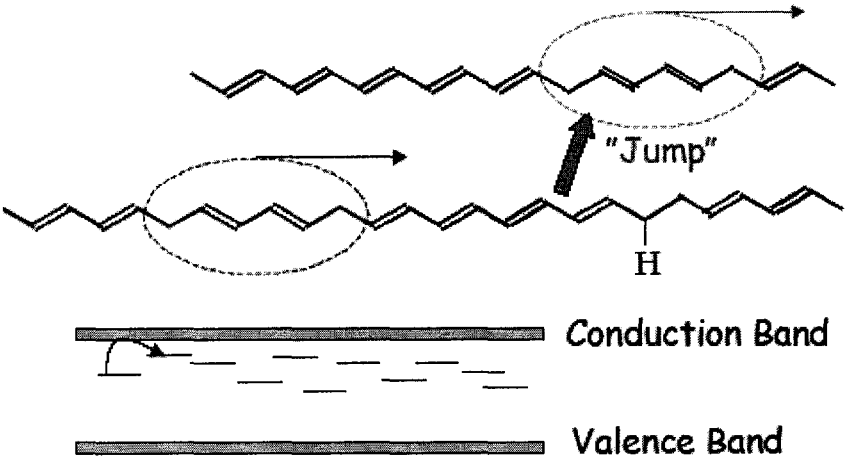

Figure 2. 8 Mechanism of charge hopping which contributes to conductivity in conducting polymers [39].

Reproduced with permission of the copyright owner. Further reproduction prohibited without permission.

2.3 Three Commonly Used Conducting Polymers

2.3.1 PPy

PPy is a class of heterocyclic conducting polymers. The monomer is called pyrrole. The chemical structure of PPy is illustrated in Figure 2.9 [40].

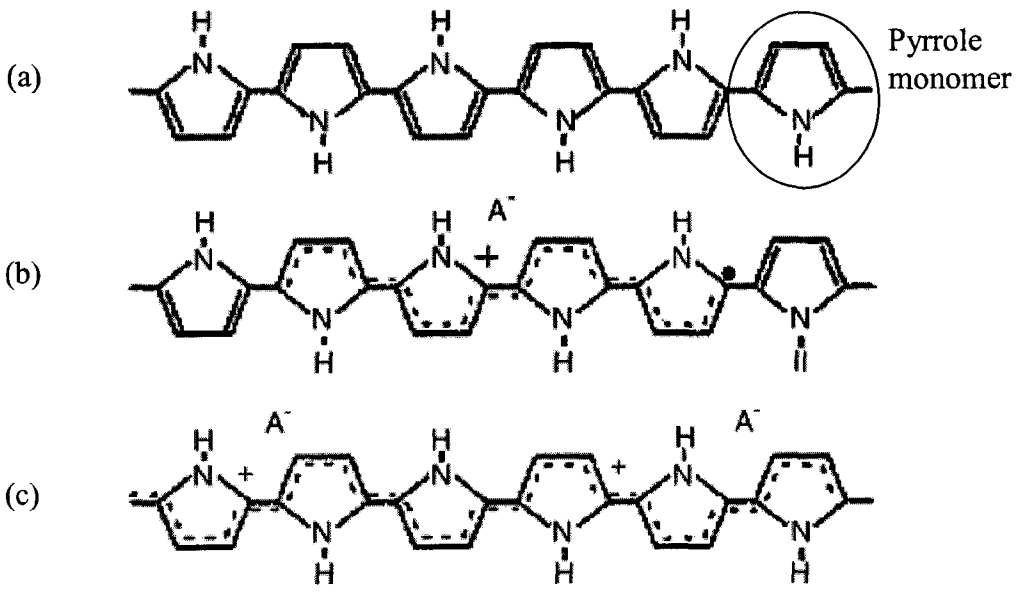

Figure 2. 9 Chemical structure of PPy: (a) neutral, (b) partially oxidized on low doping, (c) highly oxidized on heavy doping [40].

The synthesis mechanisms of PPy are electrochemical and chemical oxidative polymerization. The physical and chemical properties of PPy are dependant on the doping and polymerization conditions [41]. PPy has very wide-ranging applications, including gas sensors [42, 43], biosensors[44], and microactuators [45].

Reproduced with permission of the copyright owner. Further reproduction prohibited without permission.

2.3.2 PEDOT-PSS

The conducting polymer PEDOT-PSS was discovered by the scientists at Bayer AG in Germany. Initially, the polymer synthesized had high conductivity and was water insoluble. The conductivity of pristine PEDOT-PSS solution could be increased 100 fold by mixing tetrahydrofuran (THF), dimethyl sulfoxide (DMSO), and dimethyl formamide (DMF) [46]. The chemical structure of PEDOT-PSS is as illustrated in Figure 2.10 [47].

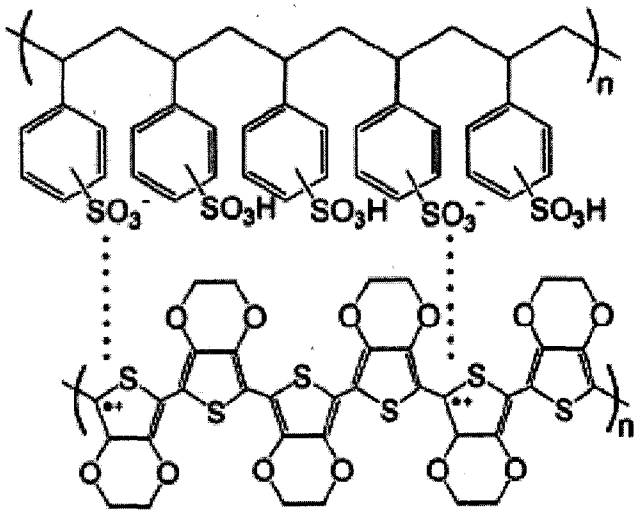

Figure 2. 10 Chemical structure of PEDOT-PSS [47].

PEDOT-PSS finds many commercial applications due to its advantages which include high stability in the p-doped state, high conductivity, good film forming capacity, and excellent transparency in the doped state [48, 49].

2.3.3 Polyaniline (PANI)

PANI is the most studied conducting polymer due to its high degree of processability, environmental stability, and interesting redox properties. It is able to remain stable in the various redox states and its conductivity can be tuned with secondary

Reproduced with permission of the copyright owner. Further reproduction prohibited without permission.

doping [50,51]. The various oxidation states of polyaniline (Figure 2.11) include leucoemraldine, emraldine, and pernigraniline.

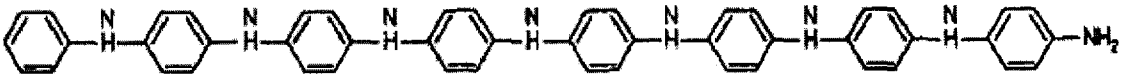

(a) Leucoemraldine

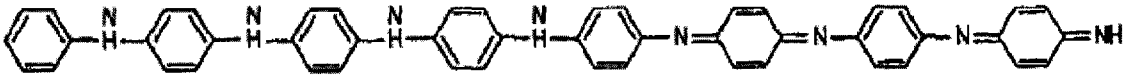

(b) Emraldine

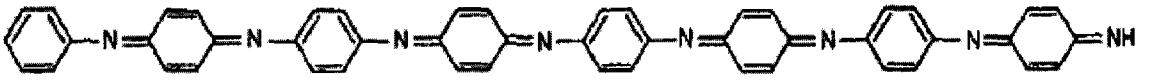

(c) Perigraniline

Figure 2. 11 Chemical structure of the various redox states of PANI [50].

Leucoemraldine or emraldine base is the fully reduced and non-conducting form of Polyaniline. Emraldine is the partially oxidized form, and pernigraniline is the fully oxidized form of Polyaniline. Pernigraniline is also known as emraldine salt and is the conducting form of the conducting polymer. Conducting Polyaniline blends may be produced using chemical and electrochemical polymerization techniques. Chemical polymerization techniques are cheap and relatively simple as compared to electrochemical polymerization. However, electrochemical polymerization has several advantages such as free standing composite polymer films. Their electrical properties may be varied by changing the electrolysis conditions [52,53].

Reproduced with permission of the copyright owner. Further reproduction prohibited without permission.

2.4 Applications of Conducting Polymers

The applications of conducting polymers range from electronic devices to chemical and biological sensors. The popularity of conducting polymers stem from various advantages associated with it. Conducting polymers have some advantages, including precise tailoring of properties, low cost, and easy processing [2]. These advantages led the research into artificial sensors employing conducting polymers. The goal is to build systems to mimic the mammalian olfactory systems. The conducting polymers produce changes in color, mass, work function, and conductivity when exposed to different chemicals [54]. The change in conductivity measurement of an exposed conducting polymer film is a popular sensing method [55]. Munoz et al. had demonstrated a vapor sensor array consisting of conducting particles dispersed inside a polymer matrix. The matrix would expand reversibly on exposure to organic vapors, causing the resistance of the sensor to increase. They found that exposing the sensor array to individual vapors produced a unique change in conductivity. Processing the conductivity data, clear patterns could be observed, identifying the individual components. This response of conducting polymers is reversible with original behavior recovered as soon as the exposure is stopped. The adsorption/desorption related conductivity changes normally occur at room temperature. These so-called "chemiresistors" are easier to implement experimentally [56,57].

Patel et al. also fabricated an organic solvent detector using carbon black particles dispersed in a polymer matrix. The organic solvents used included isooctane, ethanol, diisopropylymethylphosphonate (DIMP), and water. The conductivity change response was based on the "chemiresistor" principle and was analyzed using the Visual-Empirical

Reproduced with permission of the copyright owner. Further reproduction prohibited without permission.

Region of Influence (VERI) technique. This method was able to handle both linear as well as non-linear data [56]. Sotzing et al. demonstrated the fabrication of a vapor sensing array using the conducting polymer [57]. The sensor array was fabricated using the conventional photolithography methods of deposition and etching to define the contact lines. Afterwards, the conducting polymer solution was spin coated on top of the electrodes to yield a film thickness ranging from 90 nm to 900 nm. The sensor targets included hexane, benzene, toluene, methoxybenzene, chloroform, chlorobenzene, EtOAc, tetrahydrofuran, TFMBenzene, benzaldehyde, acetone, ethanol, methanol, nitrobenzene, and acetonitrile. The targets were differentiated based upon their relative differential resistance response upon exposure to the different vapors. This sensor performed well in resolving the polar vapors as compared to non-polar vapors. Three of the most commonly used conducting polymers are PPy [58], PANI [59], and PEDOT-PSS [60]. These polymers have been used to sense for various chemical analytes, including volatile organic gases, alcohols, industrial gases, glucose, ammonia, ions, antigens, and pH values.

A gas sensing application of PPy was demonstrated by de Melo et al [61]. Doped PPy chains were polymerized inside various dielectric polymer matrices. The dielectric polymers used consisted of poly(caprolactone) (PCP), poly(ethylene oxide) PEO, poly(methyl-methacrylate) (PMMA), poly(vinyl alcohol) (PVA), and poly(vinyl acetate) PVAC. The target gases included methanol, ethanol, carbon tetrachloride, and benzene. The sensitivities of the sensor were analyzed using the conductivity changes upon exposure. Experiments showed that the PPy-PVA and PPy-PMMA demonstrated selective response towards polar (methanol and ethanol) and non-polar vapors (benzene

Reproduced with permission of the copyright owner. Further reproduction prohibited without permission.

and carbon tetrachloride). An alcohol sensor was fabricated using PANI by Athawale et al. [62]. PANI as well as some of its substituted derivatives were tested for their sensitivities to methanol, ethanol, propanol, heptanol, and butanol. Resistance decreased when the sensors were exposed to methanol, ethanol, and propanol, and resistance increased upon exposure to butanol and heptanol. All the resistance changes were reversible; however, the response time was poor. Resistances were found to decrease for short chained alcohols and increase for the long chain alcohols. Ameer et al. [63] reported the use of PPy electronic nose for sensing toxic and non-toxic industrial gases. The concept of an electronic nose was defined by Gardner and Bartlett as an instrument with an array of sensors with partial specificity and a pattern recognition system capable of identifying simple and complex odors. Figure 2.12 illustrates the functioning of an e-nose.

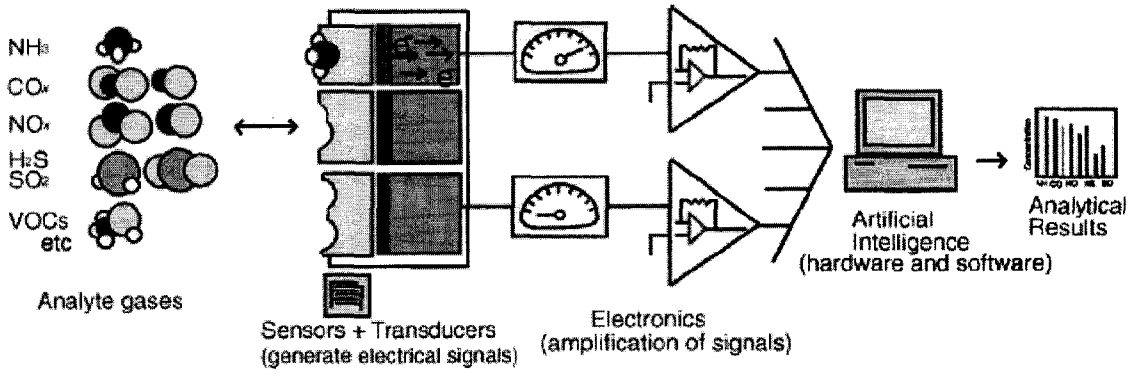

Figure 2. 12 Working principle of an electronic nose [63].

The individual sensors in the e-nose are specific towards a particular target. The responses they generate are amplified and transferred to a pattern recognition system which works on artificial intelligence. The range of targets included ammonia, nitrogen

Reproduced with permission of the copyright owner. Further reproduction prohibited without permission.

oxides, carbon monoxide, sulphur dioxide, hydrogen sulfide, methane, oxygen, hydrogen, phenol, benzene, and water vapor present in water, beverages, waste water and sewage effluent [63]. Yamauchi et al. [64] studied the glucose sensing capacity of a PPy-glucose oxidase (GOD) composite in relation to enzyme activity. Conducting polyaniline was shown to sense aqueous ammonia (NH_3) solution by Dhawan et al. [65]. They observed that that exposing the conducting polyaniline surface to aqueous NH_3 solution caused leaching of the polaronic sites resulting in increasing the surface resistance from 10^2 to 10^{10} ohm. Linfords et al. fabricated a new type of Ca^{2+} selective electrode using conducting polyaniline [66]. Polynailine was doped with an organophosphoric acid, bis[4-(1,1,3,3-tetramethylbutyl)phenyl]phosphoric acid (DTMBP-PO_4H), making it both soluble and conductive. The polyaniline membrane had three functions, including serving as the membrane matrix, improving the electron transfer at the substrate-membrane interface, and acting as sites for the Ca^{2+} selective sites DTMBP-PO_4H groups.

Torres-Rodriguez et al. demonstrated the fabrication of a PPy-biotin-based biosensor [67]. The device was fabricated by copolymerization of pyrrole monomer and pyrrole covalently linked to biotin through a spacer arm. This fabrication led to the formation of an electrically conductive polymer film with biotin grafted to the polymer network. Biomolecules with advin units could easily attach on the biotin sites on the polypyrrole surface. Karyakin et al. had fabricated a potentiometric pH sensor based on processable polyaniline [68]. Glassy carbon and screen printed carbon electrodes were modified with polaniline by dip coating. The pH sensor response was fully reversible with a potentiometric response of 90 mV/pH unit with an overall range of pH 3 to 9. A biosensing application was also demonstrated by fabricating a urea sensitive

Reproduced with permission of the copyright owner. Further reproduction prohibited without permission.

potentiometric sensor. The detection limit was 10^{-5} M urea with a maximum response of 120 mV. It displayed high sensitivity, good operational stability in routine analytical applications, and prolonged shelf life.

Reproduced with permission of the copyright owner. Further reproduction prohibited without permission.

CHAPTER 3

CONDUCTING POLYMER PATTERNING TECHNIQUES

3.1 Soft Lithography Technique

Soft lithography is a patterning technique which uses a flexible master mold for pattern transfer (Figure 3.1). The elastomer, polydimethlydioxysilane (PDMS), is used as mold for pattern transfer [69].

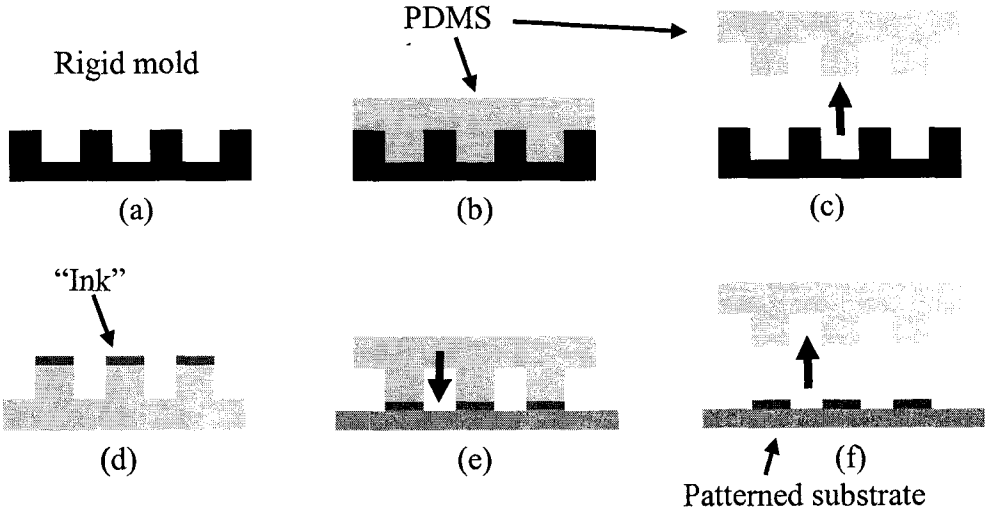

Figure 3. 1 Schematic of the soft lithography pattern transfer process: (a) the rigid mold, (b) the liquid PDMS poured into the rigid mold, (c) the cured PDMS layer peeled-off from the rigid mold, (d) "ink" applied to the PDMS stamp, (e) the inked PDMS stamp is applied to the substrate, and (f) the "ink" is transferred from the PDMS stamp on to the substrate.

Reproduced with permission of the copyright owner. Further reproduction prohibited without permission.

The PDMS mold is fabricated in the following ways: (i) a rigid mold with the desired features is fabricated first. The rigid mold may be made of silicon or SU-8. The silicon or SU-8 mold may be fabricated using the conventional photolithography method; (ii) the PDMS elastomer is mixed with the curing agent and poured into the rigid mold; (iii) the rigid mold and the liquid PDMS layer is heated to 80° C to speed up the curing process; (iv) after the PDMS layer is cured, it is peeled-off from the rigid mold; (v) the desired ink is applied to the PDMS mold; (vi) the PDMS stamp with the applied ink is put on the surface which is to be patterned (Figure 3.1). The ink is transferred from the PDMS layer onto the surface of the substrate. The soft lithography method is cheap and easy to perform. However, it suffers from the following shortcomings: (i) pairing, (ii) sagging, and (iii) deformations [69] (Figure 3.2).

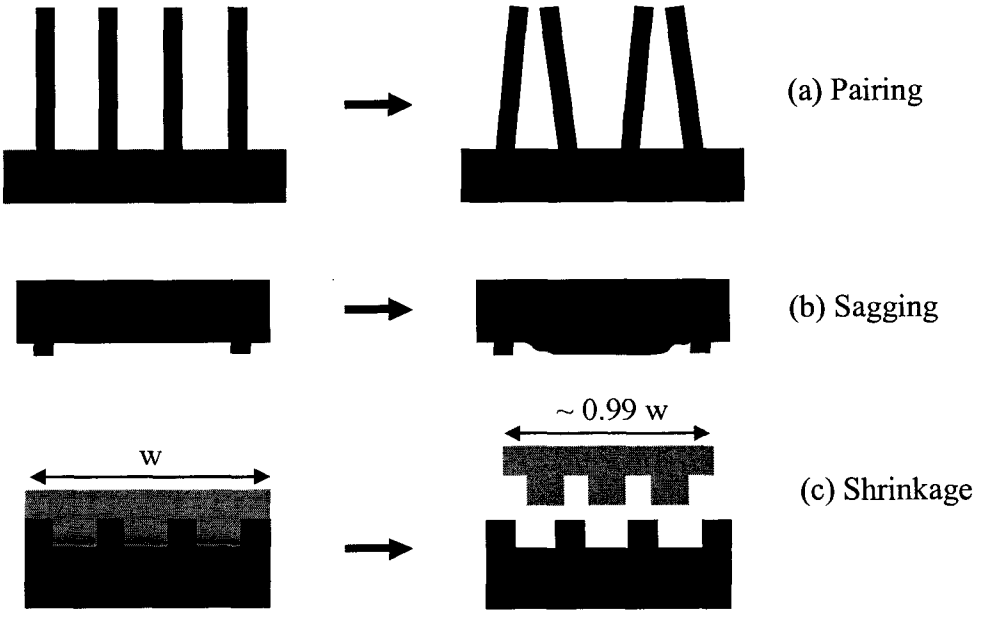

Figure 3. 2 Deformations of the PDMS in the soft lithography approach: (a) pairing deformation, (b) sagging deformation, and (c) shrinkage [69].

Reproduced with permission of the copyright owner. Further reproduction prohibited without permission.

3.2 Inkjet Printing Technique

The inkjet printing technique was developed to fabricate conducting polymer patterns. Inkjet printing technique delivers minute quantities of conducting polymer "ink" as drops at the desired location on the substrate. Instead of using the "toner" ink, modified conducting polymer solutions are used as the ink. This method was developed as an alternative method for patterning conducting polymers for applications in organic transistors, polymer arrays, and organic light emitting diodes [70, 71]. The important aspects for consideration in this technique are designing the ink dispenser head, formulating the ink solution, controlling the drop dynamics, and choosing the appropriate substrate [72]. Two different approaches exist for the inkjet printing method, (i) continuous inkjet printing and (ii) drop-on-demand inkjet printing [73]. In the continuous printing method (Figure 3.3), the ink is enclosed in a chamber and is squeezed out with sinusoidal actuation of a piezoelectric membrane. As the drops come out of the ink container, they are given a specific charge. The charge is determined by the applied signal which is modulated by the input data. As the charge droplets move further, they are deflected by the applied field between two plates. The amount of deflection a droplet suffers is determined by the nature and amount of the charge. A droplet with negligible charge will not suffer any deflection, and droplets fall on the substrate in a straight line. In the drop-on-demand printing method (Figure 3.4), the ink in the reservoir is pushed out when the piezo-actuator is actuated by input signal. The input signal is modulated by the data pulse train. The size of the drop is equal to the size of the orifice. This technique is simple and more popular.

Reproduced with permission of the copyright owner. Further reproduction prohibited without permission.

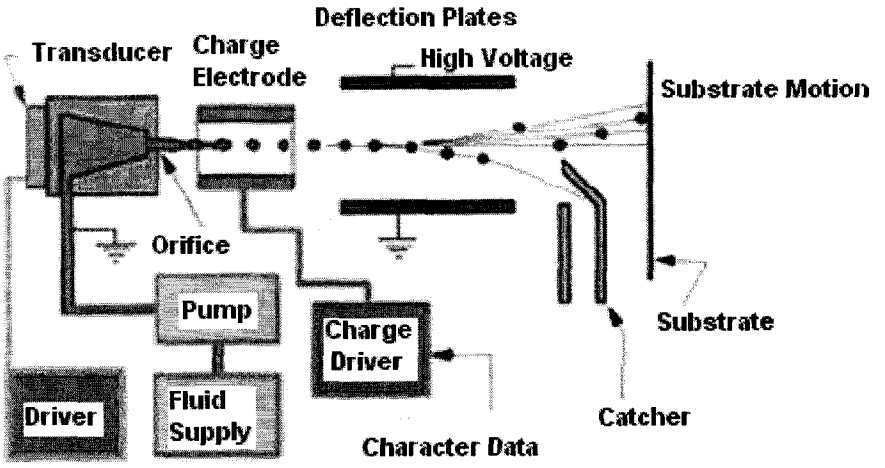

Figure 3. 3 Continuous inkjet printing technique [73].

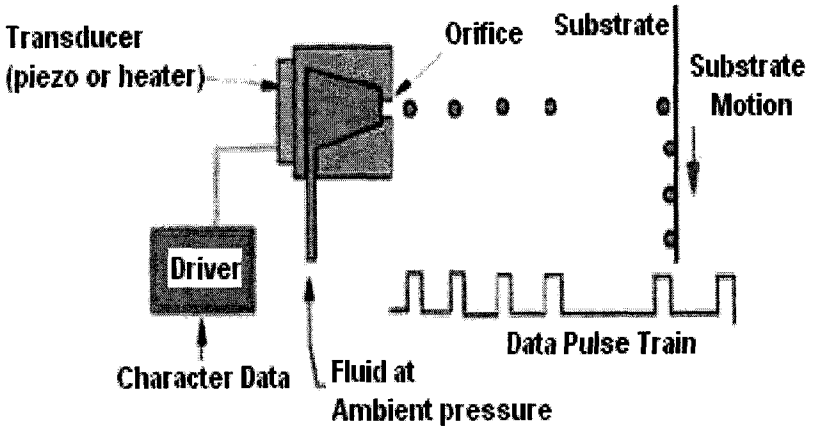

Figure 3. 4 Drop-on-demand inkjet printing technique [73].

The commercial inkjet printers may not be suitable for printing conducting polymer inks. This shortcoming may be due to the following reasons: (i) low resolution, (ii) printing only on flexible substrates such as paper and transparency sheets, (iii) alignment accuracy problems, and (iv) absence of substrate heating. An inkjet printer is commercially available from Microdrop. This Autodrop system (Figure 3.5) is capable of printing conducting polymer inks.

Reproduced with permission of the copyright owner. Further reproduction prohibited without permission.

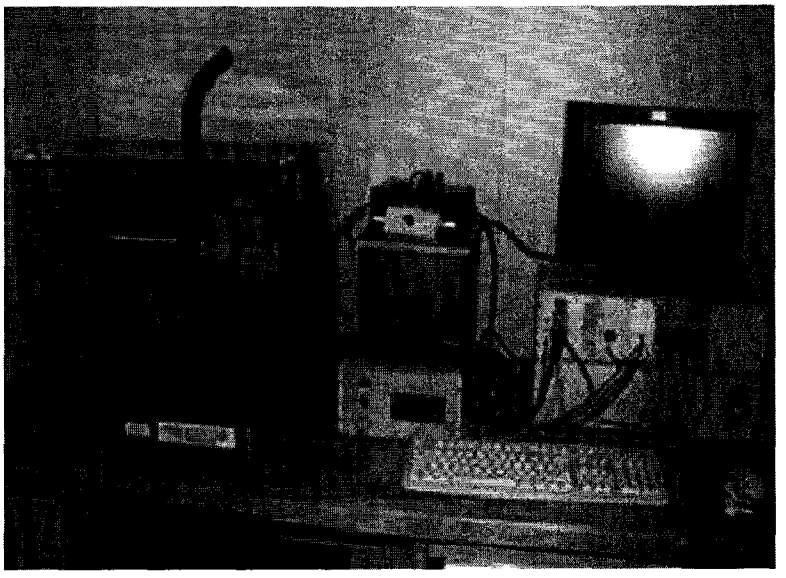

Figure 3. 5 Autodrop printing system from Microdrop.

The specifications of the autodrop system are as follows: (i) the ink reservoir volume is 4 ml, (ii) the print head is connected to the reservoir as an individual unit, (iii) four dispenser heads can be mounted for printing applications, (iv) the print head is activated by a voltage pulse, (v) the input voltage pulse width, amplitude, and frequency can be controlled with software, (vi) the position of the print head can be controlled in the XYZ directions, and (vii) the bottom stage is a hot plate with proportional, derivative, and integral control.

3.3 Hot Embossing Technique

Hot embossing is a thermoplastic molding method [74]. This process involves heating a polymer film in vacuum until the temperature is above its glass transition temperature (Tg). At this raised temperature, a rigid mold is slowly inserted uniaxially into the softened polymer, causing plastic flow of the polymer around the tool, which is inversely shaped to the desired part shape. As the mold is inserted inside the polymer,

Reproduced with permission of the copyright owner. Further reproduction prohibited without permission.

the polymer starts to flow into the mold. The amount of time needed for the polymer to fill the mold depends on the dimension and complexity of the mold design and also on the imprinting pressure and time. After the polymer has filled the mold, the temperature of the insert (substrate and mold) is reduced until the temperature is below the Tg of the polymer. After the polymer is partially solidified, the mold is pulled out of the substrate. This process is called demolding. Hot embossing is capable of producing high precision and high quality polymer microstructures. In this process the low material flow which minimizes the stress induced in the polymer. Minimal stress is advantageous for optical applications [74]. This flexible and low cost microfabrication technology is suited for high volume production [75]. Hot embossed polymer microstructures find special applications in microfluidic devices for optical [76] and biomedical applications due to several advantages, including the ease of fabricating high aspect-ratio structures in different geometries such as rectangular, rounded, etc. Low cost polymer materials with low conductivity may be used, which are suitable for electrokinetic pumping or electrophoretic separation. The general machine schematic is illustrated in Figure 3.6.

Reproduced with permission of the copyright owner. Further reproduction prohibited without permission.

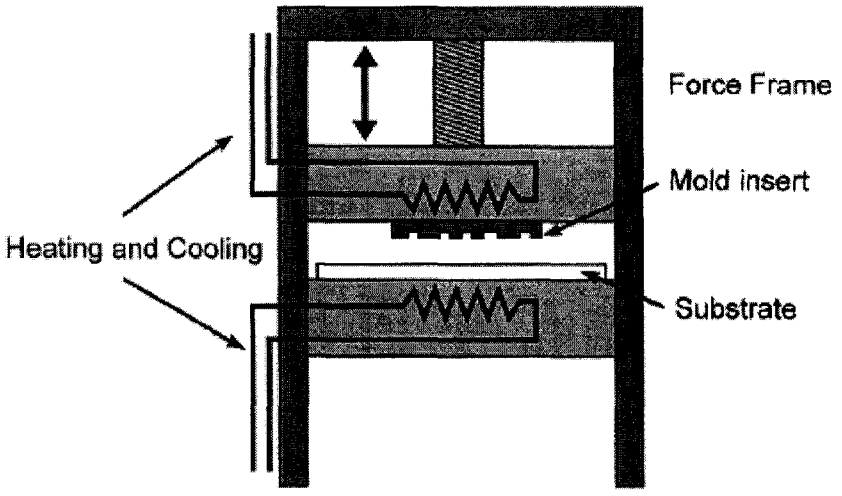

Figure 3. 6 General scheme of a hot embossing machine [75].

As in Figure 3.6, the rigid mold insert is fixed to the top plate of the machine, and the polymer substrate is fixed to the bottom plate. In case a silicon mold is used, it is fabricated using the conventional photolithography and deep reactive ion etching method. A metal mold may also be used and can be fabricated using electroplating. LIGA process may also be used to fabricate a rigid metal mold for hot embossing [77]. The embossing machine consists of a force frame which delivers the force using a spindle and a T-bar. The top and bottom plates have heating and cooling arrangements. High heat capacity oil is circulated during the cooling cycle. This arrangement allows isothermal heating and cooling. The force and temperature profiles are illustrated in Figure 3.7. During the embossing process, the top and bottom plates are heated separately in vacuum to temperatures above the Tg of the polymer. The polymers typically used are PMMA (Tg of 106° C) and Polycarbonate (Tg of 150° C). After the embossing temperature (T_{Emboss}) is reached, force is applied with the top plate moving down. The force is in the range of 20 kN-30 kN and is feedback controlled. The force and temperature is held constant for

Reproduced with permission of the copyright owner. Further reproduction prohibited without permission.

the duration of hold time. Afterwards, the temperature is reduced and after it falls below the demolding temperature (T_{Demold}), the force is released and the top plate is slowly moved upwards.

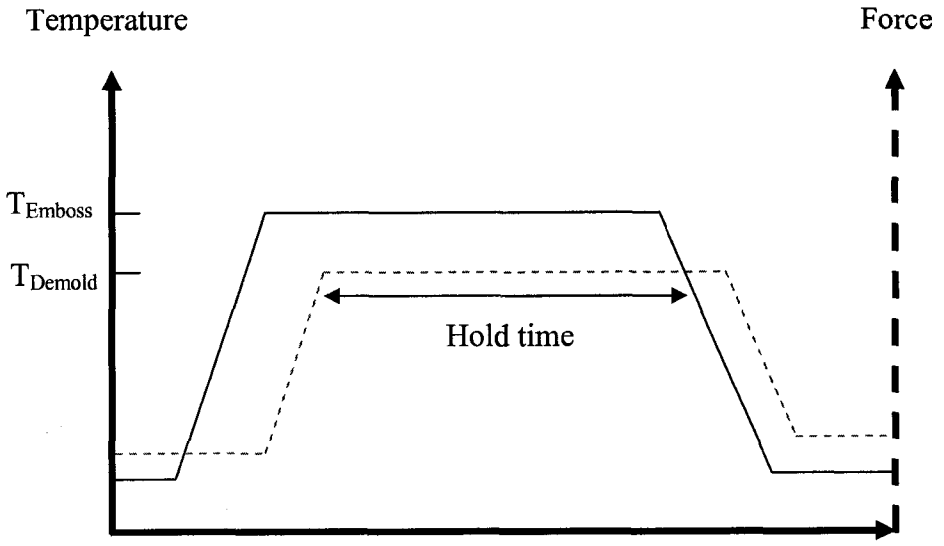

Figure 3. 7 Standard force and temperature profile during the hot embossing process.

Reproduced with permission of the copyright owner. Further reproduction prohibited without permission.

CHAPTER 4

INTERMEDIATE-LAYER LITHOGRAPHY METHOD

4.1 Process Steps in the ILL Method

This chapter introduces the Intermediate-Layer lithography (ILL) method [78,79,80]. This innovative method is used to fabricate conducting polymer patterns in the micro-scale. The fabrication steps (Figure 4.1) of the method are as follows: (i) a silicon substrate is coated with a layer of insulating thermoplastic polymer material. This polymer should be electrically non-conducting and serves as the intermediate layer; (ii) a layer of conducting polymer is spin coated on top of the intermediate layer; (iii) a silicon mold with the desired features is fabricated using conventional photolithography method. After the desired pattern is transferred from the mask to the photoresist layer on the silicon wafer, dry etching is used to further transfer the patterns onto the silicon wafer. The silicon mold is used for embossing the micropatterns; (iv) the substrate is heated to a temperature which is above the Tg of the intermediate layer polymer but below the Tg of the conducting polymer layer; (v) after the substrate is heated to the required temperature, the silicon mold is slowly inserted into the substrate; (vi) after mold insertion, the temperature of the substrate is reduced to below the Tg of the intermediate layer; (vii) after the temperature falls to below the Tg of the intermediate layer, the mold is separated

Reproduced with permission of the copyright owner. Further reproduction prohibited without permission.

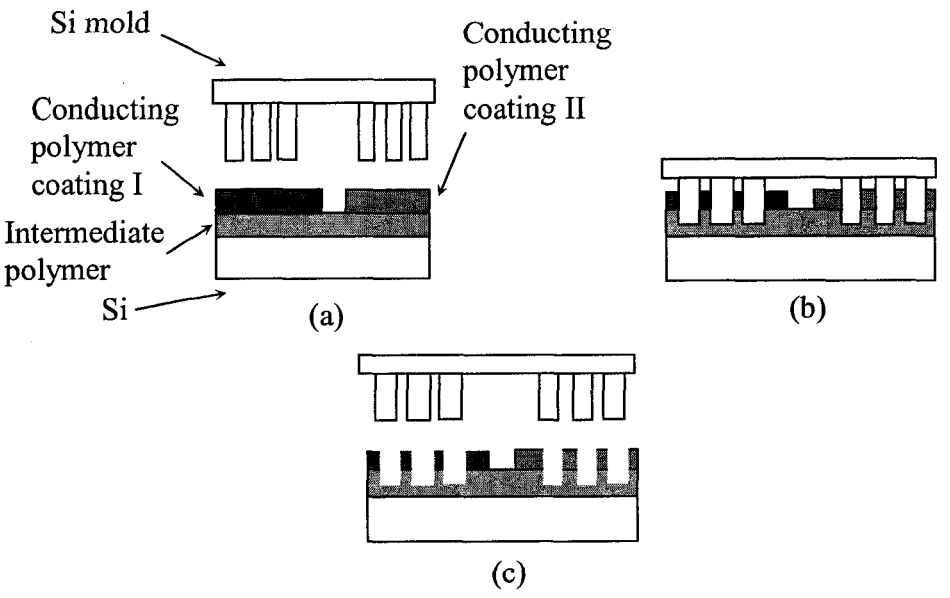

Figure 4.1 Process steps in the ILL method.

from the substrate; and (viii) the conducting polymer layer on the substrate is patterned.

In the first step of coating multiple conducting polymer layers on a common substrate, conducting polymer I is spin coated by covering the other areas of the substrate with tape and then spin coating conducting polymer II with the other areas covered by tape. This procedure is repeated for coating multiple conducting polymer layers.

4.2 Key Points of the ILL Method

The key to the ILL process is the introduction of the intermediate layer of insulating polymer; hence, this method is called the "intermediate-layer" lithography method. The ILL technique is very similar to the hot embossing process. However, in the hot embossing process, only one layer of polymer is used for embossing, giving rise to the two issues of "residual layer" and "depth of mold" (Figure 4.2). When hot embossing is used to embossing a single conducting polymer layer, the polymer layer is still connected at the base. Only the top surface of the polymer layer is deformed. This layer

Reproduced with permission of the copyright owner. Further reproduction prohibited without permission.

may be termed as the "residual layer". This residual layer connects the patterns electrically and renders the individual micropatterns ineffective. During the fabrication of the silicon mold, processing irregularities and surface roughness may lead to formation of height differences between the convex features. As illustrated in Figure 4.2a, when the height differences are more than the thickness of the polymer layer, the shorter convex features fail to get registered into the polymer layer. This failure may cause inappropriate printing. This problem is termed as the "depth of field" issue. In the ILL method, the shorter structures would still be imprinted (Figure 4.2b). The only requirement here is that the combined thickness of the intermediate layer and the conducting polymer layer should be more that the height difference existing in the silicon mold.

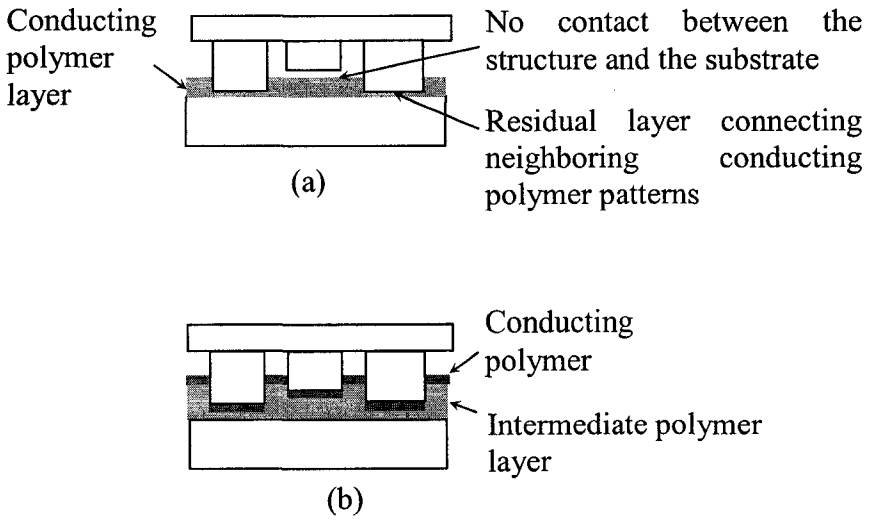

Figure 4.2 (a) "Residual layer" and "height variation" obstacles which both hot embossing and nanoimprint lithography approaches faces in patterning conducting polymers, and (b) these two obstacles are overcome using the intermediate polymer layer in the ILL approach.

Reproduced with permission of the copyright owner. Further reproduction prohibited without permission.

In the ILL method, the conducting polymer layer right below the convex mold structure is first cut-off from the neighboring layer during the mold insertion and pushed down to the bottom. This layer is cut-off due to the high shear forces generated at the two sides of the convex mold structure during mold penetration. The conducting polymer layer is also heated during the process, reducing the break stress for easy cutting-off. However, the temperature is below the Tg of the conducting polymer layer so that no chemical alteration of the layer occurs. This method of fabricating conducting polymer patterns is more of a physical process rather than a chemical one. It does not involve any aggressive chemistry. The conducting polymer layer is not subjected to any chemicals or high energy beams to avoid degradation. This patterning approach is parallel, and there is scope of high volume production.

4.3 Experimental Procedure

4.3.1 Fabrication of the Silicon Mold for ILL

The silicon mold was fabricated using conventional ultra-violet (UV) photolithography method [81] and dry etching [82]. The process for the SiO_2 mold fabrication includes the following steps: (i) baking the SiO_2 wafer at 250° C for 30 minutes to dry the surface of the wafer, (ii) after the wafer cooled down, spin coating a layer of positive photoresist, PR1813, on the wafer, (iii) soft baking the wafer at 115° C for 1 minute duration, (iv) exposing the wafer to UV light in a mask aligner, (v) developing the resist patterns in a developer solution (MF 319), (vi) baking the wafer with the developed photoresist pattern at 115° C for about 3 minutes, (vii) wet etching the 2 μm SiO_2 layer using Buffered Oxide Etch (BOE) solution, (viii) removing the photoresist layer by washing the wafer with acetone, (ix) using Deep Reactive Ion

Reproduced with permission of the copyright owner. Further reproduction prohibited without permission.

Etching (DRIE) to etch the silicon using the SiO_2 layer as mask. This step completes the SiO_2 mold fabrication (Figure 4.3). In case no oxide layer is desired on the silicon mold, a silicon wafer is chosen and patterned with the photoresist. The photoresist pattern acts as the mask for the DRIE etching. In case of positive photoresists, the parts of the photoresist which get exposed to the UV radiation dissolve in the developer solution. This dissolution is because the UV radiation breaks down the polymer chains in the photoresist. Figure 4.4 shows the silicon microwire and microheater molds fabricated using photolithography and DRIE techniques.

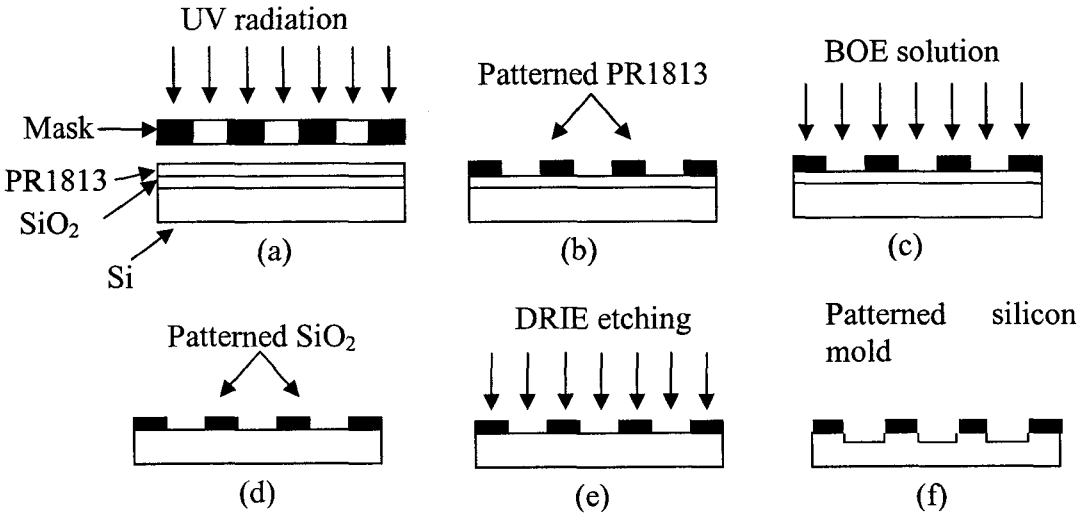

Figure 4.3 Schematic of the silicon mold fabrication steps: (a) the UV photolithography step, (b) the patterned photoresist layer, (c) the BOE etching of the SiO_2 layer, (d) the patterned SiO_2 layer, (e) the DRIE etching of silicon with SiO_2 as mask, and (f) the finished silicon mold with SiO_2 on top.

Reproduced with permission of the copyright owner. Further reproduction prohibited without permission.

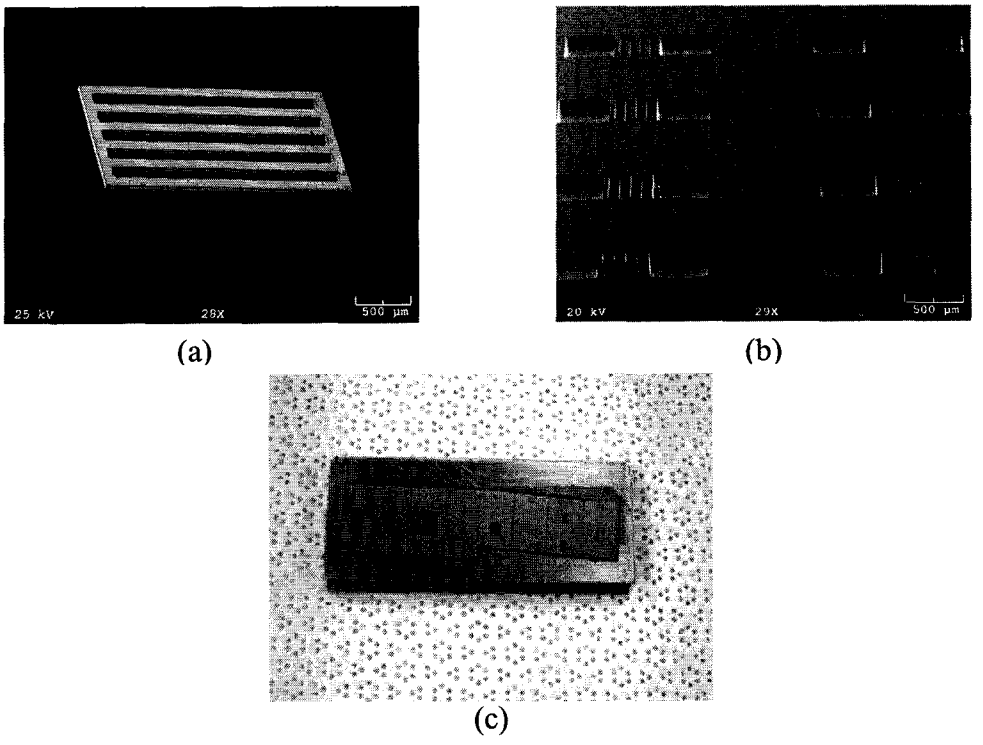

(a) (b)

(c)

Figure 4.4 (a) SEM of the microwire mold, (b) SEM of the serpentine microheater mold, and (c) optical picture of the silicon mold attached to the hot embossing tool.

BOE is composed of 1 part of concentrated hydrogen fluoride (HF) and 6 parts of ammonium fluoride (NH_4F). This solution is used to etch SiO_2. The BOE solution attacks the SiO_2 more than the photoresist layer and silicon. This etching process is isotropic in nature [81]. DRIE is a dry-etching technique commonly used in micro- and nano-fabrication to etch deep, high-aspect-ratio structures in silicon. It is accomplished by alternating sulphur hexafluoride (SF_6) plasma with Teflon (C_4F_8) deposition. The SF_6 plasma etches the silicon and the C_4F_8 layer protects the sidewalls. Both the gases are pulsed, so that the process is cyclic in nature, with etching followed by deposition. Since the sidewalls are protected, the bottom silicon layer gets etched away, and the trench depth is increased. This etching method is anisotropic in nature. The etching rate and

Reproduced with permission of the copyright owner. Further reproduction prohibited without permission.

depth can be controlled by controlling the time of etching and passivation cycles, plasma power, and flow rate of the two gases [83].

4.3.2 Experimental Procedure for ILL

For IIL, non-conducting polymethylmethacrylate (PMMA) sheets were used as the intermediate layers. The PMMA sheets were 6" X 6" and 500 μm thick. PMMA was chosen as the intermediate-layer material, because it is a good hot embossing material [84]. PMMA has a small thermal expansion coefficient of ~5.0 X 10^{-5} per °C and a small pressure shrinkage coefficient of ~3.8 X 10^{-7} per psi [84]. Its Tg is around 105° C. PPy (from Sigma Aldrich Co.), SPANI (from Sigma Aldrich Co.), and PEDOT-PSS (Baytron P HC V4 from H. C. Starck Co.) were used for the conducting polymer layer which were patterned using the ILL method. The three conducting polymers were used as received from the manufacturers, in water solutions of varying concentrations. Their thin layers were generated by spin-coating the corresponding solutions on the PMMA sheets. Before coating the conducting polymers over the PMMA, all three polymer solutions were kept in an ultrasonic bath for one hour to remove any aggregate formation in the solution from prolonged storage. The PMMA surface is hydrophobic under normal conditions due to its low surface energy. In order to make the top surface of PMMA hydrophilic so that the conducting polymers could be effectively spin-coated over it, the PMMA surface was exposed to oxygen plasma in a commercial machine (Techniques MicroRIE series 800). The plasma power was 300 watts and the duration of exposure was 45 seconds. Once high energy species bombarded the PMMA surface, the adhesion between the PMMA and conducting polymers was increased due to the increase of surface energy. Silicon molds with depths of 17 μm, 100 μm, and 120 μm were used in the ILL method. The

Reproduced with permission of the copyright owner. Further reproduction prohibited without permission.

imprinting process was done in vacuum using a commercial hot embossing system HEX 01/LT (JENOPTIK Mikrotechnik Co.), (Figure 4.5) which had a precise control over the critical process parameters.

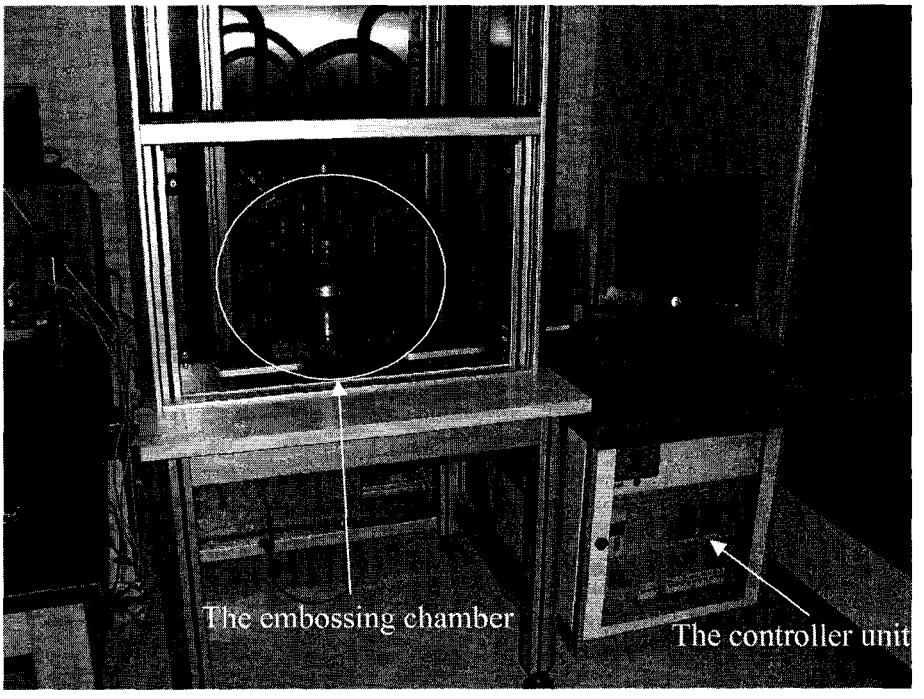

Figure 4.5 HEX 01/LT Hot embossing machine from JENOPTIK Mikrotechnik GmbH.

Embossing temperatures could be raised to 200° C with an accuracy of 0.1° C, embossing forces could be raised to 20 KN with an accuracy of 0.01 N, and position could be controlled with an accuracy of 1 μm [85]. Both the substrate and mold were heated up to the same temperature for embossing. If the mold was not heated as much as the substrate, then the mold would cool down the PMMA when the mold was placed on the substrate. This cooling would increase the viscosity of the PMMA, and the polymer would not flow effectively. Demolding temperature was below the Tg of the PMMA. Temperature control during the demolding was important. For example, cooling the

Reproduced with permission of the copyright owner. Further reproduction prohibited without permission.

sample in a fast manner would make the PMMA solidify quickly inside the silicon mold, causing stiction problem. Conducting polymer undergoes conformational changes at its Tg, which might affect the polymer matrix and conductivity. Therefore, the Tg of the conducting polymer should be higher than that of the intermediate-layer polymer. In our case, the intermediate-layer polymer was PMMA, and its Tg was lower than those of the three conducting polymers. The adopted printing temperature was 120° C, which was above the Tg of the PMMA and below that of the three conducting polymers used.

The silicon mold and substrate were aligned in the hot embossing machine. The top and bottom plates of the hot embossing machine were pre-aligned and centered. The silicon mold was attached and centered to the top plate of the embossing machine. A 170 mm X 170 mm PMMA sheet was centered on the bottom plate of the embossing machine and the mold coverage area was marked. This area was equally divided into multiple blocks and each block was coated with one conducting polymer while masking the other blocks. After spin-coating the conducting polymers on all blocks, the PMMA sheet was again centered on the bottom plate of the embossing machine, and imprinting was carried out.

In case three conducting polymers, for example, were considered, three sets of patterns were generated in the mold. The mold coverage area on the PMMA sheet was divided into three blocks for the three conducting polymers, respectively. The only alignment requirement was that the three sets of molding patterns should fall into the three blocks on the substrate during the embossing, respectively. Tape masking was used in this work. In the long run, a better masking approach should be used to precisely define the area of each block on the substrate due to two concerns. First, commercially

Reproduced with permission of the copyright owner. Further reproduction prohibited without permission.

available tapes were adopted here. Their available sizes and shapes are limited, which limits the block sizes and shapes that could be produced. Second, along their edges, there was a size variation of tens of microns, which makes the block boundary not uniform. A silicon stencil may be a potential tool to replace a tape in this masking effort, because the patterns in the silicon stencil could be well defined using photolithography. The masking using a silicon stencil is under investigation in our research group.

The generation of patterns is affected by four major parameters: insertion speed, printing pressure, printing temperature, and printing time. The insertion speed should be constant and should be as small as possible, aimed at reducing the dynamic effects on the materials to be printed. The mold insertion depth ranged from 17 μm to 120 μm. The embossing pressures used in our experiments were 2 MPa, 5 MPa, and 59.52 MPa, and the mold insertion speeds were 0.5 mm/min and 1 mm/min.

4.4 Numerical Modeling of the Embossing Process

In order to have a good understanding about the molding process, we conducted simulation using a commercial finite-element package ANSYS 8.0. Since the conducting polymer layer is much thinner than the intermediate layer in the ILL method, the conducting polymers and PMMA patterns should be generated mainly due to the flow of the PMMA at the printing temperature. Consequently, the PMMA should have dominant effects on the generated patterns. Therefore, for simplicity, during the simulation, only PMMA coated on the substrate was considered.

The deformations of solid polymers are usually characterized using the nonlinear Moony-Rivlin stress-strain relationship, instead of traditional linearly elastic stress-strain function, since this relationship is uniquely suited for rubber-like elastic deformations

Reproduced with permission of the copyright owner. Further reproduction prohibited without permission.

[86, 87]. This relationship has also been used to describe the deformation behavior of PMMA in the nanoimprint lithography method, in which a nanostructured Si mold is adopted to pattern the PMMA through a hot embossing process. According to the Mooney-Rivlin model, the stress is defined as [86, 87]:

$$\sigma_i = \lambda_i \frac{\partial W}{\partial \lambda_i}, \tag{1}$$

where λ is the expansion rate, and W is a strain density function. W is expressed as

$$W = C_{10}(I_1 - 3) + C_{01}(I_2 - 3) + \frac{1}{d}(J - 1)^2, \tag{2}$$

where $I_1 = \lambda_1^2 + \lambda_2^2 + \lambda_3^2$, $I_2 = \lambda_1^2\lambda_2^2 + \lambda_2^2\lambda_3^2 + \lambda_3^2\lambda_1^2$, I_1 is the first deviatoric strain invariant, I_2 the second deviatoric strain invariant, C_{10} and C_{01} material constants characterizing the deviatoric deformation of the material, and d the material incompressibility parameter. The initial shear modulus is defined $\mu = 2(C_{01} + C_{10})$, and the initial bulk modulus is defined as $k = \frac{2}{d}$. C_{10} and C_{10} are the 1st and the 2nd strain energy constrains, respectively. They are derived from the following approximated relations [85]:

$$C_{01} = 0.25C_{10}, 6(C_{10} + C_{01}) \approx E, \tag{3}$$

where E is the Young's modulus of the polymer. By Equation (3), we have

$$C_{01} = 0.034E, \quad C_{10} = 0.134E. \tag{4}$$

Due to the nonlinear nature of Equation (2), it is difficult to find an analytical solution. Therefore, numerical simulation is needed to find the molding deformation. Since ANSYS 8.0 allows the simulation of materials using the Moony-Rivlin stress-strain relationship, it was chosen in this work to establish the simulation model. Rectangular

Reproduced with permission of the copyright owner. Further reproduction prohibited without permission.

hyper-elastic elements were used to simulate the embossing of 5 μm and 50 μm microheater patterns in PMMA (Figures 4.6 and 4.7).

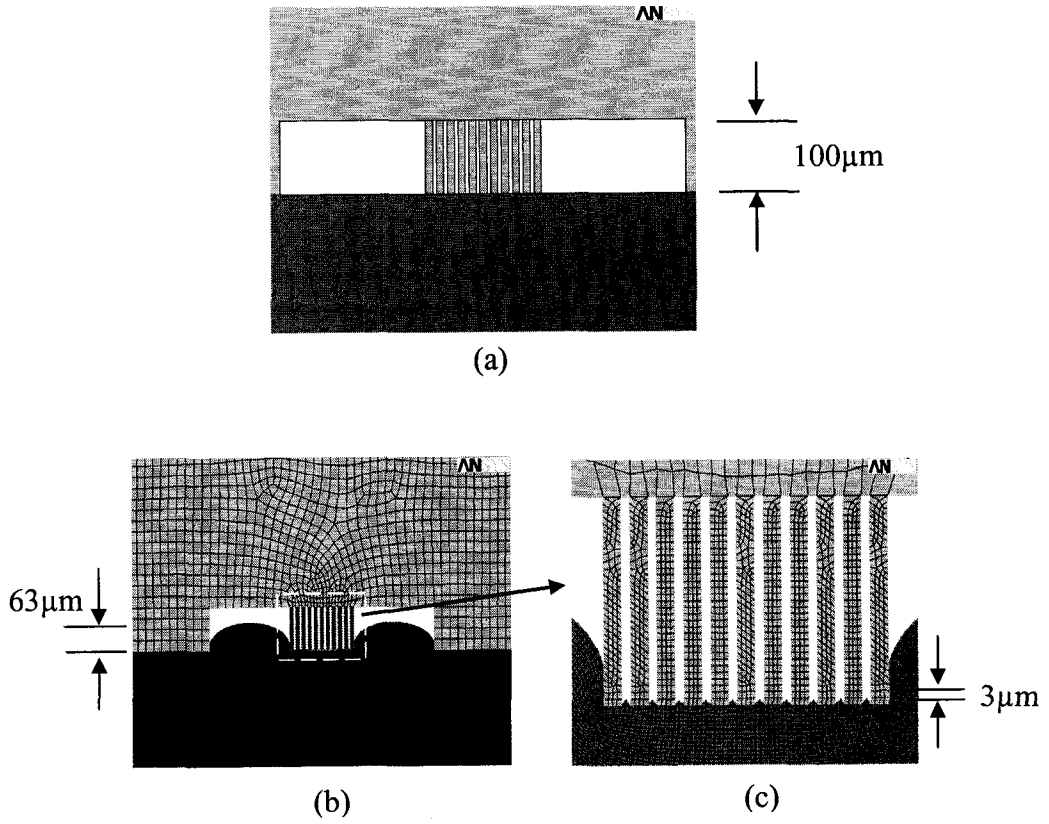

Figure 4.6 Simulation results in ANSYS for fabrication of a 5μm serpentine microheater pattern: (a) before mold insertion, and (b) after mold insertion.

Reproduced with permission of the copyright owner. Further reproduction prohibited without permission.

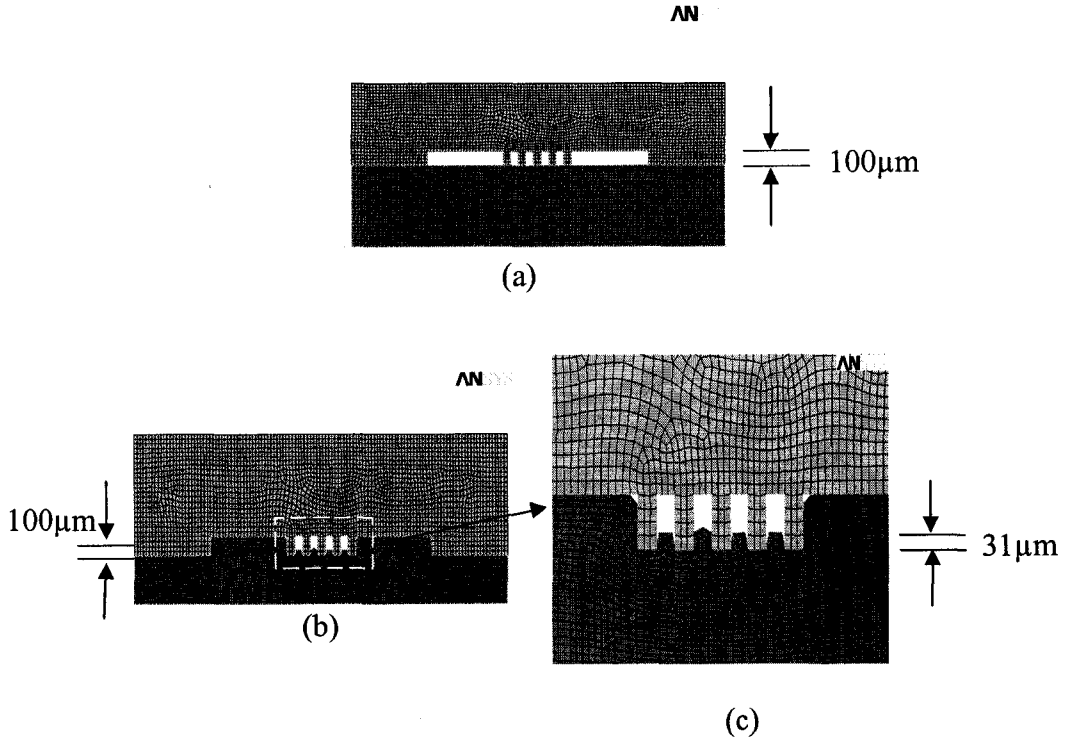

Figure 4.7 Simulation results in ANSYS for fabrication of a 50μm serpentine microheater pattern: (a) before mold insertion, and (b) after mold insertion.

Each microheater consisted of a serpentine-shaped line and two contact pads. The PMMA layer was simulated as a rubber-elastic material during the molding process. The parameters used for simulation are listed in Table 4.1.

Table 4.1 Material properties of silicon and PMMA which were used for simulations.

Properties	PMMA	Silicon
	Hyper elastic solid	Rigid solid
Young's modulus (GPa)	2.5 – 0.5	170
C_{10}	0.3325 - 0.0665	-
C_{01}	0.0825 - 0.0165	-
Poisson ratio	0.45	0.23
Density (Kg/m^3)	1.2×10^3	2.5×10^3

Reproduced with permission of the copyright owner. Further reproduction prohibited without permission.

In case the mold had a depth of 100 μm, when the heights of the 200 X 200 μm^2 and 500 X 500 μm^2 contact pads were 63 μm and 100 μm, respectively, the corresponding heights of the 5 μm- and 50 μm-wide microheater lines were 3 μm and 31 μm, recpectively (Figures 4.6 and 4.7).

As the mold had a depth of 120 μm, when the heights of the 200 X 200 μm^2 and 500 X 500 μm^2 contact pads were 75 μm and 120 μm, respectively, the corresponding heights of the 5 μm- and 50 μm-wide microheater lines were 4 μm and 38 μm, respectively. These simulation results showed that PMMA did not flow into the 5 μm and 50 μm silicon channels as efficiently as it did into the 200 X 200 μm^2 and 500 X 500 μm^2 contact pad cavities. Hence, height differences were generated between them. In order to increase the heights of small patterns, it is necessary to decrease insertion speed but increase printing time, so that polymers have more time to fill small mold cavities.

These simulation results provide a good understanding about the polymer deformations during the molding process, while they could not be used to quantitatively describe the deformation behaviors due to the following concerns. The material properties of PMMA change with temperature during the heating-up and cooling-down processes in the ILL, while the Mooney-Rivlin relationship does not describe the corresponding thermal behavior, since this relationship does not involve thermal effect. Also, the cross-section profile produced during the molding cannot be fully recovered, which is the characteristic of a plastic deformation. Therefore, the PMMA should be better modeled as a thermoplastic material during the molding case, which is also our case. Unfortunately, to our knowledge, such a thermoplastic model has not been developed yet.

Reproduced with permission of the copyright owner. Further reproduction prohibited without permission.

4.5 Experimental Results of Fabrication

The ILL method was used to fabricate straight and serpentine microwires of the three conducting polymers, PPy, PEDOT, and SPANI. Microwire and microheater patterns were fabricated, respectively, in the three different conducting polymers (Figures 4.8 and 4.9).

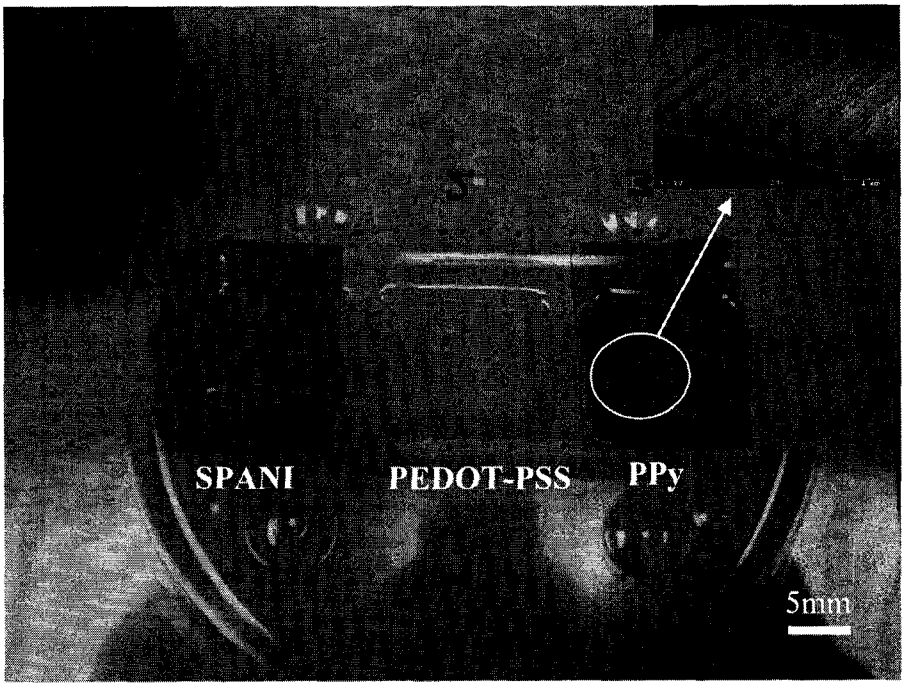

Figure 4.8 Optical picture of straight microwires of PPy, PEDOT, and SPANI fabricated simultaneously using the ILL method.

Reproduced with permission of the copyright owner. Further reproduction prohibited without permission.

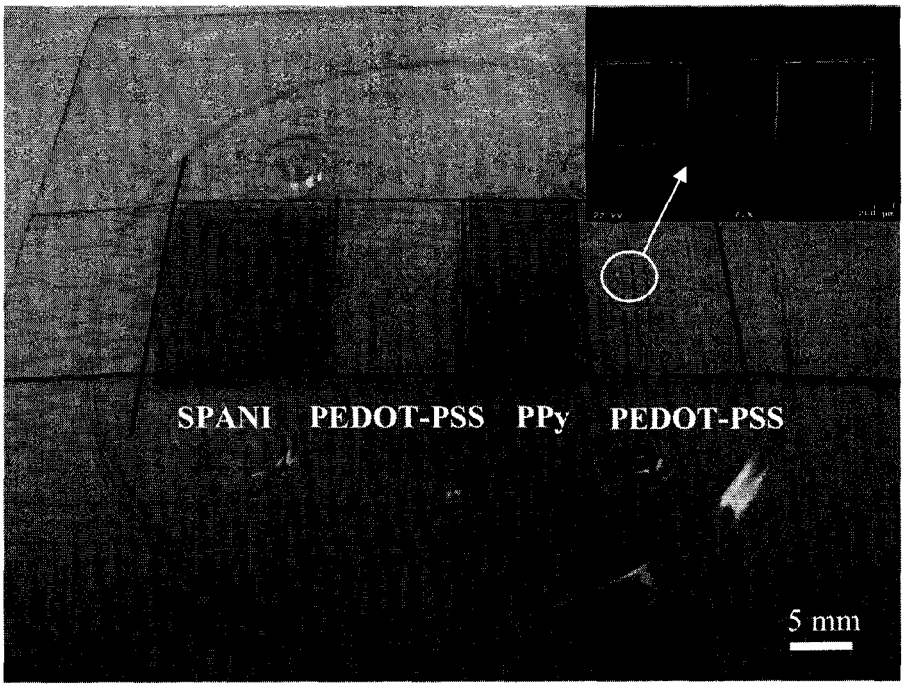

Figure 4.9 Optical pictures of serpentine microwire (microheater) patterns of PPy, PEDOT, and SPANI fabricated simultaneously using the ILL method.

The substrates were the 500 μm thick PMMA sheets. The generation of the straight microwires was used to examine whether the three conducting polymers would be cut-off. The production of the serpentine microwires was further employed to examine whether functional devices, such as the microheaters (consisting of large contacts and small lines), could be directly fabricated using the ILL method. The hot embossing recipe used for embossing the straight microwires is illustrated in Table 4.2.

Table 4.2 Hot embossing machine recipe for imprinting the 300 μm wide microwires of PPy, PEDOT and SPANI.

Initialize Force Control (true/false=0)	Initialize the force unit.
Heating (Top=90° C, Bottom=90° C)	Start heating of the tool and substrate.
Close chamber( )	Close the embossing chamber
Evacuate chamber ( )	Evacuate the embossing chamber.
Wait time (t=20 s)	Wait for process stabilization.
Touch force (Force=50 N)	Represents the initial contact force

Reproduced with permission of the copyright owner. Further reproduction prohibited without permission.

	between the tool and the substrate.
Wait time (t=20 s)	Wait for process stabilization.
Heating (Top=130° C, Bottom=130° C)	Start heating the tool and the substrate to the specified temperature limit.
Wait time (t=60 s)	Wait for process stabilization.
Temp>=(Temp=110° C, channel=10)	Wait until the temperature of the substrate is above the specified limit.
Force Control(Force=1500 N, Velocity=1.0 mm/min	Apply the specified force on the substrate.
Wait time (t=120 s)	Wait for process stabilization.
Cooling (Top=100° C, Bottom=100° C)	Start cooling the tool and the substrate.
Wait time (t=60 s)	Wait for process stabilization.
Cooling (Top=60° C, Bottom=60° C)	Continue cooling the tool and substrate until the specified temperature.
Wait time (t=60 s)	Wait for process stabilization.
Temp<=(Temp=80° C, channel=10)	Wait until the temperature of the substrate is below the specified limit.
DemoldingAdv(Stretch=1.5 mm, velocity=1.5 mm/min)	Demold the tool from the substrate with the specified velocity.
Cooling (Top=50° C, Bottom=50° C)	Continue cooling the tool and substrate until the specified temperature.
Wait time (t=60 s)	Wait for process stabilization.
Venting chamber ( )	Vent the embossing chamber.
Open chamber ( )	Open the embossing chamber.

The microwires had identical sizes. Each microwire was 300 μm wide, 80 μm deep and 5 mm long. The microheater lines had different widths. They were 5 μm, 10 μm and 50 μm wide, separately. The results of the imprinting process are tabulated in Table 4.3.

Reproduced with permission of the copyright owner. Further reproduction prohibited without permission.

Table 4. 3 Experimental results of the imprinting process using silicon molds of various dimensions.

Silicon microheater mold			Embossing results	
Physical dimensions			Height of PMMA	
Channel width (μm)	Contact pad area (μm^2)	Mold depth (μm)	Channel (μm)	Contact pad (μm)
5	200 X 200	100	5	100
10	500 X 500	120	5	120
10	500 X 500	17	15.5	17
50	500 X 500	120	30	100
50	500 X 500	120	17	17

The microheater patterns were smaller in dimension than the straight microwire patterns. The PPy, PEDOT-PSS, and SPANI coatings on the patterns were about 500 nm, 5 μm and 200 nm thick, respectively. The pattern density was increased from 8 microwires per conducting polymer to 49 microheaters per conducting polymer. The microwires were embossed at 130° C with an imprinting pressure of 59.52 MPa. The mold insertion time was 120 seconds, and the demolding temperature was 80° C.

According to the simulation results, PMMA should flow more effectively into large silicon cativities. In order to make the PMMA fill the smaller microheater patterns, the embossing time was increased to 200 s. The demolding temperature was raised to 90° C, while the demolding velocity was reduced to 0.5 mm/minute. The embossing pressure was 2 MPa.

Examination of the microwires generated in each conducting polymer indicated that these conducting polymers have been properly patterned (Figure 4.10).

Reproduced with permission of the copyright owner. Further reproduction prohibited without permission.

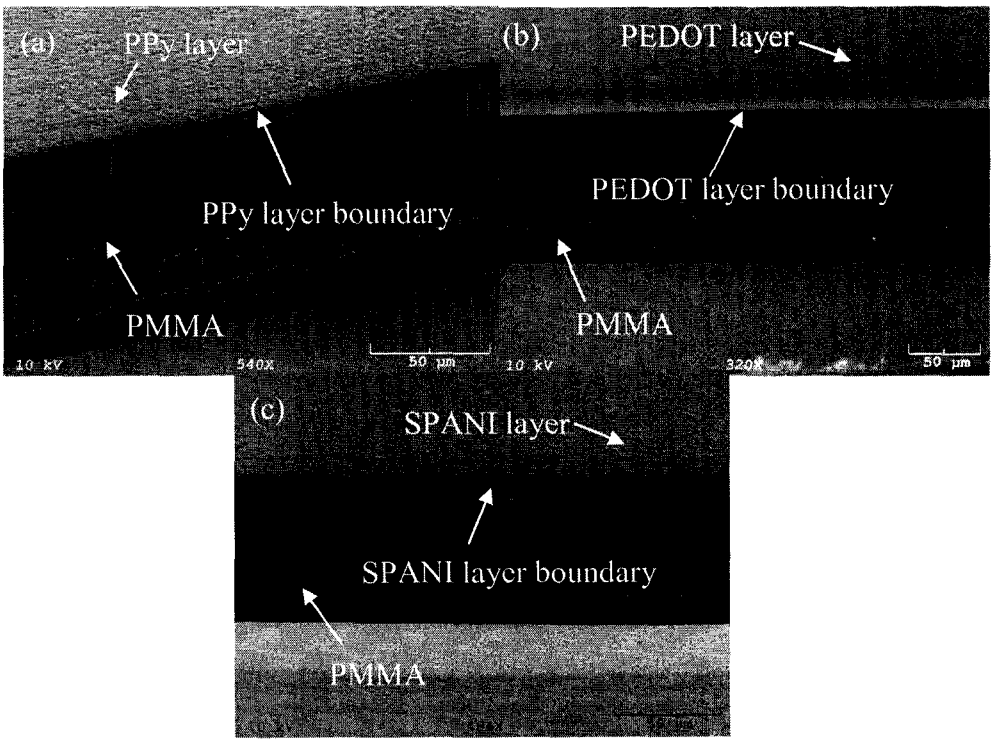

Figure 4.10 Side-view SEM pictures of the (a) PPy, (b) PEDOT, and (c) SPANI microwires.

The microwires of the three conducting polymers had identical sizes and were generated under identical molding conditions. Two differences between these patterns were (i) PPy, PEDOT-PSS and SPANI coatings on these patterns had thicknesses of about 500 nm, 5 µm and 200 nm, respectively, and (ii) these coatings had different morphologies since they were different materials. When other thicknesses and embossing conditions are used, these patterns may show more differences, which was not tested yet.

A significant height difference existed between the contact pads and the heater lines in the 5 µm and 10 µm microheater patterns. The heights of the embossed 5-µm-wide heater lines and 200 X 200 μm^2 contact pads were 6 µm and 100 µm, respectively (Figure 4.11).

Reproduced with permission of the copyright owner. Further reproduction prohibited without permission.

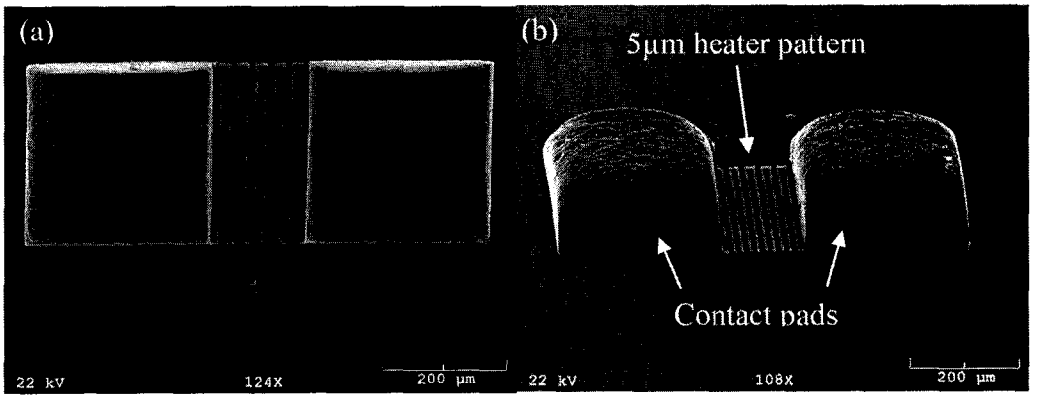

Figure 4.11 Serpentine microwires of width 5μm of PPy imprinted on PMMA: (a) SEM top view, and (b) SEM side view. The contact pads are 200μm X 200μm.

For the 50 μm-wide heater lines, the height difference was significantly reduced (Figure 4.12). The heights of the heater lines and the 500 X 500 μm^2 contact pads were 30 μm and 100 μm, respectively.

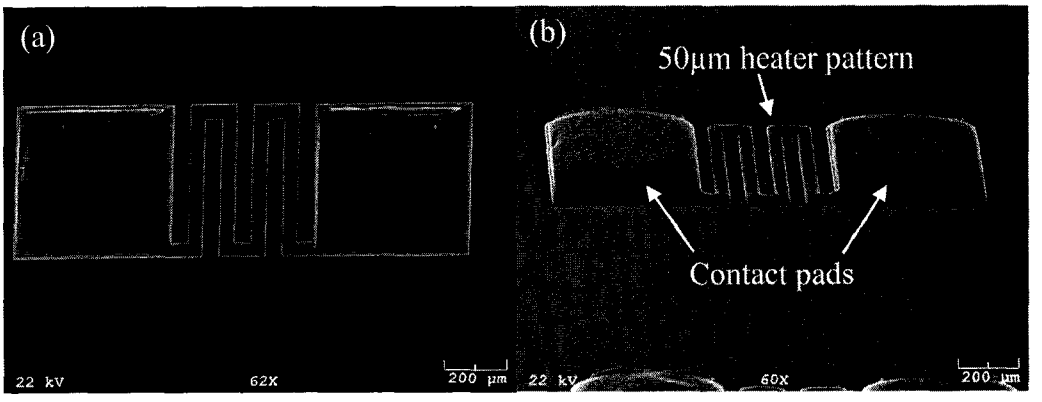

Figure 4. 12 Serpentine microwires of width 50μm of PPy imprinted on PMMA: (a) SEM top view, and (b) SEM side view. The contact pads are 500 μm X 500 μm.

The possibility of reducing the height difference between the microheater lines and the contact pads via the change of embossing conditions was also explored. For this purpose, microheater patterns of 10 μm- and 50 μm-wide lines were particularly studied. Imprinting was carried out with reduced depth of the silicon mold. The depth of the silicon mold was 17 μm, the embossing pressure was 5 MPa, and the embossing time was

Reproduced with permission of the copyright owner. Further reproduction prohibited without permission.

100 seconds. From SEM images (Figure 4.13), the height difference between contact pads and 10 μm-wide lines was 1.5 μm, and no height difference was visually observed between contact pads and 50 μm-wide lines.

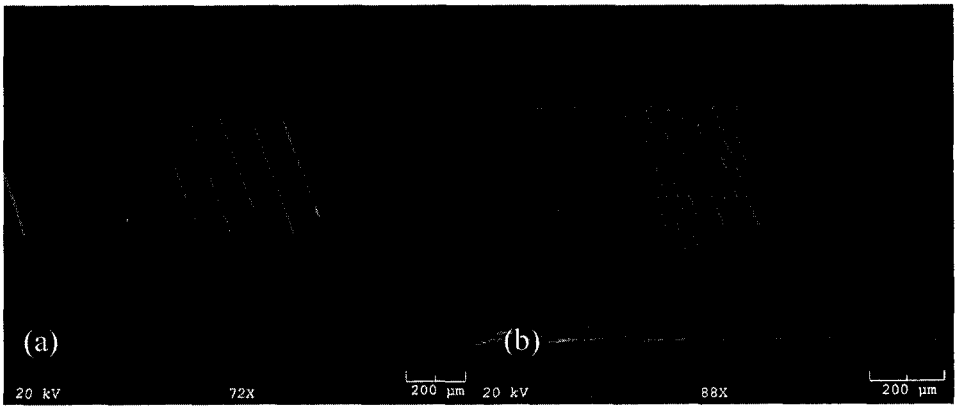

Figure 4.13 SEM pictures of serpentine PPy microwire patterns of width: (a) 50 μm, and (b) 10 μm. The silicon mold used for imprinting has a depth of 17 μm.

The contact pads in these microheater patters had a height of 17 μm. These results demonstrate that, when the Si molds are not deep, conducting polymers and PMMA will have a good filling of both large and small cavities in the molds, thus reducing the height difference between large and small patterns.

During the ILL process, the temperature of the conducting polymer coated PMMA substrate was first increased from 25° C (room temperature) to 125° C (printing temperature) and afterwards decreased from 125° C to 25° C. To investigate the effect of heating and cooling on the conductivity of the conducting polymers during the ILL, the following experiments were conducted. Additional silver epoxy contacts were made on a PPy microheater pattern and connected to the two probes of a Keithley probe station. The I-V characteristic was found after the PPy microheater pattern had been heated to a particular temperature and cooled back to room temperature. Such a procedure was

Reproduced with permission of the copyright owner. Further reproduction prohibited without permission.

repeated for temperatures of 25° C, 30° C, 50° C, 70° C, 90° C, 110° C, and 125° C. The device current was measured for a sweep of the bias voltage from 0 to 10V at each temperature reading. The value of the current at 10 V was used to plot Figure 4.14, since the I-V curve obtained by the sweeping bias voltage was linear.

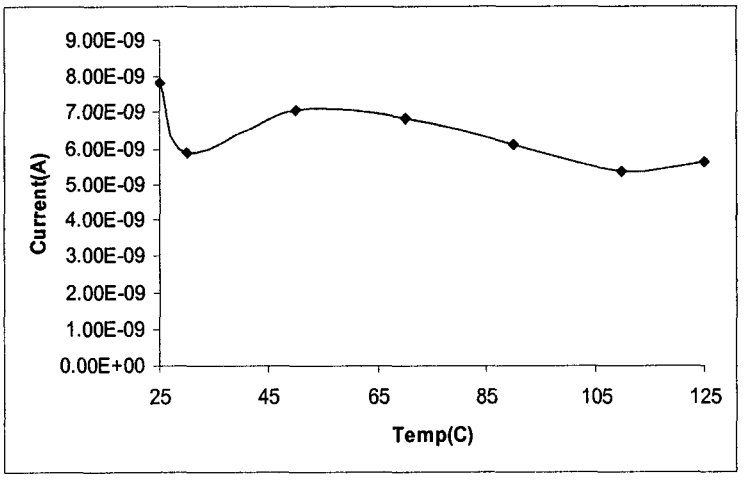

Figure 4.14 Variation in current of a 50 μm wide serpentine PPy microheater pattern when heated and cooled successively with increasing temperatures.

The inherent chemical and physical structure of a conducting polymer may be affected by temperature after the conducting polymer is heated up to an embossing temperature and cooled down to room temperature. Consequently, it is possible that conducting polymer devices of identical configurations may have different resistances (or say, different currents when the applied voltages are the same) at their operation temperature (i.e., room temperature), depending on the embossing temperatures adopted to generate these devices.

This current-temperature test was performed to find how much potential embossing temperatures affected electrical property of the corresponding devices. The

Reproduced with permission of the copyright owner. Further reproduction prohibited without permission.

data in Figure 4.14 shows the variation in the base current as a PPy microheater pattern was exposed to gradually increasing temperatures. The currents varied between $5.5x10^{-9}$ A and $9x10^{-9}$ A. This small variation should not affect the applications of conducting polymers. For example, in a sensing application, the current changes of PPy micropatterns were in the order of 10^{-7} A [88]. Therefore, it is reasonable to conclude that the temperature increase and decrease during the ILL process have a minimal effect on the electrical properties of conducting polymers.

Reproduced with permission of the copyright owner. Further reproduction prohibited without permission.

CHAPTER 5

APPLICATIONS OF THE CONDUCTING POLYMER MICROWIRES

Figure 5.1 illustrates the idea of a sensor platform by integrating several different conducting polymer micropatterns on a common substrate using the ILL method. The conducting polymer pattern density and diversity can be effectively controlled with this approach.

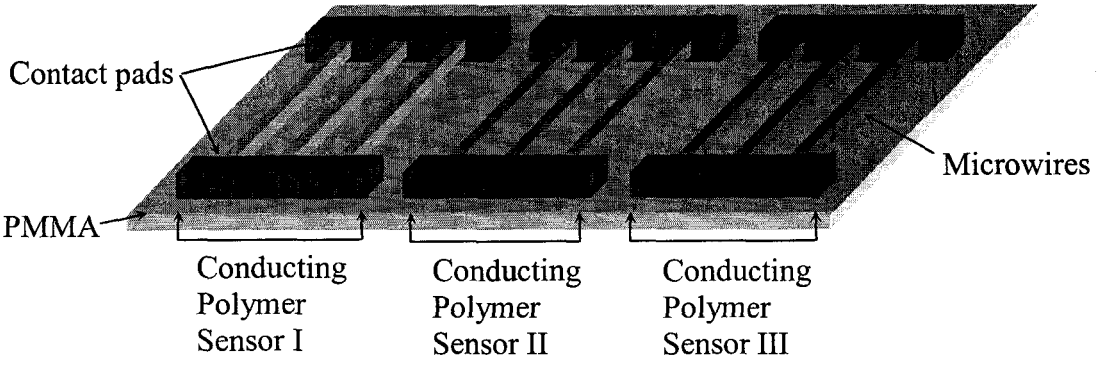

Figure 5.1 Schematic of three conducting polymer microwire sensor on a common platform.

Reproduced with permission of the copyright owner. Further reproduction prohibited without permission.

Microwires fabricated using the ILL method were exposed to humidity and volatile organic gases, including methanol, acetone, and toluene. Additional silver epoxy contacts were made on the straight microwires (Figure 5.2). The microwires behaved as "chemiresistor" sensing elements.

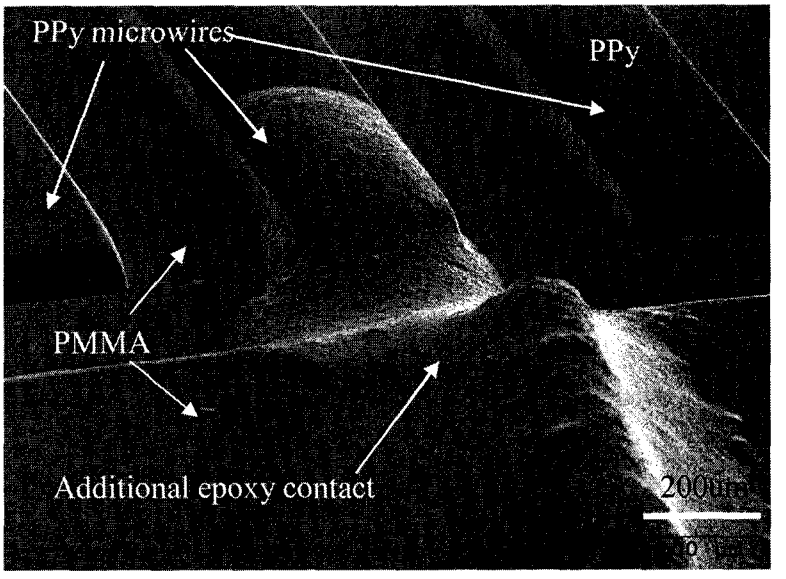

Figure 5.2 SEM picture of additional silver epoxy contact with a PPy microwire.

5.1 Humidity Exposure to PPy Microwire Sensor

A single PPy microwire (300 μm wide and 5000 μm long) was exposed to increasing levels of humidity, and its resistance change was recorded with a Keithley probe station [88]. The sensitivity index (SI) was calculated as $(R_{Humidity}-R_{Base}/R_{Base})$. For comparison, a 1 cm X 1 cm PPy film was also exposed to similar humidity levels and the SI was calculated in a similar fashion. The microwire and film sensors were enclosed inside an air-tight chamber (Figure 5.3).

Reproduced with permission of the copyright owner. Further reproduction prohibited without permission.

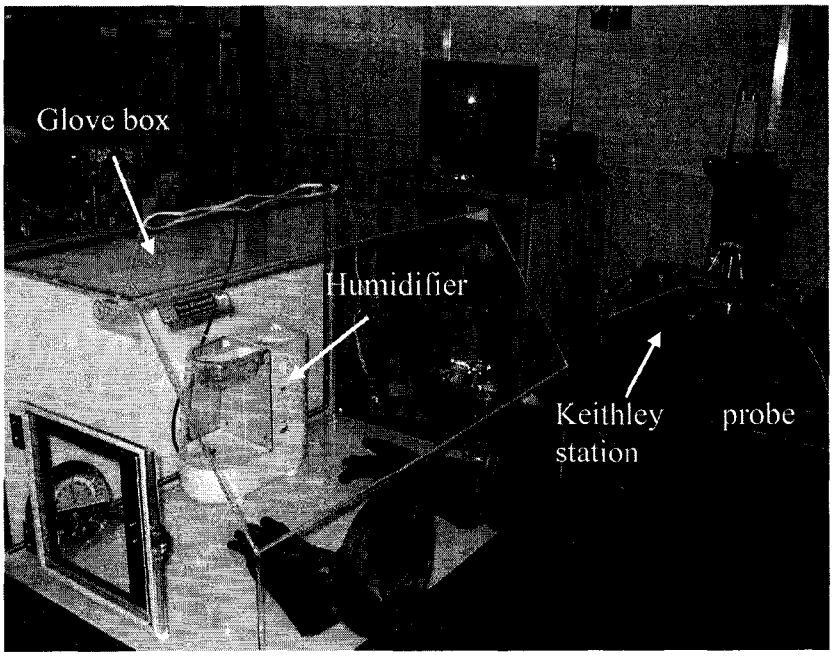

Figure 5.3 Humidity exposure experimental setup [88].

The base humidity inside the chamber was measured at the beginning of the experiment, which was equal to the room humidity level. The temperature of the setup was maintained at the room level during the experiment. The baseline resistance of the sensor was measured at the base humidity level, and the chamber was closed. The humidity of the chamber was gradually increased beyond the room humidity level and was measured constantly. As the humidity of the chamber was increased in steps, the resistance of the sensor was measured, and the corresponding SI was calculated.

Upon exposure to water vapor, the resistance of the PPy microwire and film decreased, yielding a negative value of SI (Figure 5.4). This decrease was brought about by the interaction of PPy with polar water molecules, which increased the mobility of the charge carriers in PPy [89]. The PPy current rapidly increased when the relative humidity ranged from 45% to 58%. When the relative humidity was beyond 58%, the PPy layer seemed to saturate, and the increase in current was less.

Reproduced with permission of the copyright owner. Further reproduction prohibited without permission.

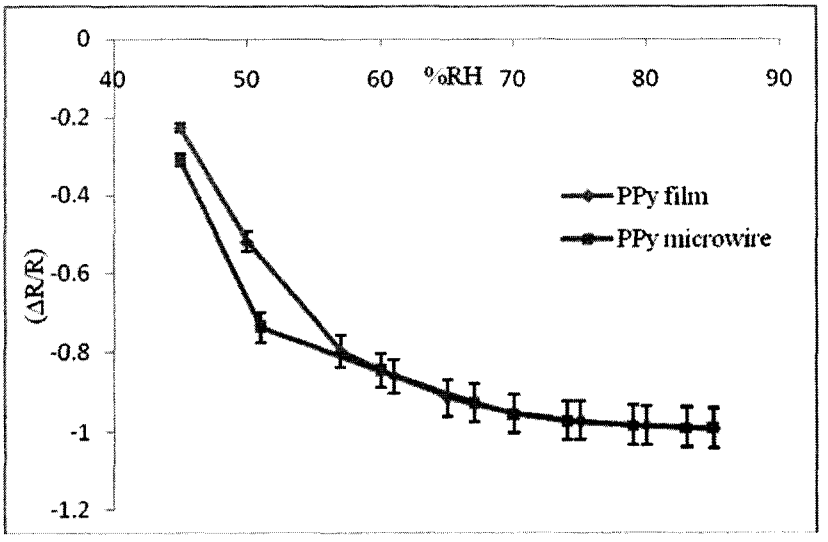

Figure 5.4 Humidity response of a single microwire and a film of PPy [88].

5.2 Binary Sensor Configuration and Detection

The idea of using multiple conducting polymer micropatterns as sensors was demonstrated via the exposure of two vapors including acetone, toluene, and methanol to PPy, SPANI, and PEDOT microwires and their response analysis. Figure 5.5 illustrates the experimental setup. An air-tight container was used to enclose two vapor sources (Vapor A and Vapor B). The vapors were of acetone, methanol, and toluene. As compressed vapors of the above three kinds were not easily available, beakers containing the three chemicals in liquid form were introduced inside the experimental chamber. Acetone, methanol, and toluene are naturally volatile compounds with high vapor pressure at standard room atmosphere. As soon as the beakers were introduced inside the chamber, the organic vapors started to diffuse inside the chamber. The microwire sensors were enclosed inside the chamber and the probes from the sensors were connected to the

Reproduced with permission of the copyright owner. Further reproduction prohibited without permission.

Keithley probe station for resistance measurements. The temperature and humidity inside the chamber were maintained at room level.

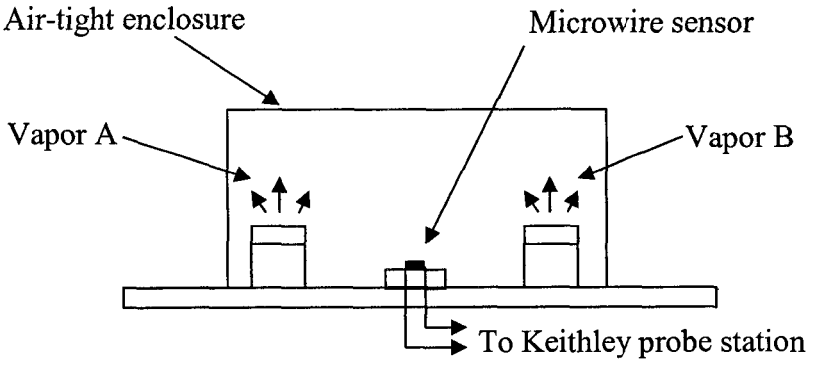

Figure 5.5 Experimental setup for the binary sensor configuration and detection scheme.

Two different sets of conducting polymer microwires were fabricated on a common PMMA substrate. The first set (Set I) had seven microwires, each of PPy and SPANI, and the second set (Set II) had seven microwires, each of PEDOT and SPANI. Set I was exposed to vapors of methanol and toluene, and Set II was exposed to vapors of acetone and toluene. The seven microwires, of each conducting polymer, were electrically connected in a parallel fashion using conductive epoxy. The initial resistance of the microwires was measured and noted as the base resistance. At first, the microwires were exposed to a single vapor for 600 s and the I-V was monitored continuously for the entire duration of exposure. After 600 s, the vapor sources were removed, and the chamber was opened to room atmosphere, stopping the exposure. Afterwards, the microwires were exposed to mixtures of methanol, toluene, and acetone in pairs, for duration of 600 s. Again, the I-V was monitored continuously for the duration of exposure. The current variation of the sensor with respect to the time of exposure was investigated to identify any particular trend in the sensor response.

Reproduced with permission of the copyright owner. Further reproduction prohibited without permission.

5.2.1 Exposure of PPy and SPANI Microwires to Methanol and Toluene.

Initially, the responses of PPy and SPANI microwires were determined separately for methanol and toluene vapor [90]. PPy microwires showed a gradual increase in current upon exposure to methanol vapor (Figure 5.6), and SI was -0.63. The reason for this trend may be attributed to the fact that methanol is a polar molecule, which helps in interchain electron transfer in PPy. Also, the small size of the methanol molecule helped it to diffuse into the polymer chain more effectively, thus aiding conduction. This behavior was similar to the humidity response.

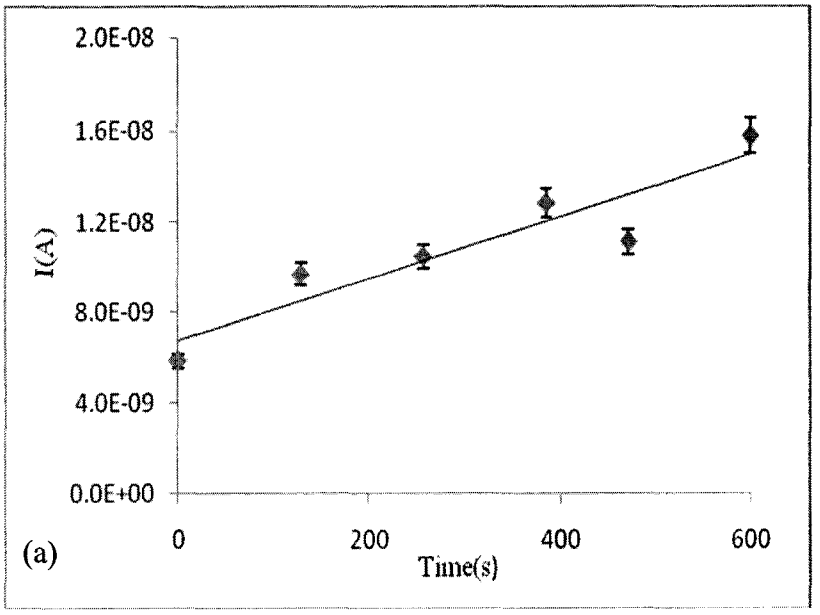

Figure 5.6 Current variation of PPy microwires to methanol exposure.

Toluene is a non-polar solvent; hence, it was not able to interact much with PPy (Figure 5.7). However, when the tolune molecules diffused inside the PPy polymer chain, it obstructed the movement of the charge carriers, thereby reducing conductivity. The SI was 1.05 after the entire duration of exposure.

Reproduced with permission of the copyright owner. Further reproduction prohibited without permission.

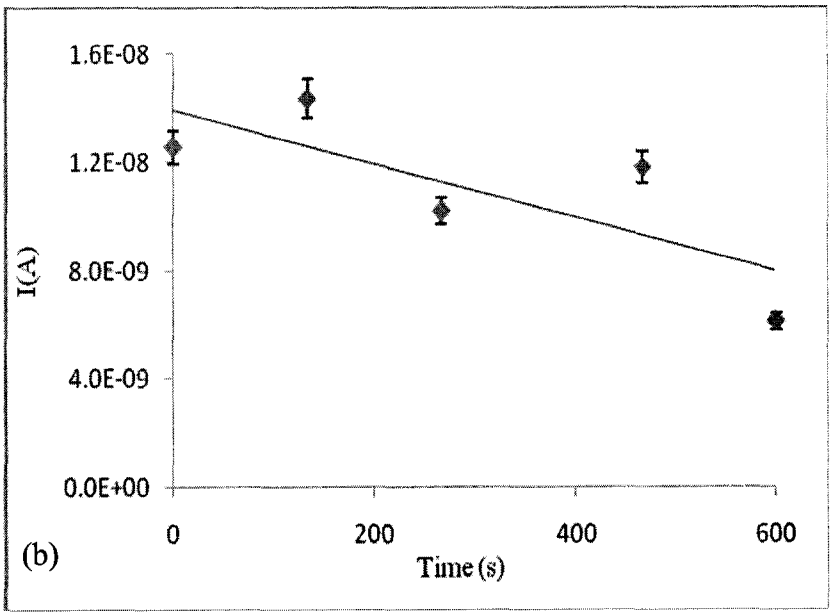

Figure 5.7 Current variation of PPy microwires when exposed to toluene.

When exposed to the mixture of methanol and toluene, the PPy current was stable for duration of about 300 s, after which it started to increase rapidly (Figure 5.8), and the SI was -0.81. This trend reflected methanol selectivity on PPy behavior over tolune in the mixture.

Reproduced with permission of the copyright owner. Further reproduction prohibited without permission.

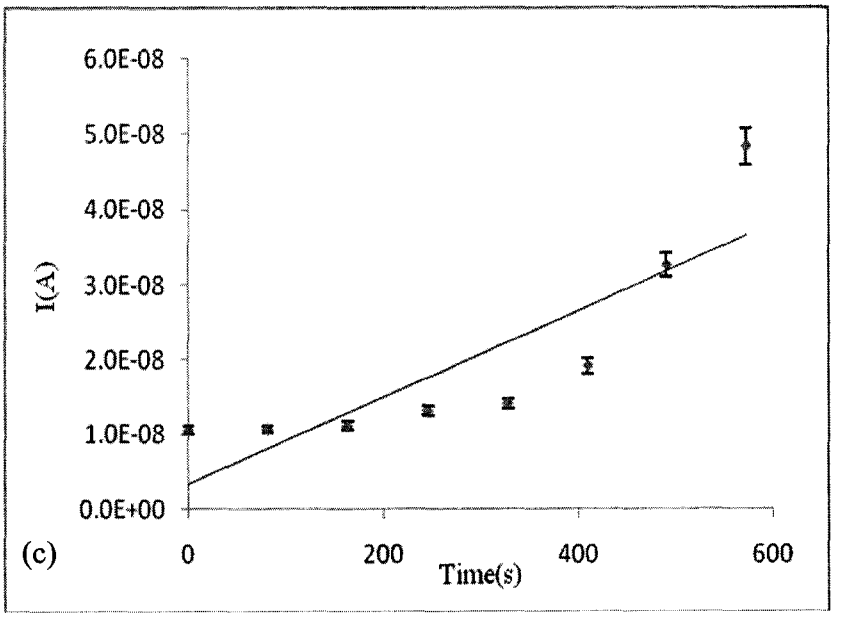

Figure 5.8 Current variation of PPy microwires when exposed to the mixture of vapors of methanol and toluene.

When the SPANI microwires were exposed to methanol vapor, the current decreased (Figure 5.9). Methanol is a polar molecule, and sulphonation of polyaniline created protonated sites which may have interacted with polar methanol molecules and reduced the number of charge carriers, thereby reducing conductivity. The overall SI was 0.24.

Reproduced with permission of the copyright owner. Further reproduction prohibited without permission.

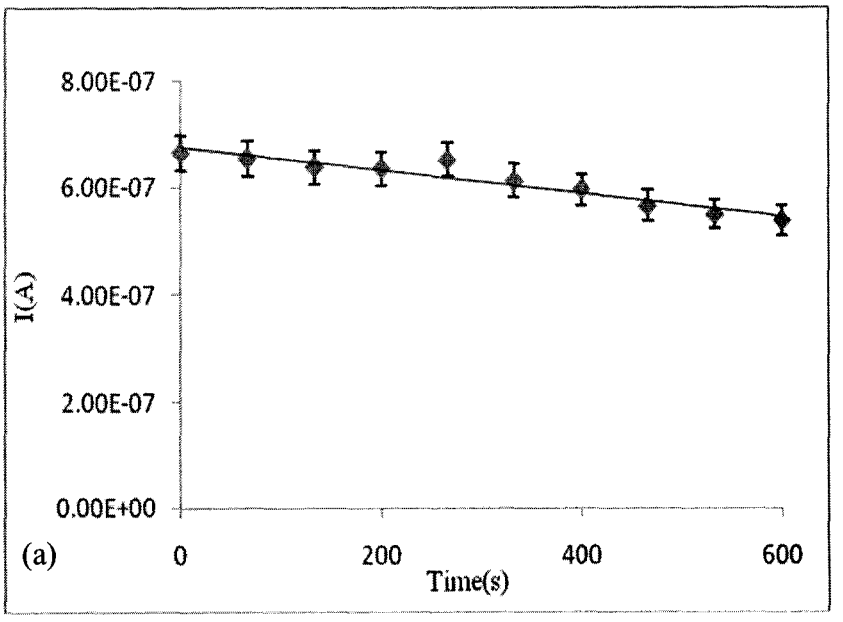

Figure 5.9 Current variation of SPANI microwires when exposed to methanol vapors.

Alternatively, methanol molecules might be diffusing inside the SPANI matrix and expanding it, thereby reducing carrier mobility and conductivity. SPANI did not respond much to non-polar toluene (Figure 5.10), which was reflected in the SI of 0.014.

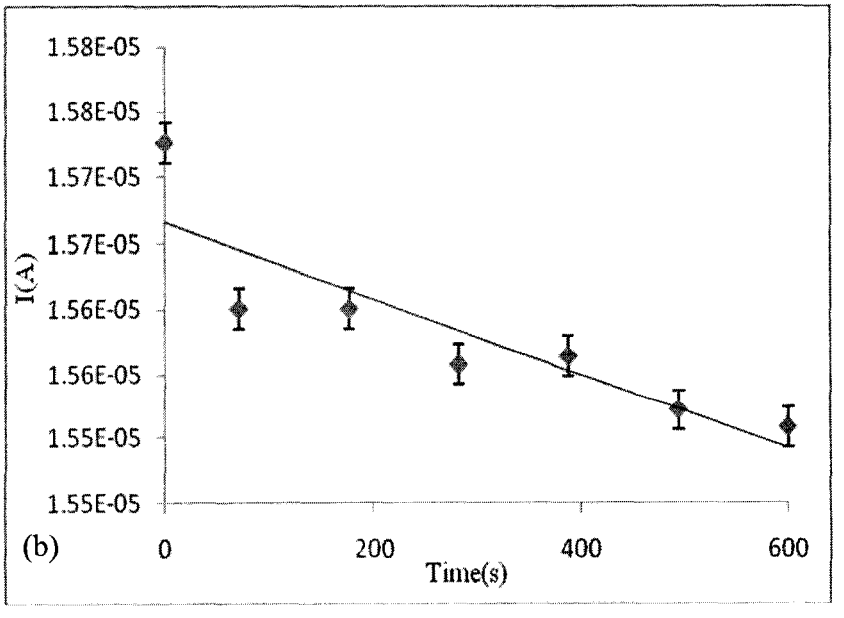

Figure 5.10 Current variation of SPANI microwires to toluene exposure.

Reproduced with permission of the copyright owner. Further reproduction prohibited without permission.

When a mixture of toluene and methanol was introduced, the SPANI microwires showed a decrease in the current trend with a SI of 0.52 (Figure 5.11). The decrease in the current of the SPANI microwires was much more in the mixture compared to the individual response. This difference may be due to the combined effect of the methanol and toluene molecules in limiting the flow of charge carriers. However, methanol had a greater influence on the SPANI microwires as compared to toluene in the mixture.

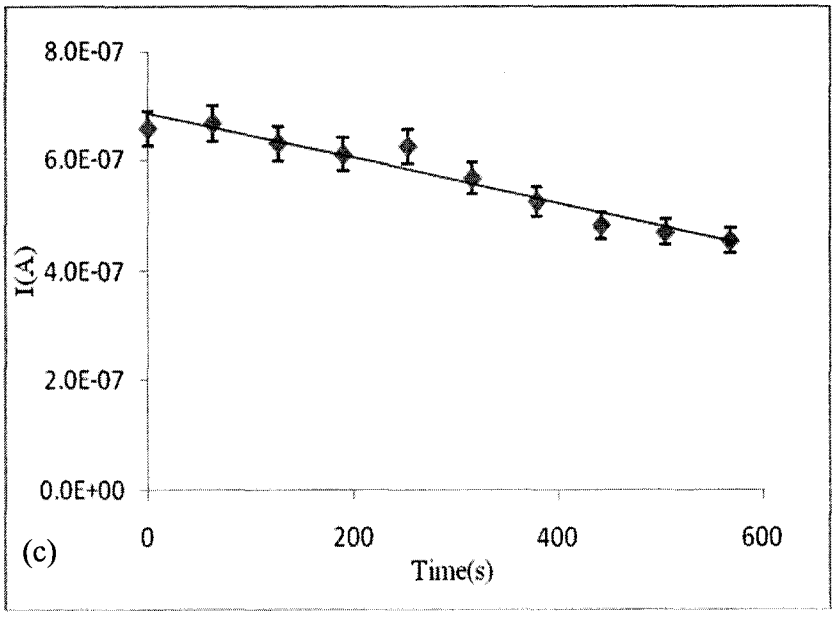

Figure 5.11 Current variation of SPANI microwires when exposed to a mixture of methanol and tolene vapors.

Comparing the response of the PPy and SPANI microwires to methanol and toluene from the sensitivity data, it was concluded that methanol affected the conductivity of both PPy and SPANI microwires more than toluene. Methanol exposure to the PPy microwires caused an increase in current with SI at -0.63. For SPANI microwires, there was a decrease in current with SI at 0.24. Toluene exerted substantial

Reproduced with permission of the copyright owner. Further reproduction prohibited without permission.

effect on the PPy microwires when exposed alone by decreasing current (SI: 1.04), but in the mixture, there was an eventual increase in current. Tolune did not affect the SPANI microwires much, and in the mixture the current showed reductions which reflected methanol dominance.

5.2.2 Exposure of PEDOT and SPANI Microwires to Acetone and Toluene

Initially, the responses of SPANI and PEDOT microwires to toluene and acetone vapors were determined [88]. Later, the microwires were exposed to the mixture of acetone and toluene.

Acetone exposure decreased the conductivity of the SPANI microwires. Acetone is a polar molecule which may be interacting with the protonated sites in SPANI, thereby reducing the number of charge carriers and decreasing conductivity (Figure 5.12).

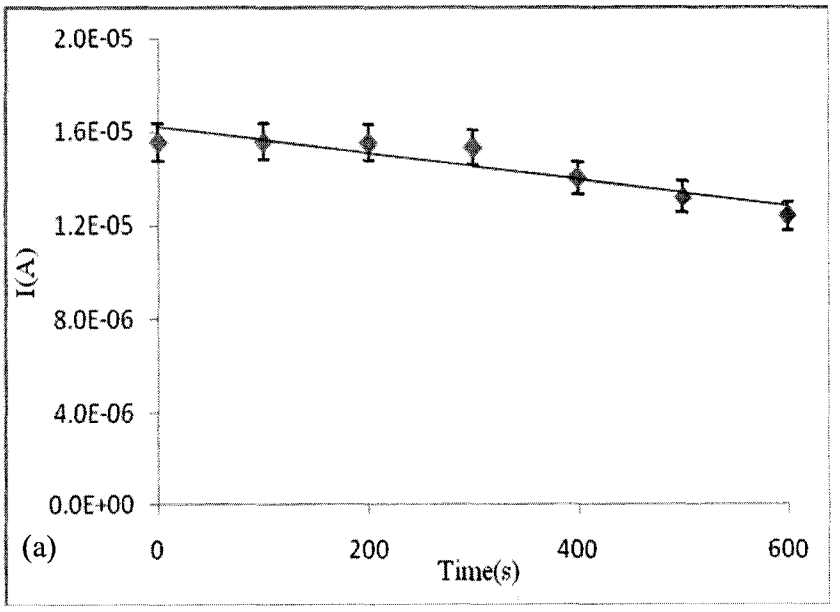

Figure 5.12 Current variation of SPANI microwires to acetone exposure.

Reproduced with permission of the copyright owner. Further reproduction prohibited without permission.

The SPANI microwires were not affected much by tolune, as it is non-polar, but over the duration of exposure, the current decreased slightly, as tolune molecules inhibited the movement of charge carriers in SPANI (SI: 0.014) (Figure 5.13). The corresponding SI was 0.26. Ladawan et al. [91] had found that acetone reduced the conductivity of PPy.

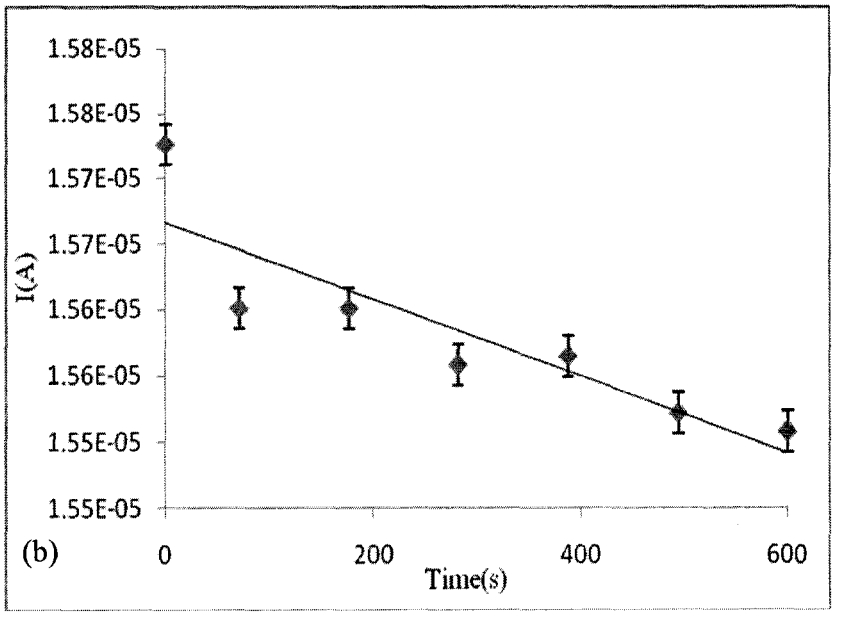

Figure 5.13 Current variation of SPANI microwires to toluene exposure.

They suggested that acetone molecules were dispersing inside the PPy matrix by hydrogen bonding and disrupting the ordered matrix of dopant ions and PPy molecules. When the SPANI microwires were exposed to a mixture of acetone and tolune vapor, the current gradually decreased (Figure 5.14), and the overall SI was 0.52. The SPANI current decreased more in the mixture of acetone and toluene vapor. Acetone exerted more influence on the SPANI microwires in the mixture with tolune.

Reproduced with permission of the copyright owner. Further reproduction prohibited without permission.

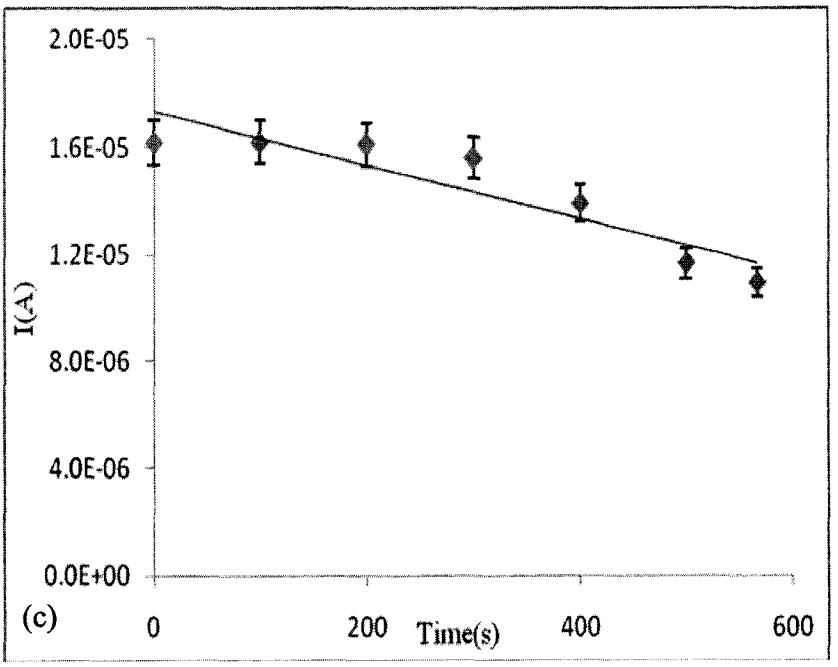

Figure 5.14 Current variation of SPANI microwires to exposure to mixture of acetone and toluene.

Exposure of the PEDOT microwires to acetone reduced its conductivity over 600 s of exposure (SI: 0.025), as charge carriers from PEDOT might be donated to acetone molecules which have a lower polarity (Figure 5.15).

Reproduced with permission of the copyright owner. Further reproduction prohibited without permission.

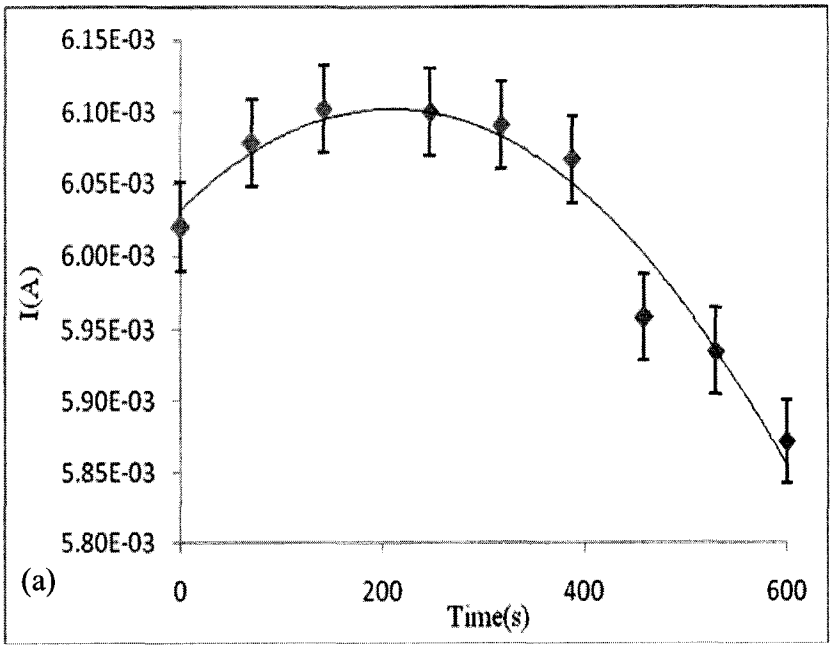

Figure 5.15 Current variation of PEDOT microwires to acetone exposure.

Another reason might be that the acetone vapor was expanding the polymer matrix, thereby reducing conductivity. With toluene, the PEDOT microwires showed a minor increase in conductivity over 600 s of exposure. The SI for the increase in current was 0.004 (Figure 5.16).

Reproduced with permission of the copyright owner. Further reproduction prohibited without permission.

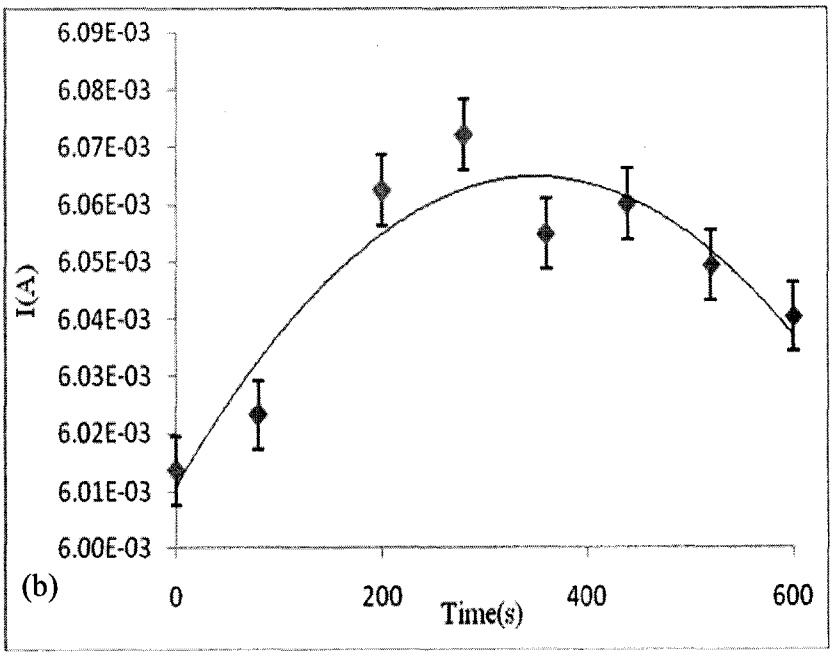

Figure 5.16 Current variation of PEDOT microwires to toluene exposure.

When the PEDOT microwires were exposed to a mixture of tolune and acetone, the conductivity was reduced over the duration of exposure (Figure 5.17). The overall SI was 0.02. The higher SI of the PEDOT microwires in the mixture indicates acetone selectivity over tolune.

Reproduced with permission of the copyright owner. Further reproduction prohibited without permission.

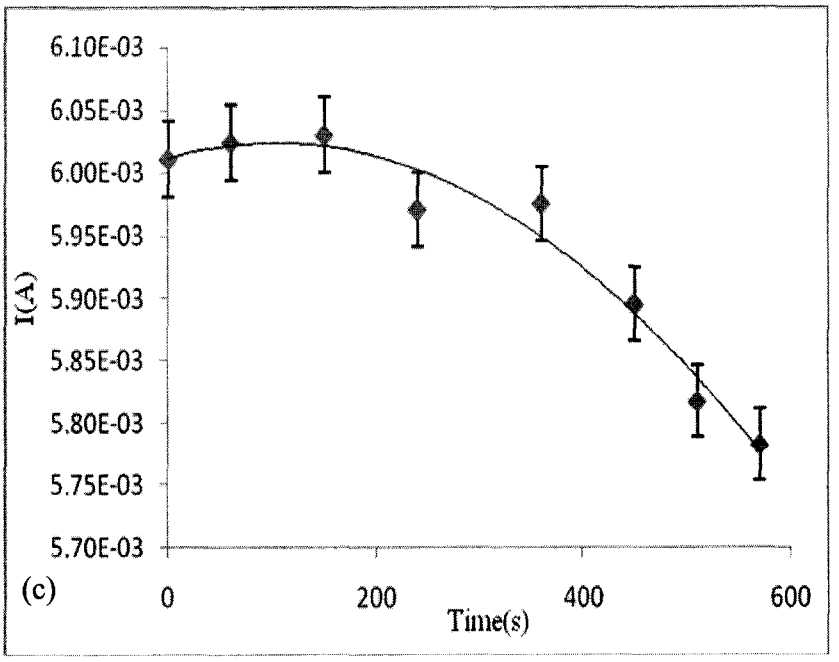

Figure 5.17 Current variation of PEDOT microwires to exposure to mixture of acetone and toluene.

From the sensitivity responses of SPANI and PEDOT microwires to individual vapors and their mixture, it was concluded that both the polymers were more responsive to acetone. Again, toluene induced minor variation in conductivity of both the polymers due to its non-polar nature. Overall, the PPy microwires showed a higher selectivity towards methanol, and the PEDOT microwires were highly sensitive towards acetone in their respective mixtures. The selectivity of the sensor can be further increased by fabricating micropatterns of different conducting polymers which are highly specific to particular targets. Preliminary examination revealed that the response and recovery times of the microwires sensors were similar to those of film sensors. The response and recovery times may vary with the individual conducting polymer and the particular analyte it is exposed to.

Reproduced with permission of the copyright owner. Further reproduction prohibited without permission.

5.3 Glucose Sensing with PPy Microwires

In order to demonstrate a biosensing application of the microwires fabricated using the ILL method, PPy microwires were modified with the required enzyme for glucose detection. The PPy microwires were coated with the enzyme glucose oxidase (GOD_{ox}) (7.8 mg/ml), ferrocenemethanol (FeMeOH) (17.8 mg/ml) and ethylenediaminetetraacetic acid (EDTA) (1.5 mM) in phosphate buffer (0.1M at pH 6.5) [92]. The device was encapsulated with a layer of cellulose acetate, a semipermeable membrane, to prevent water from entering and dissolving the PPy layer. The reactions between GOD_{ox}, glucose, and ferrocenemethanol release electrons which are transferred to the electrodes through PPy. The relevant chemical reactions are as follows: GOD_{ox} + glucose $\rightarrow$ GOD_{red} + gluconolactone; GOD_{red} + $(FeMeOH)_{ox}$ $\rightarrow$ GOD_{ox} + $(FeMeOH)_{red}$; $(FeMeOH)_{red}$ $\rightarrow$ $(FeMeOH)_{ox}$ + e^-. The electron released upon oxidation of FeMeOH reached the silver electrodes through the PPy layer. Hence, current increased at the electrodes.

Figure 5.18 shows the current variation of the PPy microwires to glucose solution of 0.3 mg/ml concentration. The current response is dynamic for the first 60 s, after which it stabilizes to a constant value.

Reproduced with permission of the copyright owner. Further reproduction prohibited without permission.

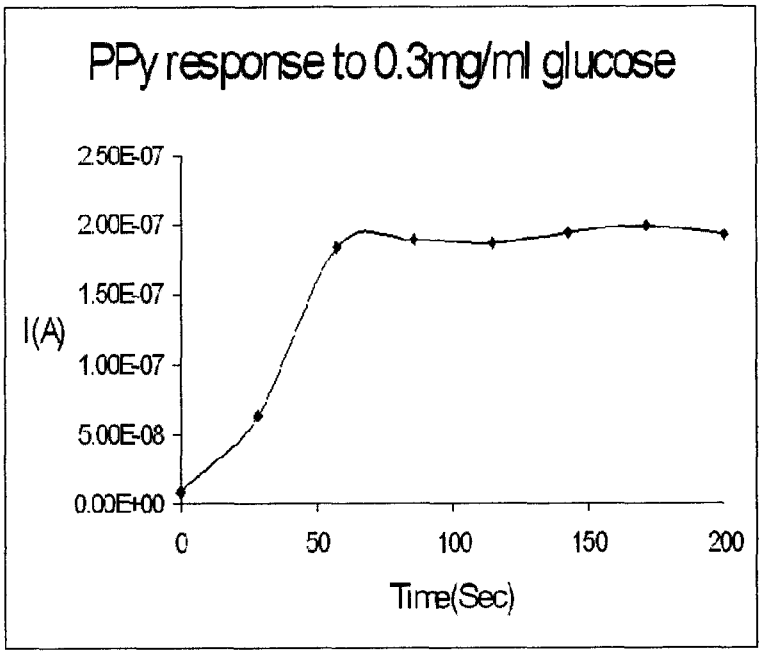

Figure 5.18 PPy microwire response to glucose solution of concentration 0.3 mg/ml.

Figure 5.19 represents the increase in the sensor current as glucose solution of successively higher concentration was used. The various concentrations of glucose solutions used were 0.2 mg/ml, 0.3 mg/ml, 0.5 mg/ml and 0.8 mg/ml.

Reproduced with permission of the copyright owner. Further reproduction prohibited without permission.

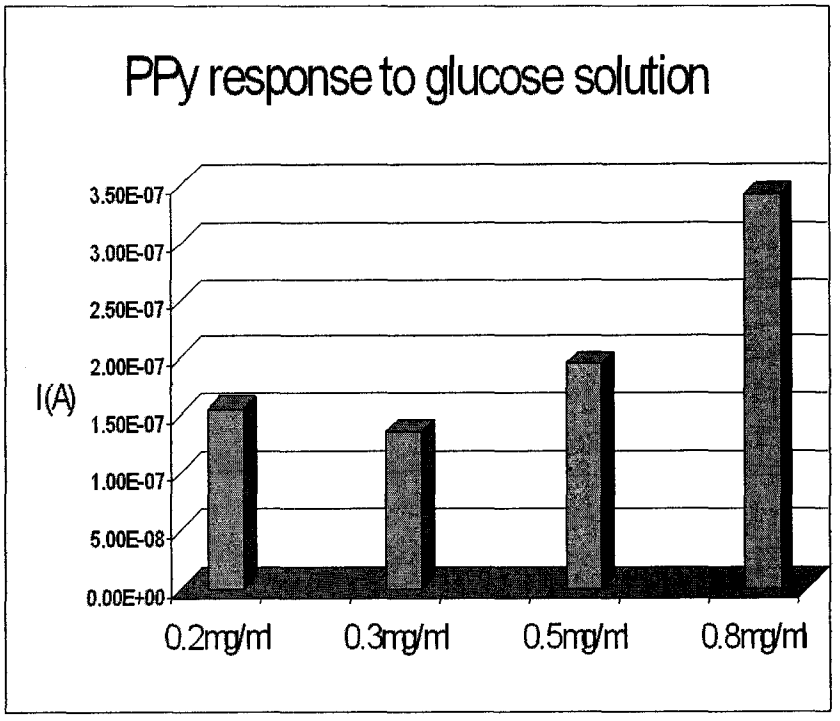

Figure 5.19 Current variation of PPy microwires to glusoce solution of various concentrations.

5.4 Surface-to-Volume Ratio and Sensitivity Comparison

As can be noted from Figure 5.4, the SI was higher for the PPy microwire than for the film within the humidity range of 45% to 58%. The entire surface area of the film may be modeled as multiple microwires of unit width, connected in parallel between the opposite edges at the electrodes [93]. These microwires may be further divided into blocks of unit area along the entire length (Figure 5.20).

Reproduced with permission of the copyright owner. Further reproduction prohibited without permission.

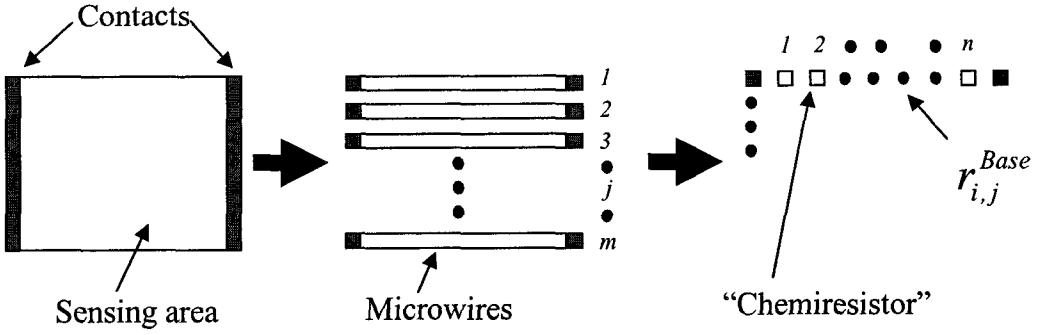

Figure 5.20 Relationship between a film sensor and an individual "chemiresistor" block.

These blocks of unit area may be regarded as individual "chemiresistor" elements, with the base resistance $r_{i,j}^{Base}$, which respond to the various concentrations of analytes with a unique change in conductivity. These "chemiresistor" blocks are electrically connected in a serial fashion between the opposite electrodes. Let the resistance of the block be $r_{i,j}^{'}$, upon exposure to an analyte. Therefore, the SI for this block would be $(\Delta R/R)_{Block} = (r_{i,j}^{'} - r_{i,j}^{Base})/(r_{i,j}^{Base})$. If the microwire is divided into "n" identical blocks, the total base resistance of a single microwire would be $n \times r_{i,j}^{Base}$. Upon exposure to analyte, the resistance would be $n \times r_{i,j}^{'}$. As there are "m" identical microwires connected in parallel, the overall base resistance would be $(n/m) \times r_{i,j}^{Base}$, and the resistance upon exposure to the analyte would be $(n/m) \times r_{i,j}^{'}$. The SI for the entire film would be

$$(\Delta R/R)_{Total} = \left\{[(n/m) \times r_{i,j}^{'} - (n/m) \times r_{i,j}^{Base}]/(n/m) \times r_{i,j}^{Base}\right\} = (\Delta R/R)_{Block}. \quad (1)$$

Reproduced with permission of the copyright owner. Further reproduction prohibited without permission.

It is observed from Equation (1) that when the SI is calculated from the overall device response, it reduces to the SI of a single "chemiresistor" unit block. The total number of blocks present on the surface does not matter, implying that SI is independent of the surface area of the sensor, whether it is a film or a microwire. The above reasoning holds true when the sensing area is uniformly and sufficiently exposed to the target analyte. However, if the analyte concentration is less, fewer molecules are available for the film sensor. In this case, when a film is exposed to the analyte molecules, a sparse distribution of the molecules on the exposed surface may be assumed. In this case some unit "chemiresistor" blocks may get exposed to the analyte, whereas other blocks may not get exposed at all. The blocks which get exposed will have a change in resistance, whereas for the other blocks, there is no change in resistance. The change in current in film sensor, brought about by the sparse distribution of the analyte molecules at lower concentrations may not be accurate. Reduction in surface area of the sensor may prove beneficial in this scenario. For the microwire sensor, a lower concentration of analyte molecules may be sufficient to cover the entire sensor and elicit an accurate response. Alternatively, the conducting polymer microwires have more exposure per unit sensing area, as compared to films at the same analyte concentration due to the higher surface-to-volume ratio of the micropatterns as compared to films. Consider a rectangular conducting polymer film, which has length a_1, width b_1, and thickness t (Figure 5.21). The sensing surface area is $(a_1 \times b_1 + 2 \times a_1 \times t + 2 \times b_1 \times t)$. The volume of the film is $(a_1 \times b_1 \times t)$. Therefore, the surface-to-volume ratio is $(1/t + 2/a_1 + 2/b_1)$.

Reproduced with permission of the copyright owner. Further reproduction prohibited without permission.

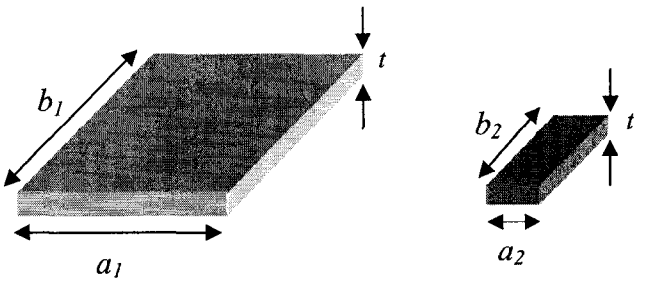

Figure 5.21 Comparison between a rectangular film and a microwire of same thickness where a1<<a2 and b1<<b2.

Similarly, for a conducting polymer microwire, which has length a_2 and width b_2, the surface-to-volume ratio is $(1/t + 2/a_2 + 2/b_2)$. Since $a_1 >> a_2$ and $b_1 >> b_2$, for a conducting polymer film of a particular thickness, its surface-to-volume ratio increases with a decrease in the length and width. The higher surface-to-volume ratio of the microwires was working to the advantage of the microwire sensor at low humidity (between 45% and 58%). Beyond 58% humidity, the film and the microwire began to saturate and the senstivity response was similar.

5.4.1 Partial Exposure of PPy Film Sensor

A simple experiment was performed to verify the fact that the response from a conducting polymer film is not accurate when the entire film surface is not exposed to an analyte. A PPy film (1 cm X 1 cm) was spin coated and made into a two probe "chemiresistor." The baseline resistance of the film was measured. The film sensor was placed inside an airtight chamber, and the two contact wires were taken out and connected to the Keithley probe station for I-V measurements (Figure 5.22).

Reproduced with permission of the copyright owner. Further reproduction prohibited without permission.

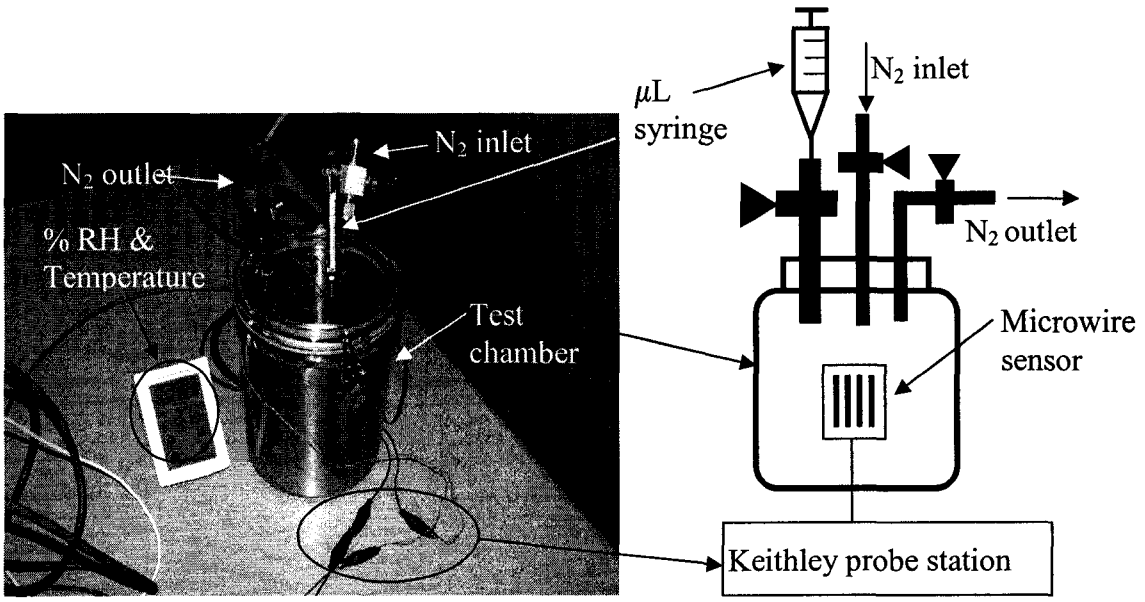

Figure 5.22 Experimental setup and schematic of the partial exposure experiment.

The humidity and temperature of the chamber were maintained at the room level. After the chamber was closed, the current of the sensor was measured at 10 V to determine the base resistance. Methanol (of known volume) was introduced into the chamber in a liquid form (as a droplet). The methanol droplet evaporated in 5-7 s inside the chamber. The final resistance was measured at the end of the exposure period of 120 s and the vapor exposure was stopped. The SI was calculated as $(R_{Methanol}\text{-}R_{Base}/R_{Base})$. After 120 s, the chamber was purged with nitrogen gas and vented. After the baseline resistance of the film recovered, the film was selectively taped to expose it partially to methanol vapor of the two concentrations, and the above procedure was repeated. The exposed area of the film was gradually decreased in steps as follows: three-quarters, half, and one-quarter.

It was found that the film was most sensitive when it was fully exposed to methanol vapor. As the film area was reduced, the sensitivity of the sensor was reduced

Reproduced with permission of the copyright owner. Further reproduction prohibited without permission.

at the same concentration of methanol vapor (Figure 5.23). The mass of methanol was calculated from the known volume and density of methanol at room temperature. The mass of air was calculated from the known volume of the chamber and the density of air at room temperature. The concentration was calculated in parts per thousand (ppth) from the ratio between the mass of methanol and that of air inside the test chamber. For a concentration of 3 ppth, the SI decreased from -0.029 for full exposure to -0.012 when only one-quarter of the film area was exposed. For 5 ppth, the SI reduced from -0.058 for full exposure to -0.026 for one-quarter of the exposed area (Figure 5.23).

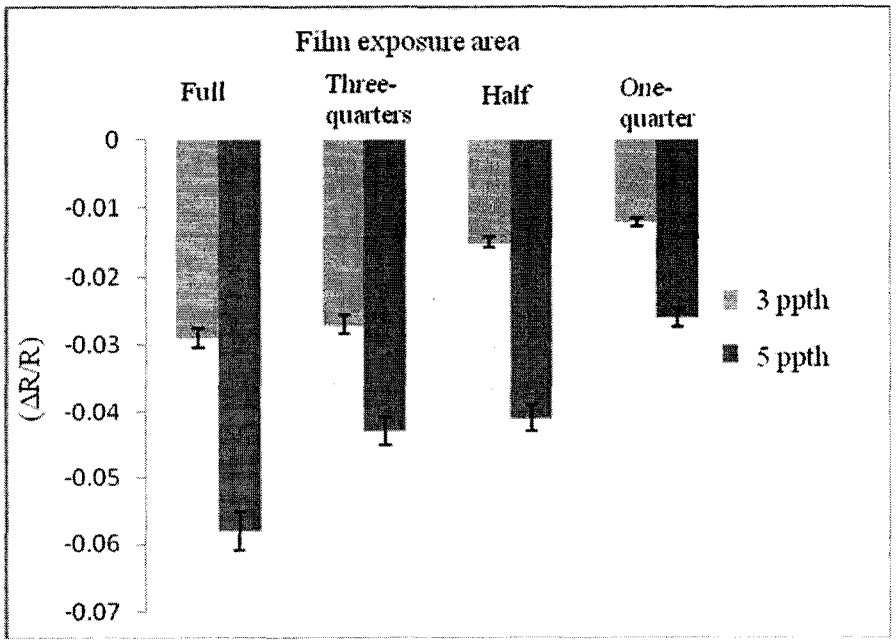

Figure 5.23 Relationship between the sensitivity of a PPy film to the exposed surface area.

Reproduced with permission of the copyright owner. Further reproduction prohibited without permission.

5.4.2 Experimental Comparison of Sensitivities of PPy and PEDOT Microwires and Film Sensor.

The sensitivity of PPy and PEDOT microwires of various surface-to-volume ratios were compared with that of a PPy and a PEDOT film of size 1 cm X 1 cm. The surface-to-volume ratio was varied by fabricating PPy and PEDOT microwires of various dimensions. The film thickness was kept constant. Silicon molds were fabricated using conventional photolithography and DRIE. The embossing temperature and pressure were 150° C and 50 MPa respectively for the ILL process. Figure 5.24 and Figure 5.25 shows one set of generated microwires of PPy which have been used for sensing. Similar microwires of PEDOT were fabricated using the same procedures. Table 5.1 lists the various dimensions of the PPy and PEDOT microwires fabricated with the ILL method.

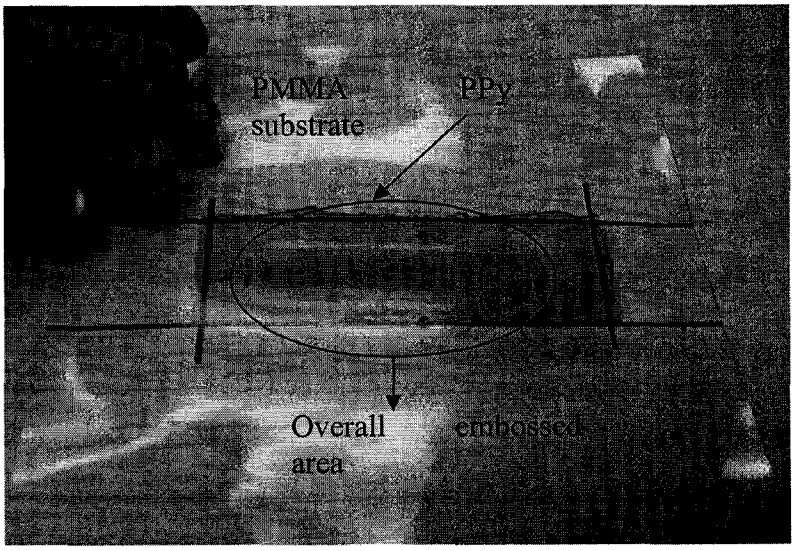

Figure 5.24 Optical picture of the overall view of the imprinted PPy microwires [91].

Reproduced with permission of the copyright owner. Further reproduction prohibited without permission.

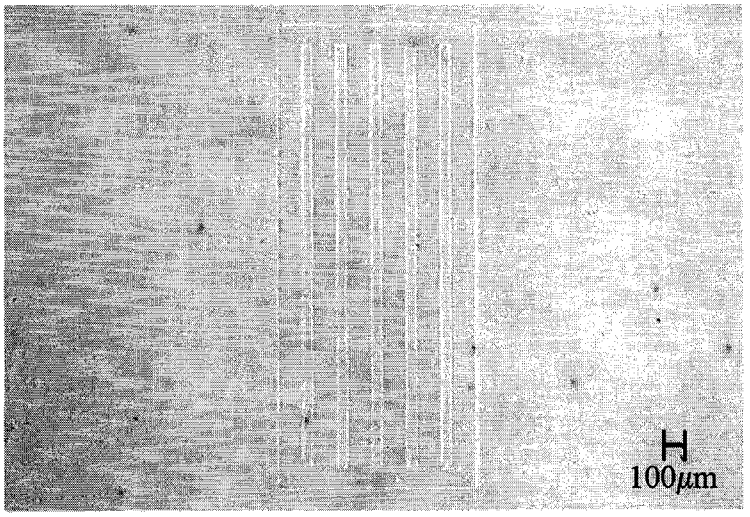

Figure 5.25 Optical picture of the close-up view of a set of PPy microwires. Each microwire is 50 μm wide and 2000 μm long [91].

Table 5.1 Dimensions of the of the PPy and PEDOT microwires fabricated with different surface-to-volume ratios

	Width (μm)	Length (μm)
Microwire Type I	300	5000
Microwire Type II	100	5000
Microwire Type III	100	2000

The experimental setup was similar to the one in Figure 5.22. The sensor was placed inside the chamber, and the two contact wires were taken out and connected to the Keithley probe station for I-V measurements. The humidity and temperature of the chamber were maintained at room level and kept constant. After the chamber was closed, the current of the sensor was measured at 10 V to determine the base resistance. Acetone (of known volume) was introduced into the chamber in a liquid form (as a droplet). This step was followed by the monitoring of the sensor's current with the applied voltage fixed at 10 V. The acetone droplet evaporated in 2 to 4 s inside the chamber. After the drop

Reproduced with permission of the copyright owner. Further reproduction prohibited without permission.

evaporated, the sensor's current was measured continuously for up to 120 s to determine the change in resistance. The sensor was comprised of six PPy and PEDOT microwires of uniform dimensions connected in parallel. There was 120 s of exposure to acetone vapor inside the chamber. After 120 s, the chamber was purged with nitrogen gas and vented. For the next round of testing, the chamber was closed and the above procedure was repeated. The mass of acetone was calculated from the known volume and density of acetone at room temperature. The mass of air was also calculated from the known volume of the chamber and density of air at room temperature. The concentration was calculated in parts per thousand (ppth) from the ratio between the masses of both acetone and air inside the test chamber. The acetone concentration was varied from 1 ppth to 7 ppth in steps for the PPy microwires and from 1 ppth to 6 ppth for the PEDOT microwires. The SI was calculated from the change in resistance upon exposure to acetone vapor as $(R_{Acetone} - R_{Base})/R_{Base}$. When the PPy and PEDOT microwires were exposed to the polar acetone molecules, there was a decrease in conductivity. The PPy and PEDOT microwires of Type III had the highest surface-to-volume ratio and the highest sensitivity response to the various acetone concentrations (Figures 5.26 and 5.27). The responses of the microwires have been approximated using a linear fit to observe the general sensitivity trends with increasing acetone concentrations.

Reproduced with permission of the copyright owner. Further reproduction prohibited without permission.

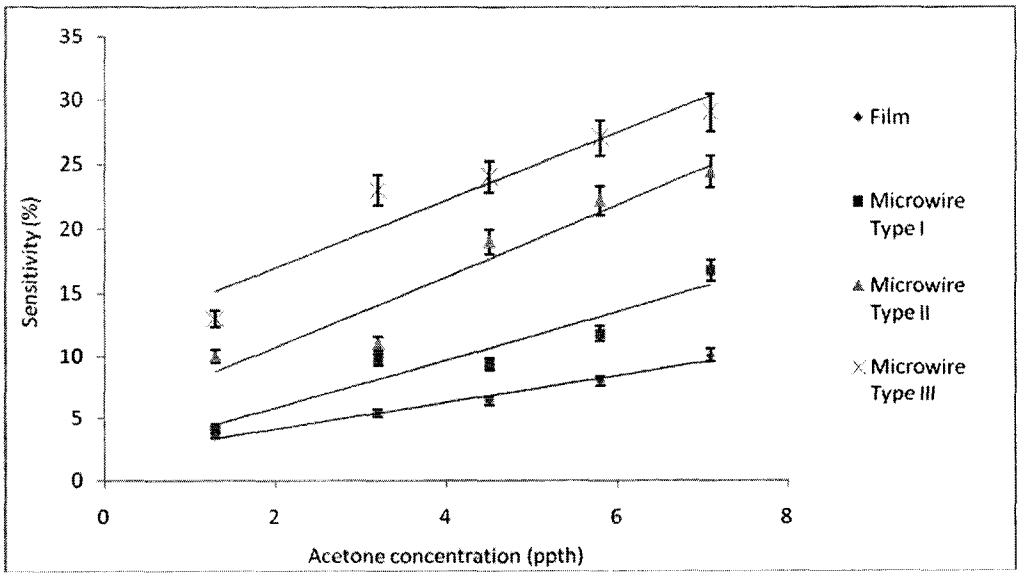

Figure 5.26 Sensitivity comparison between a PPy film and microwires of different surface-to-volume ratios.

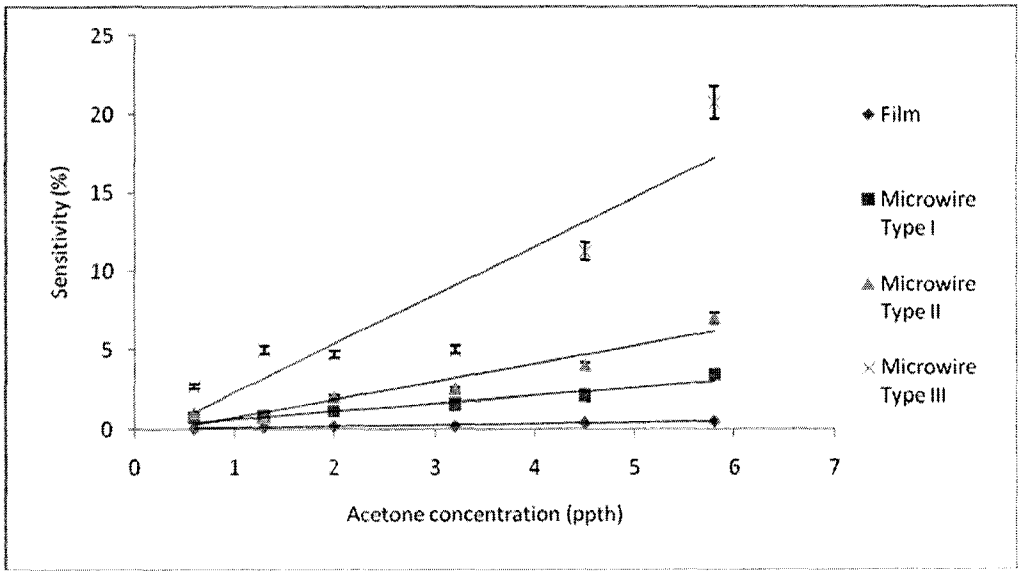

Figure 5.27 Sensitivity comparison between a PEDOT film and microwires of different surface-to-volume ratios.

Reproduced with permission of the copyright owner. Further reproduction prohibited without permission.

The responses of the PPy microwires are more widely spaced (Figure 5.26) than their PEDOT counterparts (Figure 5.27), while the overall trend was similar. In the case of PPy (Figure 5.26), the sensitivity increased from 3.6% for film sensor to 13% for Type III microwires, at a concentration of 1 ppth and from 10% for the film sensor to 29% for Type III microwires at a concentration of 7 ppth. In the case of PEDOT (Figure 5.27), the sensitivity increased from 0.05% for the film sensor to 3% for Type III microwires, at a concentration of 1ppth and from 0.5% for the film sensor to 20% for Type III microwires at a concentration of 7 ppth. This difference in sensitivity may be due to the chemical structure and individual interaction of the respective conducting polymers, PPy, and PEDOT, to acetone. More tests are required to establish the exact relationship between the change in sensitivity and that in the surface-to-volume ratio of the individual microwires. Also, the response of the Type III microwires could not be well approximated using the linear fit model. This point may be better explored by successively reducing the microwire dimensions and following their sensitivity response pattern.

Reproduced with permission of the copyright owner. Further reproduction prohibited without permission.

CHAPTER 6

FABRICATION OF PPy NANOWIRES USING THE ILL TECHNIQUE

The ILL method of fabricating conducting polymer micropatterns was extended to generate nanopatterns of PPy. Straight nanopatterns (or nanowires) of PPy of width 100 nm and 500 nm with lengths of 20 μm were fabricated using ILL. The objective of extending ILL to the nano-regime is to fabricate a sensor platform composed of multiple nano-sensing elements. The sensitivity of the sensor would be greatly enhanced by the increased surface-to-volume ratio of the nanowires. This idea was demonstrated previously by the increased sensitivity of the microwires with successively increasing surface-to-volume ratio. When multiple conducting polymers are patterned simultaneously, the sensor density could be increased greatly.

Some critical parameters concerning the nano-ILL approach are:

1. Thickness of the conducting polymer layer. The thickness needs to be less than the depth of the mold for cutting of the conducting polymer layer at the edges. The thickness of the insulating polymer layer does not matter.
2. Grain size of the conducting polymer layer. The grain size of the PPy layer was less than 100 nm.

Reproduced with permission of the copyright owner. Further reproduction prohibited without permission.

3. Embossing parameters: temperature and force of the imprinting process, demolding temperature, time of insertion, and depth of the mold.
4. Surface roughness of the silicon mold. If the surface of the silicon mold is rough due to processing or contamination, there may not be perfect contact between the mold and the substrate, resulting in improper pattern transfer.
5. Metrology of the embossed polymer: (i) using SEM to image the embossed patterns, since the stream of electrons in SEM may damage the embossed patterns, and (ii) using AFM to image the embossed patterns. The AFM cantilever tip may scratch and damage the embossed patterns on the substrate.

6.1 Silicon Nanomolds

The silicon nanomolds used in the ILL approach were fabricated using Focused Ion Beam (FIB) technique. They were obtained from the company, Applied Nano Pvt. Ltd., Santa Clara, California. The FIB technique was developed in late 1970s and early 1980s. Due to use of very short wavelengths and a large energy density, the FIB technique has become a very popular method for fabricating micro- and nano-structures [94,95,96]. This tool has become an important one in semiconductor research and processing environments. In the semiconductor industry, it is used for the localized deposition and milling of conductors and insulators. This ability is useful in mask repair, process control, and failure analysis. There are two basic working modes, including ion beam direct write and ion beam projection. In the ion beam direct write technique, an energetic beam of ions is focused on the substrate. These energetic ions knock off the host atoms from the surface upon impact. This procedure is also called FIB milling and is a maskless direct-write technology. For the ion beam projection approach, a collimated

Reproduced with permission of the copyright owner. Further reproduction prohibited without permission.

beam of ions is focused on a mask, and the resulting image is reduced and projected on the substrate. This method is also known as ion beam lithography. It is still in the developmental stage with challenges existing in the design of the ion optics. The ion sources currently available include Al, As, Au, B, Be, Bi, Cs, Cu, Ga, Er, Fe, H, In, Li, Ni, P, Pb, Pd, Pr, Pt, Si, Sn, U, and Zn. The ion species are produced from liquid-metal alloy sources, as original metals may have high melting temperature, be volatile or may be highly reactive.

The popular species for micro- and nano-fabrication are As, Be, Ga, and Si. The species As, B, and P are interesting as semiconductor doping sources. FIB has several advantages over other high energy particle techniques. In the case of FIB, the heavy ions are able to directly sputter hard materials, including semiconductors, metals, and ceramics as compared to electrons and photons. This method is also able to do away with designing complicated masks and photoresists. No backscattered electrons are generated which limits the linewidth in electron beam lithography. Using heavy ions in FIB reduces the lateral scattering as the ions strike where they are intended to strike. FIB is routinely used to fabricate nano-scale holes and channels [97]. As the dimensions of the structures have to be controlled in the nanometer scale, the milling yield with respect to the ion dose has to be precisely controlled.

Figure 6.1 represents an AFM scanned image of a silicon nano-mold. The channels are 500 nm wide and 20 μm long. The channels are spaced 500 nm apart and are about 1.5 μm in depth.

Reproduced with permission of the copyright owner. Further reproduction prohibited without permission.

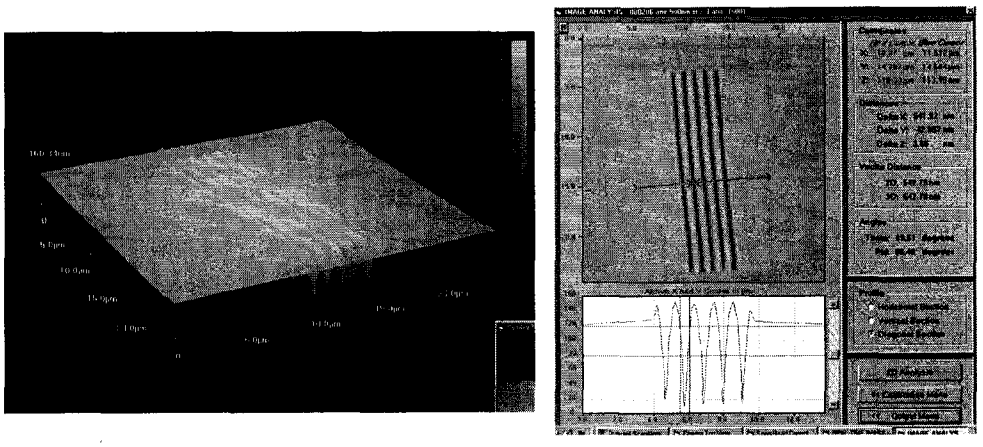

Figure 6. 1 AFM scan of a silicon nanomold containing 500 nm wide channels which are 20 μm long.

Figure 6.2 shows SEM images of another silicon nano-mold. The channels are 100 nm in width and 5 μm in length. They are spaced about 100 nm apart and are about 500 nm in depth.

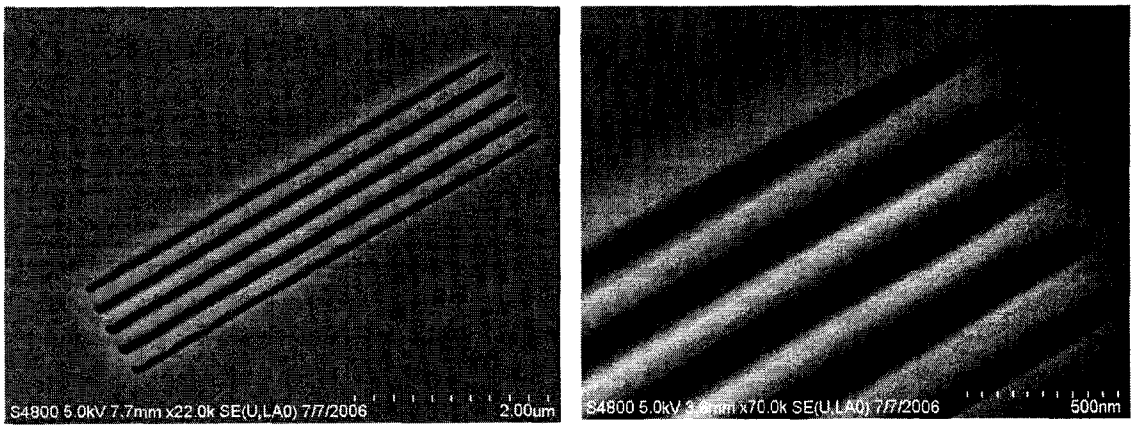

Figure 6. 2 SEM picture of a silicon nanomold with channels of width 100 nm and length 5 μm.

Reproduced with permission of the copyright owner. Further reproduction prohibited without permission.

6.2 Mold and Substrate Preparation for Nanoembossing

6.2.1 Mold Preparation for Nanoembossing

The silicon molds were cleaned with dry N_2 the first time it was to be used for the embossing process. No AFM scan of the mold was taken before embossing. This was for maintaining the pristine surface of the silicon mold and avoid contaminating the surface with the AFM cantilever probe. Also, SEM pictures of the molds were not taken before the first embossing was done. There was a possibility that the high energy electron beams from the SEM might charge the surface of the silicon mold.

After the mold was used once, it was cleaned in four steps. After each step, the mold was observed in an optical microscope to see if the channels were empty of any residual polymer after embossing. First, it was cleaned with DI water. Afterwards, it was cleaned with acetone and NanoStrip™ solution. If the mold was still not clean, it was subjected to oxygen plasma. The oxygen flow rate was about 80 sccm and the plasma power was 300 watts. The duration of exposure varied from 5-7 minutes. Aggressive cleaning procedures such as washing the mold with NanoStrip™ solution or subjecting it to oxygen plasma were avoided, as there was a possibility of increasing the surface roughness of the silicon mold. This change would induce stiction between the silicon mold and the conducting polymer layer.

6.2.2 Substrate Preparation

The substrate was carefully prepared for the nano-ILL process. PMMA was chosen as the intermediate layer due to similar reasons as in the micro-ILL process. PMMA solution in 9% chlorobenzene was obtained from Sigma Aldrich Co. The molecular weight of the PMMA used was 495 K. This solution was of moderate viscosity

Reproduced with permission of the copyright owner. Further reproduction prohibited without permission.

and allowed favorable pattern transfer in the nano-scale. PMMA solution was spin coated over a silicon wafer. The thickness of the spin coated PMMA layer was 1.2 μm. After spin coating, the PMMA layer was cured at 150° C for 1 hour. Curing the PMMA layer drove-off the solvents and solidified the layer. Additionally, it relieved it of the stresses inherent in the layer after spin coating. For the conducting polymer layer, PPy in 5% water solution was chosen. It was obtained from Sigma Aldrich Co. The PPy solution was further diluted by mixing it with DI water in the ratio of 1:2 (v/v). The PPy solution was diluted to decrease its viscosity so that upon spin coating, a very thin layer could be generated. The cured PMMA layer was subjected to oxygen plasma to make it hydrophilic. This treatment was done in an Reactive Ion Etching (RIE) machine (Techniques MicroRIE^{TM}). The plasma power was 300 watts and the oxygen flow rate was 50 sccm. The duration of exposure was 3 minutes. The oxygen plasma treatment of the PMMA surface was critical to generating a good PPy layer after spin coating. In case the surface of PMMA is not hydrophilic enough, the PPy solution would fail to form a uniform layer. This result is more likely as the PPy solution was further diluted with water. The spin speed of the diluted PPy solution was 2500 RPM. This speed generated a PPy layer which was about 75 nm in thickness. Efforts were made to decrease the thickness of the PPy film further by diluting the PPy solution with DI water in the ratios of 1:3 (v/v) and 1:4 (v/v) and also increasing the spin speed up to 3500 RPM. However, the diluted PPy solution was not able to form a uniform film and only resulted in patches on the PMMA surface. After the PPy layer was spin coated on the PMMA surface, the substrate was heated to 60° C for 1 hour. This was done to cure the PPy layer and reduce the surface stress in the layer.

Reproduced with permission of the copyright owner. Further reproduction prohibited without permission.

6.3 Nanoembossing Experimental Results

6.3.1 Nanoembossing of the 500 nm Wide Silicon Channels

The recipe for imprinting the 500 nm and 20 μm long silicon channels on the PPy is listed in Table 6.1. Position control mechanism was used for imprinting the 500 nm lines on PPy. The tool was programmed to move 1 μm inside the substrate. The temperature of the imprinting process was fixed at 160° C. The mold insert duration was 600 s. The maximum force generated in the process was 1085 N. The embossing program is listed in Table 6.1.

Table 6. 1 Embossing recipe for imprinting the 500 nm wide PPy nanowires.

Initialize Force Control (true/false=0)	Initialize the force unit.
Heating (Top=90° C, Bottom=90° C)	Start heating of the tool and substrate.
Close chamber( )	Close the embossing chamber
Evacuate chamber ( )	Evacuate the embossing chamber.
Wait time (t=20 s)	Wait for process stabilization.
Touch force (Force=50 N)	The initial contact force between the tool and the substrate.
Wait time (t=20 s)	Wait for process stabilization.
Heating (Top=130° C, Bottom=130° C)	Start heating the tool and the substrate to the specified temperature limit.
Wait time (t=60 s)	Wait for process stabilization.
Temp>=(Temp=105° C, channel=10)	Wait until the temperature of the substrate is above the specified limit.
Wait time (t=10 s)	Wait for process stabilization.
Position relative (Position = -0.001 mm, velocity=1.0 mm/min, Max force=500 N)	Move the tool down into the substrate by 1 μm.
Wait time (t=600 s)	Wait for process stabilization.
Cooling (Top=100° C, Bottom=100° C)	Start cooling the tool and the substrate.
Wait time (t=30 s)	Wait for process stabilization.
Cooling (Top=78° C, Bottom=78° C)	Continue cooling the tool and substrate until the specified temperature.
Wait time (t=60 s)	Wait for process stabilization.
Temp<=(Temp=95° C, channel=10)	Wait until the temperature of the substrate is below the specified limit.

Reproduced with permission of the copyright owner. Further reproduction prohibited without permission.

DemoldingAdv(Stretch=1.5 mm, velocity=3.0 mm/min)	Demold the tool from the substrate with the specified velocity.
Cooling (Top=50° C, Bottom=50° C)	Continue cooling the tool and substrate until the specified temperature.
Wait time (t=60 s)	Wait for process stabilization.
Venting chamber ( )	Vent the embossing chamber.
Open chamber ( )	Open the embossing chamber.

The imprinted PPy nanowires were scanned with an AFM. Figure 6.3 shows the fabricated PPy lines. The width of the lines were about 500 nm and the height was 100 nm. All the lines were imprinted uniformly and were of identical heights.

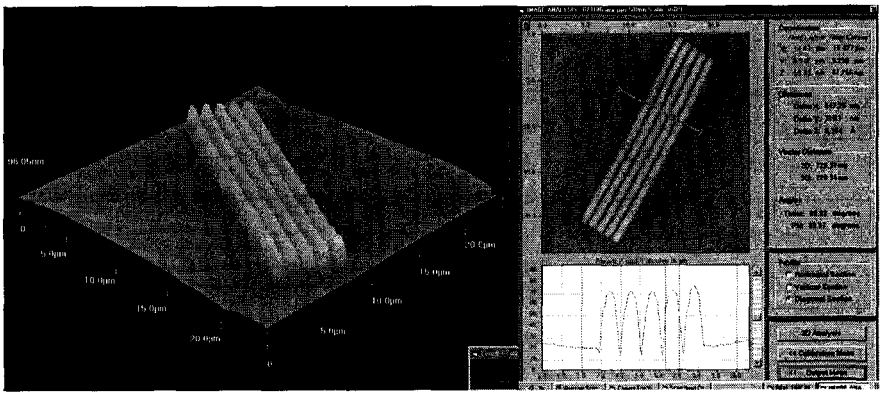

Figure 6. 3 AFM scan of the embossed PPy nanowires, 500 nm wide and 20 μm long.

6.3.2 Nanoembossing of the 100 nm Wide Silicon Channels

The 100 nm silicon channels with pitch of 1 μm were embossed using force control recipe. The embossing force was fixed at 2200 N. The mold insert duration was 500 s. The temperature of the imprinting process was fixed at 140° C. The hot embossing recipe is listed in Table 6.2.

Reproduced with permission of the copyright owner. Further reproduction prohibited without permission.

Table 6. 2 Hot embossing recipe for embossing the 100 nm wide silicon channels on PPy.

Initialize Force Control (true/false=0)	Initialize the force unit.
Heating (Top=90° C, Bottom=90° C)	Start heating of the tool and substrate.
Close chamber ( )	Close the embossing chamber
Evacuate chamber ( )	Evacuate the embossing chamber.
Wait time (t=20 s)	Wait for process stabilization.
Touch force (Force=50 N)	The initial contact force between the tool and the substrate.
Wait time (t=20 s)	Wait for process stabilization.
Heating (Top=130° C, Bottom=130° C)	Start heating the tool and the substrate to the specified temperature limit.
Wait time (t=20 s)	Wait for process stabilization.
Temp>=(Temp=110° C, channel=10)	Wait until the temperature of the substrate is above the specified limit.
Wait time (t=20 s)	Wait for process stabilization.
Heating (Top=140° C, Bottom=140° C)	Start heating the tool and the substrate to the specified temperature limit.
Force Control (Force=2200 N, Velocity=1.0 mm/min	Apply the specified force on the substrate.
Wait time (t=500 s)	Wait for process stabilization.
Cooling (Top=100° C, Bottom=100° C)	Start cooling the tool and the substrate.
Wait time (t=60 s)	Wait for process stabilization.
Cooling (Top=75° C, Bottom=75° C)	Continue cooling the tool and substrate until the specified temperature.
Wait time (t=60 s)	Wait for process stabilization.
Temp<=(Temp=95° C, channel=10)	Wait until the temperature of the substrate is below the specified limit.
DemoldingAdv(Stretch=1.5 mm, velocity=1.0 mm/min)	Demold the tool from the substrate with the specified velocity.
Cooling (Top=50° C, Bottom=50° C)	Continue cooling the tool and substrate until the specified temperature.
Wait time (t=60 s)	Wait for process stabilization.
Venting chamber ( )	Vent the embossing chamber.
Open chamber ( )	Open the embossing chamber.

The result of the imprinting process was partial pattern transfer (Figure 6.4). This result occurred as the nanochannels were partially filled up with PPy. The PPy flow into the channels was non-uniform to form the edges of the channels, while leaving the

Reproduced with permission of the copyright owner. Further reproduction prohibited without permission.

middle portion unfilled. This difference may be due to inadequate imprinting force or lesser duration of imprint.

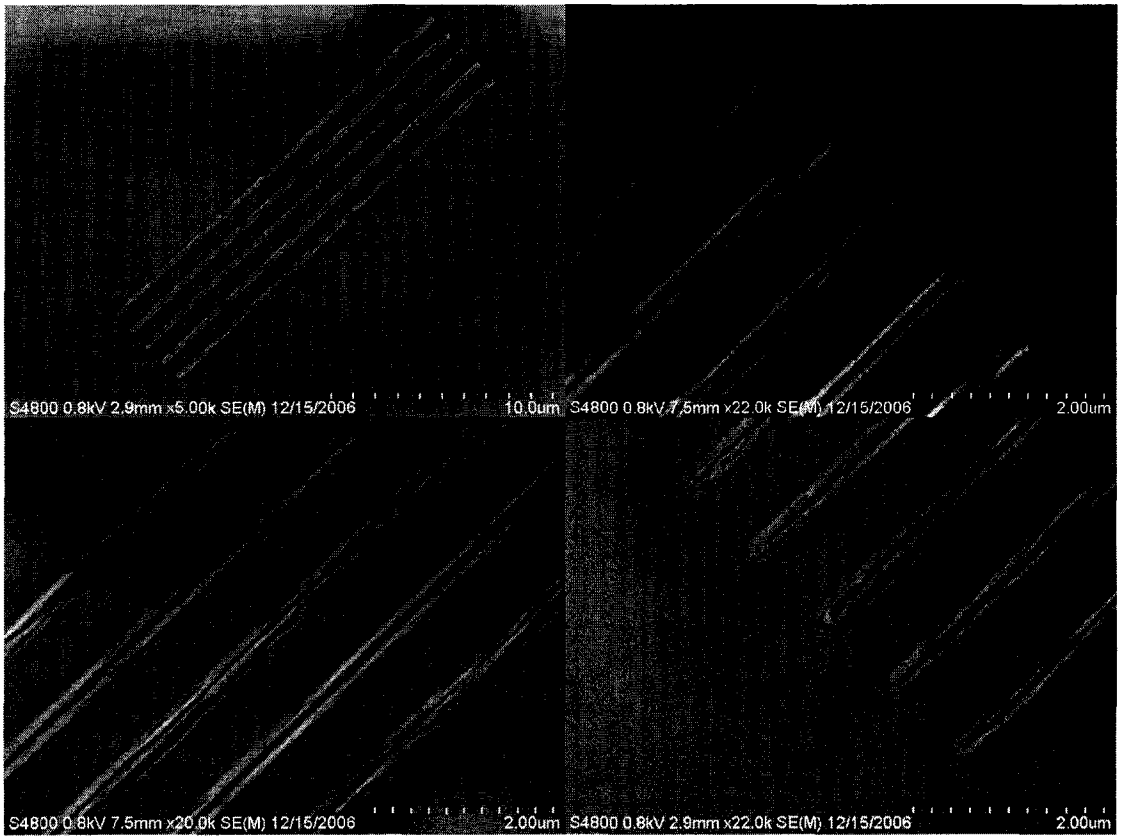

Figure 6. 4 SEM pictures of the partially filled PPy nanowires, 100 nm wide and 20 μm long. The pitch of the lines was 1 μm.

In order to achieve satisfactory pattern transfer, the embossing force was increased to 2300 N. The temperature and duration of imprint were 140° C and 500 s respectively. Force control recipe was used for the imprinting. Figure 6.5 shows the SEM image of the embossed PPy nanowires. Increasing the embossing resulted in better pattern transfer results.

Reproduced with permission of the copyright owner. Further reproduction prohibited without permission.

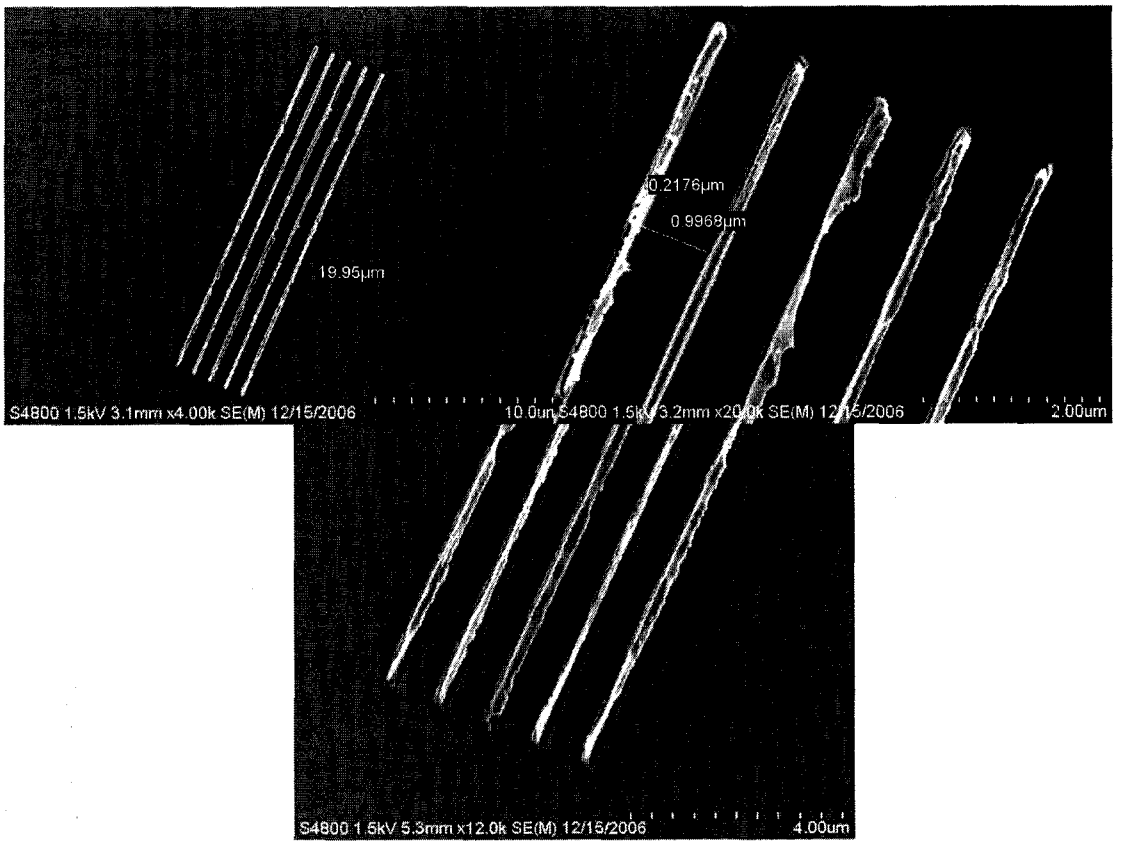

Figure 6. 5 PPy nanowires 100 nm wide and 20 μm long. The pitch of the lines was 1 μm.

6.3.3 Nanoembossing of the 100 nm Wide Silicon Nanochannels with a Pitch of 500 nm

Imprinting was done with a silicon mold with 100 nm wide and 20 μm long channels. The pitch of the channels was 500 nm. The pitch of the silicon nanochannels was varied in order to investigate the effect of channel spacing on the pattern transfer result. A force control mechanism was chosen, and the embossing force was fixed at 2350 N. The embossing temperature and duration were 140° C and 500 s, respectively. The resulting pattern transfer was satisfactory with complete filling of the nanochannels (Figure 6.6).

Reproduced with permission of the copyright owner. Further reproduction prohibited without permission.

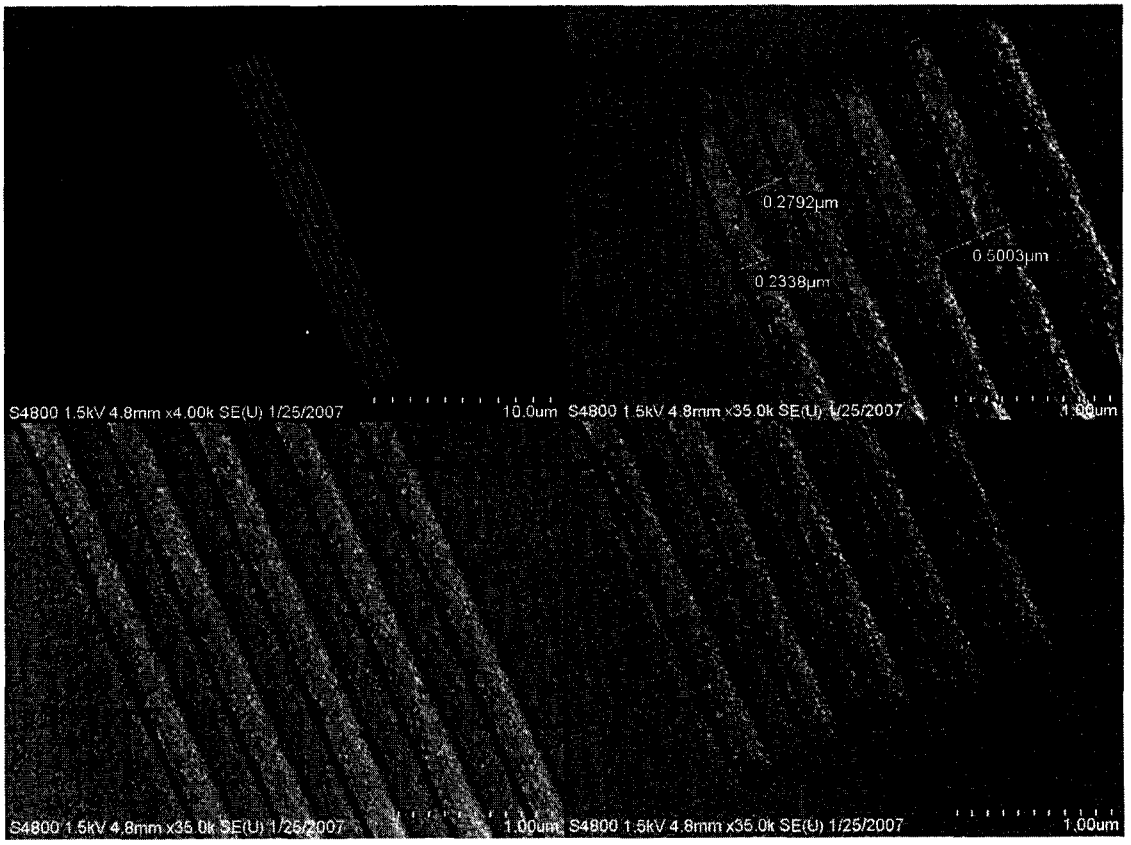

Figure 6. 6 SEM pictures of the embossed PPy nanowire, 100 nm wide and 20 μm long. The pitch of the nanowires was 500 nm.

Reproduced with permission of the copyright owner. Further reproduction prohibited without permission.

CHAPTER 7

CONCLUSIONS AND FUTURE DIRECTION

7.1 Conclusions

A novel ILL method to pattern conducting polymers was proposed. The purpose was to overcome the shortcomings of the current conducting polymer patterning techniques, which include inkjet printing, soft lithography, UV lithography, and hot embossing. Using the ILL method, microwire and microheater patterns varying in dimensions and made of PPy, PEDOT-PSS and SPANI were fabricated simultaneously on a common substrate. During the fabrication of the 5 μm and 10 μm wide microheater patterns, there was evidence of non-uniform fluid flow. This variation occurred when the silicon mold had large and small features in close proximity. Also a height difference occurred between the smaller and larger imprinted features. This aspect was simulated in ANSYS to gain a better understanding of the molding process. The simulation results were similar to the experimental results, confirming non-uniform fluid flow phenomenon. The ILL technique successfully overcame the "depth of mold" and "residual layer" issues. This method generated conducting polymer micropatterns with good resolution and high throughput and has the potential of becoming an important technique for massive production of conducting polymers patterns. The ILL method gives substantial flexibility of generating several different conducting polymer micropatterns on a common

Reproduced with permission of the copyright owner. Further reproduction prohibited without permission.

substrate. The imprinted microwires of PPy, PEDOT-PSS, and SPANI were used as sensing components to detect various analytes. The sensitivity response to humidity of a single PPy microwire was compared with a PPy film of larger dimensions. The PPy microwire exhibited greater sensitivity at lesser humidity levels as compared to the PPy film. It was observed that at higher humidity levels, both the film and microwire responses are similar. Film sensors did not give accurate response when partially exposed to methanol vapor. This scenario may arise when detecting targets in little quantities. This finding was confirmed by exposing a PPy film sensor to methanol vapor of two concentrations (3 ppth and 5 ppth). The exposed surface area of the film sensor was successively reduced. The sensitivity results showed that as the surface area of the sensor was reduced, the SI decreased, even though the concentration of the analyte remained the same. The high surface-to-volume ratio of the micropatterns helped increase the sensitivity of the microwires.

The relationship between the surface-to-volume ratio and sensitivity of the microwires at various analyte concentrations was investigated. PPy and PEDOT microwires of different surface-to-volume ratios were fabricated. The microwires were exposed to acetone vapor of concentrations varying from 1 ppth to 7 ppth. There was an increase in sensitivity with increasing surface-to-volume ratio. This change implied that smaller microwires were more sensitivive than the larger ones at same concentration of the analyte. A layer of GOD was applied on top of the PPy microwires for glucose sensing. The concentration of the glucose solution was varied from 2 mg/ml to 8 mg/ml. There was an increase in response current as the glucose concentration was increased.

Reproduced with permission of the copyright owner. Further reproduction prohibited without permission.

Two sets of microwires of PPy, PEOT-PSS, and SPANI were fabricated on a common substrate. PPy and SPANI microwires were used to sense for methanol and toluene, and PEDOT-PSS and SPANI microwires were employed to distinguish between acetone and toluene. From the electrical response, it was concluded that methanol and acetone dominated the conductivity characteristics of the three conducting polymer microwires. Tolune did not affect the conductivity of the PPy, SPANI and PEDOT microwires in mixtures due to its non-polar nature. Finally, the ILL method was used to imprint nano-channels in PPy. Nano-channels of width 100 nm and 500 nm were etched into a silicon substrate using FIB technique. After embossing, PPy nanowires of width 200 nm and 500 nm were obtained.

7.2 Future Direction

In the near future, we would like to continue to explore nano-imprinting using the ILL method. The goal is to be able to fabricate multiple nanopatterns of different conducting polymers simultaneously. The nanopatterns are required to be cut-off and isolated in the intermediate-layer polymer similar to their micro counterparts. The imprinting process has to be optimized for repeatability and consistency with control over the critical process parameters. The flow dynamics of the intermediate-layer and conducting polymers need to be studied. Different conducting polymers and alternative intermediate-layer polymers need to be explored for nanoembossing. New designs of nanopatterns need to be developed, which would be individually addressable for sensing applications. System integration of a fabricated nanosensor platform with the appropriate signal processing circuitry also needs to be considered for any sensing application.

Reproduced with permission of the copyright owner. Further reproduction prohibited without permission.

REFERENCES

[1] The Nobel Prize in Chemistry, *Conducting Polymers*, pp. 1-16, 2000.

[2] Basudam Adhikar and Sharmistha Majumdar. "Polymers in sensor applications," *Progress in Polymer Science,* Vol. 29, pp. 699-766, 2004.

[3] W. Mokua, D. Kohl and G. Heiland. "An SnO2 thin film for sensing arsine," *Sensors Actuators,* Vol. 4, pp. 283-289, 1985.

[4] G. S. V. Coles, K. J. Gallagher and J. Watson. "Fabrication and preliminary tests on Tin(IV) oxide-based gas sensors," *Sensors Actuators,* Vol. 7, pp. 89-96, 1985.

[5] P. J. Shaver. "Activated tungsten oxide gas detectors," *Applied Physics Letters,* Vol. 124, pp. 1443-1446, 1967.

[6] N. Yamazoe, J. Hisamoto, N. Miura and S. Kuwata. "Potentiometric solid-state oxygen sensorusing lanthanum fluoride operative at room temperature," *Sensors Actuators,* Vol.12, pp. 415-423, 1987.

[7] G. Berthet, J. P. Blanc, J. P. Germain, A. Larbi, C. Marleysson and H. Robert. "Electroactive polymes in thin layers: a potential application as gas sensor," *Synthetic Metals,* Vol. 18, pp. 715-720, 1987.

[8] K. Nagata, M. Nishino and K. S. Goto. "Humidity sensor with Strontium cerium ytterbium oxide solid electrolyte for high temperature use," *Journal of Electrochemical Society,* Vol. 63, pp. 28-29, 1987.

[9] J. Wang and P. Tuzhi. "Selectivity and sensitivity improvements at perfluorinated isomer/cellulose acetate bilayer electrodes," *Analytical Chemistry,* Vol. 56, pp. 3257-3261, 1985.

[10] U. Wuthier, H. V. Pham, R. Zuend, D. Welti, R. J. J. Funck, A. Bezegh, D. Ammann, E. Pretsch and W. Simon. "Tin organic compounds as neutral carriers for anion selective electrodes," *Analytical Chemistry,* Vol. 56, pp. 535-538, 1984.

Reproduced with permission of the copyright owner. Further reproduction prohibited without permission.

[11] P. Schulthess, D. Ammann, B. Kraulter, C. Caderas, R. Stepanek and W. Simon. "Nitirite-selective liquid membrane electrode," *Analytical Chemistry,* Vol. 57, pp. 1397-1340, 1985.

[12] G. Inzelt, M. Pineri, J. W. Schultze and M. A. Vorotyntsev. "Electron and proton conducting polymers: recent developments and prospects," *Electrochimical Acta,* Vol. 45, pp. 2403-2421, 2000.

[13] B. Wessling. "Passivation of metals by coating with polyaniline: Corrosion potential shift and morphological changes," *Advanced Materials,* Vol. 6, pp. 226-228, 1994.

[14] D. W. DeBerry. "Modifications of the electrochemical and corrosion behavior of stainless steels with an electroactive coating," *Journal of Electrochemical Society,* Vol. 132, pp. 1022-1026, 1985.

[15] N. Ahmed and A. G. MacDiarmid. "Inhibition of corrosion of steels with the exploitation of conducting polymers," *Synthetic Metals,* Vol. 78, pp. 103-110, 1996.

[16] D. Xie, Y. Jiang, W. Paw, D. Li, Z. Wu and Y. Li. "Fabrication and characterization of Polyaniline based gas sensors by ultra-thin film technology," *Sensors Actuators B,* Vol. 81, pp. 158-161, 2002.

[17] Q. Contractor, T. N. Sureshkumar, R. Narayanan, S. Sukeerthi, R. Lal and R. S. Srinivasa. "Conducitnng polymer-based biosensors," *Electrochimica Acta,* Vol. 39, pp. 1321-1324, 1994.

[18] L. S. Hwang, J. M. Ko, H. W. Rhee and C. Y. Kim. "A polymer humidity sensor," *Synthetic Metals,* Vol. 57, pp. 3671-3676, 1993.

[19] Andrzej Lewandowski, Katarzyna Skorupska and Jadwiga Malinska. "Novel poly(vinyl alcohol)–KOH–H_2O alkaline polymer electrolyte," *Solid State Ionics,* Vol. 3, pp. 265-271, 2000.

[20] C. Arbizzani, M. Mastragostino and L. Meneghello. "Polymer-based redox supercapacitors: A comparative study," *Electrochimica Acta,* Vol. 41, pp. 21-26, 1996.

[21] F. Jonas and G. Heywang. "Technical applications for conductive polymers," *Electrochimica Acta,* Vol. 39, pp. 1345-1347, 1996.

[22] J. C. Gustafsson-Carlberg, O. Inganas, M. R. Andersson, C. Booth, A. Azens and C. G. Granqvist. "Tuning the bandgap for polymeric smart windows and displays," *Electrochimica Acta,* Vol. 13, pp. 2233-2235, 1995.

Reproduced with permission of the copyright owner. Further reproduction prohibited without permission.

[23] Hayer, A. Köhler, E. Arisi, I. Bergenti, A. Dediu, C. Taliani, M. Al-Suti and M.S. Khan. "Polymer light-emitting diodes with spin-polarised charge injection," *Synthetic Metals*, Vol. 147, pp. 155-158, 2004.

[24] Lei Wen and N. M. Kocherginsky. "Doping-dependent ion selectivity of polyaniline membranes," *Synthetic Metals,* Vol. 106, pp. 19-27, 1996.

[25] Lisowska-Oleksiak, U. Lesińska, A.P. Nowak and M. Bocheńska. "Ionophores in polymeric membranes for selective ion recognition; impedance studies," *Electrochimica Acta,* Vol. 51, pp. 2120-2272, 2006.

[26] Colin Pratt, *Report on conducting polymers*, pp. 1-15, 1996.

[27] Larry Rupptecht, *Conductive polymers and plastics,* Plastic design library, New York, 1999.

[28] G. MacDiarmid. "Synthetic Metals: A novel role for organic polymers" *Angewandte Chemie International Edition,* Vol. 40, pp. 2581-2590, 2001.

[29] S. Roth and H. Bleier. "Solitons in polyacetylene," *Advances in Physics*, Vol. 36, pp. 385–462, 1987.

[30] J. Heeger, S. Kivelson, J. R. Schrieffer and W. P. Su. "Solitons in conducting polymers," *Reviews of Modern Physics*, Vol. 60, pp. 781–850, 1988.

[31] S. Kivelson. "Electron hopping conduction in the soliton model of polyacetylene," *Physical Review Letters,* Vol. 46, pp. 1344-1348, 1981.

[32] A. J. Epstein, H. Rommelman, R. Bigelow, H. W. Gibson, D. M. Hoffmann and D. B. Tanner. "Role of solitons in nearly metallic polyacetylene," *Physical Review Letters,* Vol. 50, pp. 1866–1869, 1983.

[33] S. Stafstrom and J. L Bredas. "Evolution of the electronic structure of polyacetylene and polythiophene as a function of doping level and lattice conformation," *Physical Review B,* Vol. 38, pp. 4180–4191, 1988.

[34] P. J. Phillips. "Polymer crystals," *Reports on Progress in Physics,* Vol. 53, pp. 549-604, 1980.

[35] S. K. M. Jönsson, W. R. Salaneck and M. Fahlman. "Spectroscopy of ethylenedioxy- thiophene-derived systems: from gasphase to surfaces and interfaces found in organic electronics," *Journal of Electron Spectroscopy and Related Phenomena,* Vol. 137, pp. 805–809, 2004.

Reproduced with permission of the copyright owner. Further reproduction prohibited without permission.

[36] S. Timpanaro, M. Kemerink, F. J. Touwslager, M. M. Kok and S.Schrader. "Morphology and conductivity of PEDOT/PSS films studied by scanning–tunneling microscopy," *Chemical Physics Letters,* Vol. 394, pp. 339–343, 2004.

[37] J. Y. Kim, J. H. Jung, D. E. Lee and J. Joo. "Enhancement of electrical conductivity of poly(3,4-ethylenedioxythiophene)/poly(4-styrenesulfonate) by a change of solvents," *Synthetic Metals,* Vol. 126, pp. 311–316, 2002.

[38] Aleshin, R. Kiebooms, R. Menon and A. J. Heeger. "Electronic transport in doped poly(3,4-ethylenedioxythiophene) near the metal-insulator transition," *Synthetic Metals*, Vol. 90, pp. 61-68, 1997.

[39] F. Mott and E. Davis. *Electronic processes in non-crystalline materials*, Oxford: Clarendon Press, 1979.

[40] S. Geetha, C. R. K. Rao, M. Vijayan and D. C. Trivedi. "Biosensing and drug delivery by polypyrrole," *Analytica Acta,* Vol. 568, pp. 119-125, 2006.

[41] Lin-Xia Wang, Xin-Gia Li and Yu-Liang Yang. "Preparation, properties and applications of polypyrroles," *Reactive and Functional Polymers,* Vol. 47, pp. 125-139, 2001.

[42] D. Kincal, A. Kumar, A. D. Child and J. R. Reynolds. "Conductivity switching in polypyrrole-coated textile fabrics as gas sensors," *Synthetic Metals,* Vol. 92, pp. 53-56, 1998.

[43] N. T. Kemp, G. U. Fianagan, A. B. Kaiser, H.J. Trodahl, B. Chapman, A.C. Partridge and R.G. Buckley. "Temperature-dependent conductivity of conducting polymers exposed to gases," *Synthetic Metals,* Vol. 101, pp. 434-435, 1999.

[44] Juan C. Vidal, Esperanza García and Juan R. Castillo. "In situ preparation of a cholesterol biosensor: entrapment of cholesterol oxidase in an overoxidized polypyrrole film electrodeposited in a flow system: Determination of total cholesterol in serum," *Analytica Chimica Acta,* Vol. 385, pp. 213-222, 1999.

[45] E. Smela. "Microfabrication of PPy microactuators and other conjugated polymer devices," *Journal of Micromechanics and Microengineering,* Vol. 9, pp. 1-18, 1999.

[46] J. Y. Kim, J. H. Jung D. E. Lee and J. Joo. "Enhancement of electrical conductivity of poly(3,4-ethylenedioxythiophene)/poly(4-styrenesulfonate) by a change of solvents," *Synthetic Metals,* Vol. 126, pp. 311-316, 2002.

[47] W. H. Kim, A. J. Ma¨kinen, N. Nikolov, R. Shashidhar, H. Kim and Z. H. Kafafi. "Molecular organic light-emitting diodes using highly conducting polymers as anodes," *Applied Physics Letters,* Vol. 80, pp. 3844-3846, 2002.

Reproduced with permission of the copyright owner. Further reproduction prohibited without permission.

[48] S. K. M. Jo¨nsson, J. Birgerson, X. Crispin, G. Greczynski, W. Osikowicz, A. W. D. van der Gon, W. R. Salaneck and M. Fahlman. "The effects of solvents on the morphology and sheet resistance in poly(3,4-ethylenedioxythiophene)–polystyrenesulfonic acid (PEDOT–PSS) films," *Synthetic Metals,* Vol. 139, pp. 1-9, 2003.

[49] X. Crispin, S. Marciniak, W. Osikowicz, G. Zotti, A. W. D. van der Gon, F. Louwet, M. Fahlman, L. Groenendaal, F. de Schryver and W. R. Salaneck. "Conductivity, morphology, interfacial chemistry, and stability of poly(3,4-ethylene dioxythiophene)-poly(styrene sulfonate): A photoelectron spectroscopy study," *Journal of Polymer Science.,* Vol. 41, pp. 2561-2583, 2003.

[50] E. T. Kang, K. G. Neoh and K. L. Tan. "Polyaniline: A polymer with many interesting intrinsic oxidation redox states," *Progress in Polymer Science,* Vol. 23, pp. 277-324, 1998.

[51] E. M. Genies, A. Boyle, M. Lapkowski and C. Tsintavis. "Polyaniline: A historical survey," *Synthetic Metals,* Vol. 36, pp. 139-182, 1990.

[52] J. Anand, S. Palaniappan and D. N. Sathyanarayana. "Conducting Polyaniline blends and composites," *Progress in Polymer Science,* Vol. 23, pp. 993-1018, 1998.

[53] E. Smela, Wen Lu and B. R. Mattes. "Polyaniline actuators Part 1. PANI(AMPS) in HCl," *Synthetic Metals,* Vol. 151, pp. 25-42, 2005.

[54] J.W. Gardner and P.N. Bartlett. "A brief history of electronic noses," *Sensors and Actuators B,* Vol. 18-19, pp. 210-211, 1994.

[55] C. Munoz, G. Steinthal and S. Sunshine. "Conductive polymer-carbon black composites-based sensor array for use in sensor array," *Sensor Review,* Vol. 19, pp. 300-305, 1999.

[56] S. V. Patel, M. W. Jenkins, R. C. Hughes, W, G. Yelton and A. J. Ricco. "Differentiation of chemical components in a binary solvent vapor mixture using carbon/polymer composite-based chemiresistor," *Analytical Chemistry,* Vol. 72, pp. 1532-1542, 2000.

[57] G. A. Sotzing, S. M. Briglin, R. H. Grubbs and N. S. Lewis. "Preparation and properties of vapor detector arrays formed from Poly(3,4-ethylenedioxy)thiophene-Poly(styrenesulphonate)/Insulating polymer composites," *Analytical Chemistry,* Vol. 72, pp. 3181-3190, 2000.

[58] R. H. M. van de Leur and A. van der Waal. "Gas and vapor detection using Polypyrrole," *Synthetic Metals,* Vol. 102, pp. 1330-1331, 1999.

Reproduced with permission of the copyright owner. Further reproduction prohibited without permission.

[59] S. T. McGovern, G. M. Spinks and G. G. Wallace. "Micro-humidity sensors based on a processable Polyaniline blend," *Sensors and Actuators B,* Vol. 107, pp. 657-665, 2005.

[60] W. A. Daoud, J. H. Xin and Y. S. Szeto. "Polyethylenedioxythiophene coatings for humidity, temperature and strain sensing polyamide fibers," *Sensors and Actuators B,* Vol. 109, pp. 329-333, 2005.

[61] P. de Melo, B. B. Neto,E. G. de Lima, L. F. B de Lira and J. E. C. de Souza. "Use of conducting Polypyrrole blends as gas sensors," *Sensors and Actuators B,* Vol. 109, pp. 348-354, 2005.

[62] A. Athawale and M. V. Kulkarni. "Polyaniline and its substituted derivatives as sensor for aliphatic alcohols," *Sensors and Actuators B,* Vol. 67, pp. 173-177, 2000.

[63] Q. Ameer and S. Adeloju. "Polypyrrole-based electronic noses for environmental and industrial analysis," *Sensors and Actuators B,* Vol. 106, pp. 541-552, 2005.

[64] T. Yamauchi, K. Kojima, K. Oshima, M. Shimomura and S. Miyauchi. "Glucose-sensing characteristics of conducting polymer bound with glucose oxidase," *Synthetic Metals,* Vol. 102, pp. 1320, 1999.

[65] S. K. Dhawan, D. Kumar, M. K. Ram, S. Chandra and D. C. Trivedi. "Application of conducting Polyaniline as sensor material for ammonia," S*ensors and Actuators B,* Vol. 40, pp. 99-103, 1997.

[66] T. Linfords and A. Ivaska. "Calcium-selective electrode based on Polyaniline functioalized with bis[4-(1,1,3,3-tetramethylbutyl)phenyl]phosphate," *Analytica Chimica Acta,* Vol. 437, pp. 171-182, 2001.

[67] L. M. Torres-Rodriguez, M. Billon, A. Roget and G. Bidan. "A Polypyrrole-biotin based biosensor: elaboration and characterization," *Synthetic Metals,* Vol. 102, pp. 1328-1329, 1999.

[68] A. Karyakin, M. Vuki, L. V. Lukachova, E. E. Karyakina, A. V. Orlov, G. P. Karpachova and J. Wang. "Processable Polyaniline as an advanced potentiometric pH transducer," *Analytical Chemistry,* Vol. 71, pp. 2534-2540, 1999.

[69] Y Xia and G. M. Whitesides. "Soft lithography," *Angewandte Chemie International Edition,* Vol. 37, pp. 550-575, 1998.

[70] R. F. Service. "Printable electronics that stick around," *Science*, Vol. 304, pp. 675-678, 2004.

Reproduced with permission of the copyright owner. Further reproduction prohibited without permission.

[71] R. K. Holman, S. A. Uhland, M. J. Cima and E. Sachs. "Surface Adsorption Effects in the Inkjet Printing of an Aqueous Polymer Solution on a Porous Oxide Ceramic Substrate," *Journal of Colloid and Interface Science,* Vol. 247, pp. 266-274, 2002.

[72] P. Calvert. "Inkjet Printing for Materials and Devices," *Chemical Materials,* Vol. 13, pp. 3299, 2001.

[73] V. G. Shah and D. B. Wallace. "Low-cost Solar Cell Fabrication by Drop-on-Demand Ink-jet Printing," *Proceedings of IMAPS, 37th Annual International Symposium on Microelectronics,* Vol. 24, pp. 15-17, 2004

[74] M. Heckele, W. Bacher and K. D. Muller. "Hot embossing-The molding technique for plastic microstructures," *Microsystem Technologies,* Vol. 4, pp. 122-124, 1998.

[75] Holger Becker and Ulf Heim. "Hot embossing as a method for fabrication of polymer high aspect ratio structures," *Sensors and Actuators B,* Vol. 83, pp. 130-135, 2000.

[76] X. C. Shan, T. Ikehara, Y. Murakoshi and R. Maeda. "Applications of micro hot embossing for optical switch formation," *Sensors and Actuator A,* Vol. 119, pp. 433-440, 2005.

[77] L. L. Hunter. "Investigation of sidewall cracking in PMMA LIGA structures," *Journal of Micromechanics and Microengineering,* Vol. 16, pp. 1181-1188, 2006.

[78] Luo, R. Poddar and X. Liu. "Innovative approach for replicating micropatterns in a conducting polymer," *Journal of Vacuum Science and Technology B,* Vol. 24, pp. L19-L22, 2006.

[79] A. Chakraborty, X. Liu, and C. Luo. "An intermediate-layer lithography method for generating multiple microstructures made of different conducting polymers," *Microsystem Technologies* (in press; available on the journal website), 2006.

[80] X. Liu, A. Chakraborty and C. Luo. "Generation of all-polymeric diodes and capacitors using an innovative intermediate-layer lithography," A*dvances in Solid-State Technology* (invited book chapter, accepted for publication), 2007.

[81] Marc J. Madou, *Fundamentals of Microfabrication,* CRC Press, 2002.

[82] G. T. Kovacs, *Micromachined Transducer Sourcebook,* McGraw-Hill Publications, 1998.

[83] G. T. Kovacs, N. I. Maluf and K. Peterson. "Bulk micromachining of silicon," *Proceedings of the IEEE,* Vol. 86, pp. 1536-1551, 1998.

Reproduced with permission of the copyright owner. Further reproduction prohibited without permission.

[84] Stephen Y Chou, Peter R. Krauss and P. J. Renstorm. "Nanoimprint Lithography," *Journal of Vacuum Science and Technology B,* Vol. 14, pp. 4129-4133, 1996.

[85] Operating Manual, Hot embossing system HEX 01/LT, JENOPTIK MICROTECHNIK GmbH, 1996.

[86] M. Mooney. "A theory of large elastic deformation," *Journal of Applied Physics*, Vol. 11, pp. 582-597, 1940.

[87] Y. Hirai, M. Fujiwara, T. Okuno and Y. Tanaka. "Study of resist deformation in nanoimprint lithography," *Journal of Vacuum Science and Technology B*, Vol. 19, pp. 2811-2815, 2001.

[88] A. Chakraborty, G. Parthasarathi, W. Zhao and C. Luo. "Electronic nose for detecting multiple targets," *SPIE Proceedings on Micro (MEMS) and Nanotechnologies for Space Applications*, Vol. 3550, pp. 50-56, 2006.

[89] K. Suri, S. Annapoorni, A. K. Sarkar and R. P. Tandon. "Gas and humidity sensors based on iron oxide-polypyrrole nanocomposites," *Sensors and Actuators B,* Vol. 81, pp. 277-282, 2002.

[90] A. Chakraborty, G. Parthasarathi and C. Luo. "Multiple arrays of conducting polymer microwire based sensors," *Proceedings of ASME/JSME Joint Conference on Micromechatronics for Information and Precision Equipment (MIPE),* Vol. 4320, pp. 1- 8, 2006.

[91] R. Ladawan, A. Sirivat and J. Schwank. "Electrical conductivity response of polypyrrole to acetone vapor: effect of dopant anions and interaction mechanisms," *Synthetic Metals,* Vol. 140, pp. 15-21, 2004.

[92] L. Setti, A. F. Morgera, B. Ballarin, A. Filippino, D. Frascaro and C. Piana. "An amperometric glucose biosensor prototype fabricated by thermal inkjet printing," *Biosensors and Bioelectronics,* Vol. 20, pp. 2019-2026, 2005.

[93] A. Chakraborty, G. Parthasarathi and C. Luo. "Investigation of the conducting polymer microsensors generated using an intermediate-layer lithography method," *Micro (MEMS) and Nanotechnologies for Defense and Security,* Vol. 6556, pp. 10-17, 2007.

[94] Watt, A. A. Bettiol, J. A. Van Kan, E. J. Teo and M. B. H. Breese. "Ion beam lithography and nanofabrication: A review," *International Journal of Nanoscience,* Vol. 3, pp. 269-286, 2005.

Reproduced with permission of the copyright owner. Further reproduction prohibited without permission.

[95] A.A.Tseng. "Recent developments in micromilling using focused ion beam technology," *Journal of Micromechanics and Microengineering,* Vol. 14, pp. R15-R34, 2004.

[96] S. Reyntjens and R. Puers. "A review of focused ion beam applications in microsystem technology," *Journal of Micromechanics and Microengineering,* Vol. 11, pp. 287-300, 2001.

[97] A. A. Tseng. "Recent developments in nanofabrication using focused ion beams," *Small,* Vol. 10, pp. 924-939, 2005.

Reproduced with permission of the copyright owner. Further reproduction prohibited without permission.